DISSERTATION

SNOW SUBLIMATION AND SEASONAL SNOWPACK VARIABILITY

Submitted by

Graham A. Sexstone

Department of Geosciences

In partial fulfillment of the requirements

For the Degree of Doctor of Philosophy

Colorado State University

Fort Collins, Colorado

Fall 2016

Doctoral Committee:

Advisor: Steven R. Fassnacht

David W. Clow
Christopher A. Hiemstra
Gregory L. Butters

ABSTRACT

SNOW SUBLIMATION AND SEASONAL SNOWPACK VARIABILITY

In the western United States, seasonal melt from snow in mountainous regions serves as an essential water resource for ecological and anthropological needs, and improving our abilities to quantify the amount of water stored in the seasonal snowpack and provide short-term forecasts of snowmelt inputs into river systems is a critical science endeavor. Two important uncertainties in characterizing the seasonal evolution of snow in mountainous environments are related to the inherent spatial variability of snow in complex terrain and the magnitude and variability of snow sublimation fluxes between snow and the atmosphere; these uncertainties motivate this collection of research which includes three studies conducted in the north-central Colorado Rocky Mountains. The first study uses fine resolution airborne lidar snow depth datasets to evaluate the spatial variability of snow within areas comparable to coarse scale model grids (i.e. subgrid variability at 500 m resolution). Snow depth coefficient of variation, which was used as a metric for evaluating subgrid snow variability, exhibited substantial variability in mountainous terrain and was well correlated with mean snow depth, land cover type, as well as canopy and topography characteristics. Results highlight that simple statistical models for predicting subgrid snow depth coefficient of variation in alpine and subalpine areas can provide useful parameterizations of subgrid snow distributions. Given that snow sublimation fluxes are expected to exert important influences on snow distributions, the second and third studies focus on measuring and modeling the variability and importance of snow sublimation. To evaluate the relative merits and measurement uncertainty of methods for quantifying snow sublimation in

mountainous environments, a comparison was made between the eddy covariance, Bowen ratio-energy balance, bulk aerodynamic flux, and aerodynamic profile methods within two forested openings. Biases between methods are evaluated over a range of environmental conditions, which highlight limitations and uncertainties of each method as well as the challenges related to measuring surface sublimation in snow-covered regions. Results provide guidance for future investigations seeking to quantify snow sublimation through station measurements and suggest that the eddy covariance and/or bulk aerodynamic flux methods are superior for estimating surface sublimation in snow-covered forested openings. To evaluate the spatial variability and importance of snow sublimation, a process-based snow model is applied across a 3600 km^2 domain over five water years. *In-situ* eddy covariance observations of snow sublimation compare well with modeled snow sublimation at sites dominated by surface and canopy sublimation, but highlight challenges with model evaluation at sites where blowing sublimation is prominent. Modeled snow sublimation shows considerable spatial variability at the hillslope scale that is evident across elevation gradients and between land cover types. Snow sublimation from forested areas (canopy plus surface sublimation) accounted for the majority of modeled sublimation losses across the study domain and highlights the importance of sublimation from snow stored in the forest canopy in this region. Model simulations suggest that snow sublimation is a significant component of the winter water balance, accounting for losses equivalent to 43 percent of total snowfall, and strongly influences snow distributions in this region. Results from this study have important implications for future water management and decision making.

ACKNOWLEDGEMENTS

This collection of research would not have been possible without the funding provided by the USGS Water Availability and Use Science Program; USGS Water, Energy, and Biogeochemical Budgets Program; NASA Terrestrial Hydrology Program (award NNX11AQ66G); and the Colorado Water Conservation Board. Additionally, I would like to acknowledge the support provided by the USGS Colorado Water Science Center throughout my graduate work.

I am grateful to have had the opportunity to learn from and work with my advisor, Dr. Steven Fassnacht, throughout my M.S. and Ph.D. programs at Colorado State University. He is my mentor and friend, and has played such an important role in my development as a scientist and researcher. I would also like to thank Dr. Dave Clow (USGS) for his insight, confidence in my abilities, and rigorous expectations that have continually pushed my research forward. He has provided tremendous opportunities for me working with the USGS that are greatly appreciated. Thanks to Dr. Chris Hiemstra (CRREL) for serving on my committee, his valuable insight, and always going above and beyond looking for data sources that could aid this research. Also, thanks to Dr. Greg Butters for serving on my committee and his inspiring teaching during my graduate coursework.

Dr. Glen Liston (CIRA) was very helpful with my queries related to running SnowModel and provided insight and helpful discussions related to modeling snow processes. Thanks to Dave Stannard (USGS) for the many discussions on the atmospheric boundary layer over snow covers and his contributions to this research. Dr. Juan Ignacio López-Moreno's (IPE CSIC) insight related to snow variability and his contributions to this research are greatly appreciated.

Thanks to Colin Penn (USGS) and Garrett Port (USGS) whose help in the field was instrumental for the success of this work. Additionally, thanks for the Fassnacht Snow Lab for the writing retreats, presentation reviews, and good company over the years. Thanks to Dr. John Knowles (CU) and Sean Burns (CU) for their willingness to share their eddy covariance data that was a tremendous resource for this research. Dr. Dean Anderson (USGS) was very helpful with the initial deployment of the eddy covariance instrumentation used in this research. Lastly, I would like to acknowledge the work of the late Dr. Edgar Andreas. Dr. Andreas contributed helpful discussions on turbulent fluxes over snow-covered surfaces and provided the bulk flux algorithm that was used in this study.

There are many data sources that were utilized as part of this research that need to be acknowledged. Data sources include the: Boulder Creek Critical Zone Observatory lidar datasets, Ameriflux program US-NR1 datasets, Natural Resource Conservation Service SNOTEL datasets, Niwot Ridge Long Term Ecological Research meteorological datasets, and Colorado Avalanche Information Center meteorological datasets. The availability and accessibility of high quality datasets such as these will be instrumental for future advances in science.

DEDICATION

This dissertation is dedicated to my parents Alan and Julie, who taught me the importance of hard work and introduced me to the wonders of nature and science.

To my wife Colleen, whose never-ending patience, love, and support is my foundation that has made this undertaking a possibility.

And to my son Crosby, who gives me happiness and motivation that I couldn't have imagined. May you someday find your passion that inspires you to do great things.

TABLE OF CONTENTS

CHAPTER 1 – INTRODUCTION

Seasonal snow covers are relied on by human populations as an essential water resource in many regions throughout the world [*Barnett et al.*, 2005], particularly in semi-arid and arid lands that rely heavily on water originating in mountainous areas [*Viviroli et al.*, 2003]. In the mountains of the western United States (U.S.), where most of annual precipitation falls as snow [*Serreze et al.*, 1999], seasonal snowmelt runoff is a major source for streamflow and subsurface recharge, delivering water for drinking, irrigation, industry, energy production, and ecosystems across much of the region [*Bales et al.*, 2006]. Snow-covered mountainous terrain in this region serves as a large natural reservoir that stores water through the winter, and releases it downstream during the spring and summer months each year. It has been estimated that snowmelt contributes to between 70 and 80% of annual runoff in the western U.S. [*Doesken and Judson*, 1996]. Therefore, in headwater states such as Colorado, an area with already over-allocated water resources [*Painter et al.*, 2010], quantifying the amount of water stored within seasonal snow is critical to account for water that will often be utilized to meet demands hundreds of miles away. Additionally, given the increasing pressures on water resources in the western U.S. from population growth as well as the risk of changing snow dynamics in response to climate change [e.g., *Knowles et al.*, 2006; *Mote*, 2006; *McCabe and Wolock*, 2007; *Rauscher et al.*, 2008; *Stewart*, 2009; *Clow*, 2010; *Harpold et al.*, 2012], future water management in this region will pose significant challenges. Current water resources forecasting methods are based upon statistical relations between index snow measurements and observed streamflow and have been shown to perform best during average conditions well represented by the past [*Pagano et al.*, 2014], and the skill of these forecasts will likely continue to decrease as past observations

become less representative of current conditions [*Milly et al.*, 2008]. Therefore, improving our abilities to quantify the seasonal evolution of snow water equivalent (SWE) within mountainous regions and provide short-term forecasts of snowmelt inputs into river systems is a critical endeavor and is central to the motivation of the dissertation.

Chapter 1 of this dissertation provides background on the nature of spatial and temporal snow variability in complex mountainous terrain as well as the drivers of this heterogeneity. Also, an overview of the methodologies currently used to resolve snow variability and their limitations are provided. The motivations of this dissertation research as well as the objectives of each dissertation chapter are outlined.

1.1 Background

1.1.1 Spatial and Temporal Variability of the Snowpack

The snowpack exhibits marked variability both spatially and temporally across the landscape [*López-Moreno et al.*, 2015] that is shaped by different processes at varying spatial scales [*Blöschl*, 1999]. At the plot scale (1 to 10s m), microtopography and forest canopy cover often control the distribution of snow [e.g., *Musselman et al.*, 2008; *López-Moreno et al.*, 2011], while snow sublimation, wind redistribution of snow, and solar radiative irradiance tend to dictate the evolution of the snowpack at the hillslope or watershed scale (100s to 1000s m). At the basin scale (100s to 1000s km), where the physical process scale of climatic conditions may be represented by a correlation length on the order of 10 km [*Blöschl*, 1999], snow variability in mountainous regions is controlled by orographic precipitation and storm track movement. Therefore, the variability of the snowpack through space and time at a given scale of interest is driven by the influences of weather patterns (e.g. precipitation, temperature, vapor pressure, wind, and net radiation) and their interactions with topography and forest canopy. Given the

complexity related to the processes and interactions controlling snow evolution, considerable research has focused on understanding the nature and drivers of snowpack variability.

Forest canopy can have a strong influence on snow cover heterogeneity observed over short distances due to a variety of physical process interactions. Snow interception within the forest canopy [e.g., *Hedstrom and Pomeroy*, 1998] and subsequent canopy sublimation [e.g., *Montesi et al.*, 2004; *Molotch et al.*, 2007] often results in a reduced snow accumulation underneath the canopy [e.g., *Musselman et al.*, 2008; *Veatch et al.*, 2009]. Additionally, in environments with interspersed canopy cover and high exposure to wind (especially near tree line), trees have a strong influence on aerodynamic properties and thus the redistribution of snow by wind, with blowing snow often depositing in drifts on the leeward side of trees [*Hiemstra et al.*, 2006; *Deems*, 2007]. Forest canopy cover also exhibits a strong control on the snowpack energy balance through solar radiation [e.g., *Ellis and Pomeroy*, 2007], longwave radiation [e.g., *Pomeroy et al.*, 2009], and advective fluxes of water, heat, and momentum [e.g., *Liston*, 1995]. The influence of canopy cover on sub-canopy shortwave irradiance has been shown to be well correlated with the variability of snowmelt rates [e.g., *Musselman et al.*, 2012].

Terrain position and orientation and its interaction with meteorology also impose a strong control on snowpack variability. The transfer of water directly between the snowpack and atmosphere through snow sublimation from the surface [e.g., *Fassnacht*, 2004; *Reba et al.*, 2012; *Sexstone et al.*, 2016b] and blowing snow [e.g., *Pomeroy and Essery*, 1999] is an important process influencing snow water evolution and is especially enhanced in terrain with high exposure to wind and solar radiation, such as alpine areas [e.g., *Hood et al.*, 1999; *Strasser et al.*, 2008; *Knowles et al.*, 2012]. Wind redistribution of snow is another important driver of snow distribution and variability that is highly correlated with the influence of terrain on the

aerodynamics of wind; the snowpack tends to scour on the windward side of terrain elements and accumulate on the leeward side due to these effects [*Winstral et al.*, 2002]. The degree of topographic slope, which impacts the stability of the snowpack, can also influence snow accumulation through sloughing and avalanching [e.g., *Kerr et al.*, 2013], and cause preferential accumulation of snow in areas of convex topography (e.g. low lying gullies) [e.g., *Lapen and Martz*, 1996]. Lastly, topographic position and orientation can have a strong influence on the exposure of the snowpack to solar radiation [*Dozier*, 1980]. Solar radiation is the dominant component of the overall snow energy balance and therefore plays an important role in the timing and rate of snowmelt [*Marks and Dozier*, 1992].

The geographic controls on mountain meteorology, such as elevation, latitude, and continentality [*Barry*, 2008], can also control snow variability, especially at the basin scale. Snow accumulation tends to increase with elevation because of orographic precipitation patterns and the effects of air temperature (i.e. the fraction of precipitation falling as snow and snow cover duration) [e.g., *Fassnacht and Soulis*, 2002]. Additionally, latitude can influence snow accumulation and melt because of decreasing temperature and net radiation as well as changing vegetation growth patterns with latitude [*Barry*, 2008]. Continentality (i.e. geographic location) can influence the distribution of snow in various ways that depend on site location and scale. The distance to a mountain barrier and/or an ocean can influence snow accumulation patterns [e.g., *Fassnacht et al.*, 2003; *López-Moreno and Nogués-Bravo*, 2006]. Furthermore, geographic differences in snow accumulation and ablation can be caused by the preferential movement of storm tracks through a region. *Sexstone and Fassnacht* [2014] found that elevation and geographic location showed a strong relation with SWE at the basin scale, suggesting these

variables represent consistent drivers of the spatial variability of SWE, such as orographic precipitation patterns and storm track movement.

1.1.2 Measuring and Modeling Snow Variability

Given the complexities that shape the spatial and temporal variations of snow in mountainous regions, accurately measuring and modeling snow distributions is a significant challenge. Ground-based and remotely sensed observations as well as various modeling methods each show important strengths and limitations [*Dozier*, 2011]. An overview of methods currently used to characterize the spatial distribution of snow is provided below.

1.1.2.1 Remote Sensing Observations

Satellite and airborne remote sensing platforms offer an exceptional opportunity to monitor snowpack variability across spatial and temporal scales that cannot be monitored by traditional field measurements. Remote sensing observations of snow have shown significant advances over the past fifteen years [*Nolin*, 2010]; however, there are still major challenges limiting the direct observation of snow distributions in complex terrain. Operationally, spaceborne snow remote sensing products are either coarse-resolution data with broad observational frequency or fine-resolution data with longer time steps. Despite these limitations, snow covered area (SCA) is a key spaceborne snow observation that provides important information about the spatial and temporal coverage of snow and is essential for constraining the extent of snow cover in spatial estimations of SWE. Additionally, SCA is a central observation to a reconstruction modeling analysis of SWE that is based on the timing snow cover disappearance [*Martinec and Rango*, 1981]. Snow water equivalent reconstruction [e.g., *Molotch and Bales*, 2005] has shown robust performance by a variety of studies [*Dozier*, 2011], but this

method can be only applied subsequent to snow disappearance which limits its application for streamflow forecasting.

More recently, airborne and terrestrial-based lidar (light detection and ranging) remote sensing observations are of particular interest for monitoring snow distributions. This is because these lidar observations have shown the ability to measure fine resolution (~1 m) snow depth across the watershed scale [e.g., *Hopkinson et al.*, 2004; *Cline et al.*, 2009; *Grünewald et al.*, 2013; *Painter et al.*, 2016], which decimeter scale accuracy [e.g., *Deems*, 2007]. In principle, lidar measurements can be used to calculate snow depth by differencing retrievals made of surface elevation from both snow-on and snow free observations [*Deems et al.*, 2013]. Although snow depth observations from airborne and terrestrial lidar show considerable promise, these observations are limited because they are not operational and require considerable time and expense for a mission to be conducted (i.e., these observations have limited spatial and temporal coverage). Additionally, potential errors induced by both topography and canopy must be considered when utilizing lidar-based snow depth [*Deems et al.*, 2013].

1.1.2.2 Statistical Modeling

The correlation of topography with the drivers of snowpack variability in mountainous regions has encouraged research on the relation between terrain characteristics and snowpack properties [e.g., *Meiman*, 1968] through the development of statistical models [e.g., *Elder et al.*, 1991]. Using topographic variables derived from digital elevation models (DEMs) as explanatory variables along with measurements of snowpack properties as response variables, models have successfully been used to characterize the heterogeneity of snow water equivalent, snow depth, and/or snow density across the landscape. Studies have commonly used either multiple linear regression [e.g., *Fassnacht et al.*, 2003; *Jost et al.*, 2007; *Sexstone and Fassnacht*, 2014] or

binary regression trees [e.g., *Balk and Elder*, 2000; *Erxleben et al.*, 2002; *Winstral et al.*, 2002; *Molotch et al.*, 2005] for these efforts. These statistical models have been developed using manual field-based snow measurements [e.g., *Balk and Elder*, 2000], operational NRCS snow measurements [e.g., *Fassnacht et al.*, 2003], or a combination of both [e.g., *Sexstone and Fassnacht*, 2014]. However, representative field-based measurements are often needed for strong model performance, as operational measurements alone cannot accurately characterize the snowpack variability that vitally impacts snowmelt runoff [*Bales et al.*, 2006]. Statistically-based modeling of snow distributions has provided important insight into understanding the nature of snow variability, but is also limited for directly improving snowmelt runoff forecasts because of the sparse availability of representative snowpack measurements [e.g., *Fassnacht et al.*, 2012; *Meromy et al.*, 2013] both spatially and temporally that are needed to develop these models. Therefore, there is a need for future research to evaluate how to incorporate the relations of snow distribution with topographic and canopy features, that tend to repeat annually [*Sturm and Wagner*, 2010], within techniques for estimating snow distribution that have a more reliable spatial coverage, such as remote sensing observations or process-based snow models.

1.1.2.3 Physically Based Modeling

Physically based snow models have made considerable advances in recent years that show promise for simulating the spatial distribution of the snowpack across the landscape [e.g., *Lehning et al.*, 2006; *Liston and Elder*, 2006b; *Pomeroy et al.*, 2007]. These distributed models use more readily available meteorological forcing data and energy balance calculations to simulate the energy fluxes away from and toward the snowpack, accounting for physical processes driving snow accumulation, evolution, redistribution, and ablation throughout the snow season. Given the numerical treatment of each physical process, these models also offer the

unique ability to improve both understanding of snow process interactions and prediction of SWE distributions without relying on historic relations. The spatially distributed snowpack evolution modeling system SnowModel [*Liston and Elder*, 2006b] is used in this dissertation research and will be described in subsequent chapters.

Although process based snow models show promise for improving estimates of snow distribution and snowmelt runoff, these models are not often critically evaluated, largely because of the difficulty of making high quality ground and remote sensing observations across expansive model domains. Given the uncertainties in modeling snow water content and its seasonal evolution, and the importance of snowmelt in the annual water balance, research is needed to conduct a more comprehensive evaluation of data needs and model capabilities for quantifying the distribution and variability of the snowpack across snow dominated regions. Particularly, research needs to be focused on evaluating model representations of processes that are important for driving snow distributions, such as snow sublimation. Additionally, continued work on the utility of assimilating ground-based snow measurements and remote sensing observations into snow models is also needed [e.g., *Liston and Hiemstra*, 2008; *Fletcher et al.*, 2012].

1.2 The Importance of Snow Sublimation in Snow Distributions

Snow sublimation is defined as the transfer of water directly between snow and the atmosphere through phase change, and encompasses water vapor fluxes between the atmosphere and the snow surface (surface sublimation), snow held within the forest canopy (canopy sublimation), and snow being transported by wind (blowing sublimation). Snow sublimation has been shown to be an important process in the annual water balance across many snow-covered regions [e.g., *Pomeroy and Gray*, 1995; *Strasser et al.*, 2008; *MacDonald et al.*, 2010; *Knowles*

et al., 2015b]. However, given the spatial and temporal sparsity of studies that have collected snow sublimation measurements and the lack of an operational network for measuring this process, there is considerable uncertainty in the variability and importance of snow sublimation and how this process shapes the spatial and temporal evolution snow distributions [*Liston and Sturm*, 2004], particularly in complex mountainous terrain. Process-based snow models provide the unique ability to model the spatial and temporal variability of surface, canopy, and blowing sublimation; however, careful measurements of water vapor fluxes between snow and the atmosphere are needed for evaluating model representations.

1.3 Research Motivation and Objectives

Given that process-based snow models may provide an important utility for future snowmelt runoff forecasting in the western U.S., there is a need for research to critically evaluate and potentially improve model representations of snow processes. Two important uncertainties in characterizing the seasonal evolution of the snowpack are the nature and scale of the spatial variability of snow in complex mountainous terrain, and the magnitude and variability of seasonal snow sublimation fluxes between the snowpack and atmosphere. Therefore, the science question motivating this research is: *How does snow sublimation vary spatially and temporally in seasonally snow-covered environments and what is the role of this process in shaping the spatial distribution of the snowpack across varying land covers within mountainous terrain?* Through a combination of ground-based measurements, remote sensing observations, and snow evolution modeling within the northern Colorado Rocky Mountains, this collection of research focuses on key gaps in knowledge that are central to this overarching science question.

This dissertation research is presented as three articles prepared for peer-reviewed journals (Chapters 2 through 4) followed by a synthesis of research contributions (Chapter 5).

Chapter 2 [*Sexstone et al.*, 2016a submitted] uses airborne lidar datasets to evaluate the variability of subgrid snow distributions across a range of mountainous terrain and land cover characteristics and highlights the utility of airborne lidar for evaluating and improving snow model representations. In Chapter 3 [*Sexstone et al.*, 2016b], measurements of seasonal snow sublimation by four methods are collected from two forested openings and a comparison of the relative merits and propagated uncertainty of each method is provided. Lastly, in Chapter 4 [*Sexstone et al.*, 2016c in preparation], a process-based snow model is run for five water years across a 3600 km^2 model domain in the northern Colorado Rocky Mountains. Model results are used to quantify the spatial and temporal variability and importance of snow sublimation and are evaluated by ground-based eddy covariance measurements.

CHAPTER 2 – SUBGRID SNOW DEPTH COEFFICIENT OF VARIATION WITHIN COMPLEX MOUNTAINOUS TERRAIN[1]

2.1 Summary

Given the substantial variability of snow in complex mountainous terrain, a considerable challenge of coarse scale modeling applications is accurately representing the subgrid variability of snowpack properties. The snow depth coefficient of variation (CV_{ds}) is an important metric for characterizing subgrid snow distributions but has not been well defined by a parameterization for mountainous environments. This study utilizes lidar-derived snow depth datasets from mountainous terrain in Colorado, USA to evaluate the variability of subgrid snow distributions within a grid size comparable to a 1000 m resolution common for hydrologic and land surface models. The subgrid CV_{ds} exhibited a wide range of variability across the 321 km^2 study area (0.15 to 2.74) and was significantly greater in alpine areas compared to subalpine areas. Mean snow depth was well correlated with CV_{ds} variability in both alpine and subalpine areas, as CV_{ds} decreased nonlinearly with increasing snow depths. This negative correlation is attributed to the static size of roughness elements (topography and canopy) that strongly influence seasonal snow variability. Subgrid CV_{ds} was also strongly related to topography and forest variables; important drivers of CV_{ds} included the subgrid variability of terrain exposure to wind in alpine areas and the mean and variability of forest metrics in subalpine areas. Two simple statistical models were developed (alpine and subalpine) for predicting subgrid CV_{ds} that show reasonable performance statistics. The methodology presented here can be used for parameterizing CV_{ds} in snow-

[1] Chapter 2 was submitted to *The Cryosphere* and is currently under review. Additional authors are S.R. Fassnacht, J.I. López-Moreno, and C.A. Hiemstra.

dominated mountainous regions, and highlights the utility of using lidar-derived snow datasets for improving model representations of snow processes.

2.2 Introduction

Snow plays an important role in hydrological, ecological, and atmospheric processes within much of the Earth System, and for this reason, considerable research has focused on understanding the spatial and temporal distribution of snow depth (d_s) and snow water equivalent (*SWE*) across the landscape [e.g., *Clark et al.*, 2011]. Snowpacks exhibit substantial spatiotemporal variability [e.g., *López-Moreno et al.*, 2015] that is shaped by processes at varying spatial scales [*Blöschl*, 1999]. The variability of the snowpack through space and time at a given scale of interest is often driven by meteorology and its interactions with topography and forest features. Mountainous areas, which often accumulate large seasonal snowpacks, generally exhibit a high range of snow variability because of these effects [*Sturm et al.*, 1995]. Given that this variability occurs over relatively short distances [e.g., *Fassnacht and Deems*, 2006; *López-Moreno et al.*, 2011], accurately modeling the distribution of snow in mountainous areas requires a detailed understanding of the characteristics of snow variability at the model scale of interest [*Trujillo and Lehning*, 2015].

An important challenge of physically-based modeling is often the ability to represent within grid processes, or the subgrid spatial variability, of critical input parameters [*Seyfried and Wilcox*, 1995]. Accurate representation of subgrid snow distribution is critical for reliably simulating energy and mass exchanges between the land and atmosphere in snow-covered regions [*Liston*, 1999], yet various studies have highlighted a deficiency with this representation in hydrologic and land-surface models [e.g., *Pomeroy et al.*, 1998; *Slater et al.*, 2001; *Liston*, 2004; *Clark et al.*, 2011; *Liston and Hiemstra*, 2011]. *Liston* [2004] presented an approach of

effectively representing subgrid snow distributions in coarse-scale models by using a lognormal probability density function and an assigned coefficient of variation (*CV*). This approach only requires an estimation of the *CV* parameter (i.e. standard deviation divided by the mean), which has generally been estimated from field data and is a measure of snow variability that allows for comparisons that are independent of the amount of snow accumulation. Representative values of the *CV* of snow water equivalent (CV_{SWE}) and snow depth (CV_{ds}) have been published by many field studies [refer to Table 1 and Figure 2 from *Clark et al.*, 2011] and have been summarized based on vegetation and landform type [*Pomeroy et al.*, 1998] and classified globally, based on air temperature, topography, and wind speed regimes [*Liston*, 2004]. However, the range of published CV_{SWE} and CV_{ds} in complex mountainous terrain (i.e. the mountain snow class from *Sturm et al*. [1995]) is quite variable and a parameterization has not been well defined.

The recent developments of snow depth mapping capabilities from ground-based and airborne lidar [e.g., *Deems et al.*, 2013] as well as digital photogrammetry [e.g., *Bühler et al.*, 2015; *Nolan et al.*, 2015] have provided a high definition view of snow depth distributions, albeit at fixed locations in space and time, that have not been historically available by traditional field measurements. These detailed snow depth datasets have aided in an improved understanding of the scaling properties of snow distributions [e.g., *Deems et al.*, 2006; *Trujillo et al.*, 2007], the temporal evolution of snow distributions [e.g., *Grünewald et al.*, 2010; *López-Moreno et al.*, 2015], the relation of snow depth with topography [e.g., *Grünewald et al.*, 2013; *Kirchner et al.*, 2014; *Revuelto et al.*, 2014] and canopy [e.g., *Broxton et al.*, 2015; *Revuelto et al.*, 2015; *Zheng et al.*, 2016] characteristics, as well as the nature of fine scale subgrid variability of snow depth [*López-Moreno et al.*, 2015]. *Grünewald et al.* [2013] present a novel study in which lidar-derived snow depth datasets are aggregated to coarse scale grids to evaluate the drivers of snow

distribution at the catchment scale. Evaluations of lidar snow depth datasets within coarser scale grid resolutions can be analogous to the grid resolution of many modeling applications, thus lidar-derived snow datasets have potential to serve as an important tool for evaluating the representation of subgrid snow distributions within physically based models.

In this study, we use the snow depth coefficient of variation (CV_{ds}) as a metric of subgrid snow variability within complex mountainous terrain similarly to *López-Moreno et al.* [2015], however we use a grid size comparable to a 1000 m resolution common for hydrologic and land surface models. The objectives of this research were to (1) determine the range of CV_{ds} values that are observed within varying grid resolutions throughout the study area, (2) evaluate the effects of mean snow depth, forest, and topography characteristics on subgrid CV_{ds}, and (3) develop a methodology for parameterizing CV_{ds} within complex mountainous terrain. This research aims to help advance understanding of the variability of subgrid snow distributions, and support the development of more accurate representations of subgrid snow variability that can be used within physically based models.

2.3 Methods

2.3.1 Site description

The study area is in the Front Range Mountains of north-central Colorado, located in the western United States (Figure 2.1). Spatial lidar datasets collected by the Boulder Creek Critical Zone Observatory (CZO) (http://criticalzone.org/boulder/, accessed 17 April 2016) were investigated in this study. The study area (321 km^2) ranges in elevation from 2190 m to 4117 m and is dominated by ponderosa pine (*Pinus ponderosa*) and lodgepole pine (*Pinus contorta*) at lower elevations, Engelmann spruce (*Picea engelmannii*) and subalpine fir (*Abies lasiocarpa*) forests at higher elevations, and alpine tundra at the highest elevations (Figure 2.1). The mean

winter (1 October to 1 May) precipitation and temperature for water years 2006 - 2010 at the Niwot SNOTEL site (3021 m; Figure 2.1) is 452 mm and 2.7°C [*Harpold et al.,* 2014b]. The mountainous terrain in this region is complex, varying from gentle topography at lower elevations to steep and rugged slopes closer to the Continental Divide. The majority of the study area has a southeastern aspect and is located on the eastern side of the Continental Divide (Figure 2.1). The Front Range Mountains are characterized by a continental seasonal snowpack [*Trujillo and Molotch,* 2014], with the persistent snow zone at elevations greater than 3050 m [*Richer et al.*, 2013], generally exhibiting peak snow accumulation during the springtime months of April and May each year.

2.3.2 Spatial datasets

This analysis uses publically available lidar-derived snow depth (d_s), elevation (z), and vegetation height (VH) raster datasets (1 m resolution) from the Boulder Creek CZO (ftp://snowserver.colorado.edu/pub/WesternCZO_LiDAR_data, accessed 27 August 2015) that are described in detail by *Harpold et al.* [2014b]. Airborne lidar campaigns were completed during snow-covered (May 2010) and snow free (August 2010) periods across the study area and lidar surfaces were differenced to derive d_s [*Harpold et al.*, 2014b]. The snow-covered lidar returns were collected on two dates, 05 May 2010 and 20 May 2010, and the combined snow-covered lidar extent is 321 km^2 (Figure 2.1). A comparison of the lidar d_s dataset to *in-situ* d_s sensors within research catchments in the Boulder Creek CZO showed a root mean squared error (RMSE) of 27 cm and 7 cm at the Como Creek catchment (16 sensors) and Gordon Gulch catchment (5 sensors), respectively [*Harpold et al.*, 2014b].

The lidar-derived digital elevation model (DEM) was resampled from a 1 m to a 10 m resolution for representation of the resolution of commonly available DEMs (USGS National

Elevation Dataset, http://ned.usgs.gov) and was subsequently used to derive topography variables for each 10 m cell that have been shown to influence d_s distributions [e.g., *Elder et al.*, 1998; *Winstral et al.*, 2002; *Erickson et al.*, 2005; *Kerr et al.*, 2013; *Revuelto et al.*, 2014] using a Geographic Information System (GIS). Surface slope (S) was calculated by fitting a plane to a 3 x 3 cell window around each DEM cell. Winter clear-sky incoming solar radiation ($Q_{sw\downarrow}$) was determined using the Area Solar Radiation tool in ArcGIS, which calculates mean incoming solar radiation for clear-sky conditions across a DEM surface for a specified time interval based on solar zenith angle and terrain shading. The time interval used for the calculation of $Q_{sw\downarrow}$ was 01 October through 01 May. Aspect was not considered because it was highly correlated with $Q_{sw\downarrow}$. Maximum upwind slope (Sx) [*Winstral et al.*, 2002], which can be used as a measure of the exposure to or sheltering from wind, was calculated for each cell as:

$$Sx_{\alpha,d\max}(x_i, y_i) = \max\left(\tan^{-1}\left\{ \frac{z(x_v, y_v) - z(x_i, y_i)}{\left[(x_v - x_i)^2 + (y_v - y_i)^2\right]^{0.5}} \right\} \right) \tag{2.1}$$

where α is the azimuth of the search direction, *dmax* is the maximum distance for the search direction, z is elevation, and (x_v, y_v) are all cells along the vector defined by α and *dmax*. Given the prevailing westerly winds within the study area [*Winstral et al.*, 2002; *Erickson et al.*, 2005], an average Sx was calculated for a *dmax* of 200 m and a range of α from 240° to 300° at 5° increments [e.g., *Molotch et al.*, 2005]. Topographic position index (*TPI*) [*Weiss*, 2001], which is a measure of the relative position of the cell to surrounding topography, was calculated for each cell as:

$$TPI = z_0 - \bar{z} \tag{2.2}$$

$$\bar{z} = \frac{1}{n_R} \sum_{i \in R} z_i \tag{2.3}$$

where z_0 is the elevation of the cell and $\bar{z}$ is the average elevation of the surrounding cells within a specified cell window (R). TPI was calculated for 3 x 3 (i.e. 30 m resolution), 11 x 11, and 21 x 21 windows around each cell.

Additional forest canopy spatial datasets were also used in this study. WorldView-2 (WV2) satellite imagery (DigitalGlobe, Inc., USA) from a cloud free sky condition on 26 September 2013 was acquired. The WV2 imagery has a high spatial (3 m) and spectral resolution (8 multispectral bands) and was used to compute the Normalized Difference Vegetation Index (*NDVI*) for the study area at a 3 m resolution. Additionally, a 30 m resolution 2011 canopy density (*CD*) dataset was downloaded for the study area (http://www.mrlc.gov/nlcd2011.php, accessed 04 December 2015).

2.3.3 Aggregation of study grids

Operational snow models [e.g., *Carroll et al.*, 2006] often have a 1000 m horizontal grid resolution and snow representations within land surface models [e.g., *Slater et al.*, 2001] have generally been designed for a coarser resolution [e.g., *Yang et al.*, 1997] but are being developed to operate at finer scales [e.g., *Kumar et al.*, 2006; *Wood et al.*, 2011; *Bierkens et al.*, 2015]. This study attempts to evaluate the subgrid variability of d_s at a comparable grid resolution to this 1000 m model grid size. Therefore, the subgrid variability of d_s within study grids of 100 m, 200 m, 300 m, 400 m, 500 m, 750 m, and 1000 m resolutions was evaluated. For example, subgrid statistics for each 500 m study grid (with 100% d_s coverage) were calculated based on 250000 lidar-derived d_s cells. The goal of this was to identify an appropriate grid size for evaluation that exhibited similar characteristics of snow variability to the 1000 m resolution grids, but maximized the number of grids available for analysis within the study area. At least 80% coverage of each study grid by the lidar d_s datasets was required, and the d_s dataset with the

greatest coverage was utilized for cases of the overlapping snow-covered lidar datasets (Figure 2.1). When the 05 May 2010 and 20 May 2010 lidar d_s datasets were overlapping and both datasets had 100% study grid coverage, the 05 May 2010 dataset was used. In order to assess the influence of using lidar-derived snow depth from two different days, the snow depth distributions within the overlapping area of the two lidar campaigns (7.92 km^2; Figure 2.1) were compared.

For each study grid, the mean and standard deviation of d_s were determined and used to calculate CV_{ds}. The mean and standard deviation of each of the topography and vegetation datasets outlined above were also calculated for each study grid. A categorical variable representing ecosystem type was also determined for each study grid. The alpine ecosystem type was assigned to study grids that had a mean elevation greater than 3300 m and a mean *VH* less than 0.5 m, while the remaining study grids were assigned to the subalpine ecosystem type (Figure 2.1); treeline elevation in this area generally varies between 3400 m and 3700 m [*Suding et al.*, 2015]. Lastly, only study grids with a mean elevation greater than 3000 m (i.e. the persistent snow zone) were evaluated in this study (Figure 2.1).

2.3.4 Statistical analysis

Pairwise relations between CV_{ds} and d_s, topography variables (mean and standard deviation), and vegetation variables (mean and standard deviation) were explored for both alpine and subalpine study grids to evaluate drivers of subgrid d_s variability. CV_{ds} was expected to have a strong nonlinear relation with d_s [*Fassnacht and Hultstrand*, 2015]; therefore, this relation was detrended for both the alpine and subalpine study grids, and residuals were used to evaluate further topography and vegetation effects on CV_{ds} using Pearson's *r* coefficient. Additionally, multiple linear regression models were developed to predict CV_{ds} for both alpine and subalpine study grids. We evaluated a range of independent variables to be included within the multiple

linear regression models (refer to variables in Table 2.1). However, given that the goal of the model analysis was to provide a methodology for parameterizing CV_{ds}, some of the variables were deemed unsuitable and excluded from model testing. For example, mean *z* was not included in model testing as it was believed to be a site specific variable that may not have been transferable to independent data. Additionally, *VH* was not tested within the models as spatial datasets of this variable are not commonly available, unlike the USGS National Land Cover Database (http://www.mrlc.gov/index.php) canopy density product or remote sensing forest metrics such as *NDVI*. Variables included in the models were selected by an all-subsets regression procedure in which both Mallows' C_p [*Mallows*, 1973] and Akaike information criterion (AIC) [*Akaike*, 1974] were used as a measure of relative goodness of fit of the models [e.g., *Sexstone and Fassnacht*, 2014]. Final independent variables within the models were required to be statistically significant (p value < 0.05) and not exhibit multicollinearity. Multicollinearity was defined as model parameters exhibiting a variance inflation factor greater than 2. Given that a non-normal distribution of snow depth [*Liston*, 2004] and other topography and vegetation variables was expected, various transformations of model variables were explored. Model diagnostics of residuals were used to ensure the model assumptions of normality, linearity, and homoscedasticity. Model performance was evaluated using the Nash-Sutcliffe efficiency (NSE) and RMSE. Additionally, model verification was assessed using a 10-fold cross-verification procedure which runs 10 iterations of removing a randomly-selected 10 percent of the dataset, fitting the regression to the remainder of the data, and subsequently comparing modeled values to the independent observations that were removed.

2.4 Results

2.4.1 Snowpack conditions

In a hypothetical uniform snowmelt scenario [e.g., *Egli and Jonas*, 2009], the subgrid mean d_s is expected to decrease faster than the σ_{ds}, thus the CV_{ds} will increase without a corresponding increase in subgrid snow variability [*Winstral and Marks*, 2014]. Therefore, in this study, an evaluation of the snowpack conditions was important for assessing if the subgrid CV_{ds} may have been influenced by a melting snowpack. *SWE* data from nine Natural Resources Conservation Service (NRCS) SNOTEL stations located in the Front Range Mountains of northern Colorado (Figure 2.1) were evaluated to assess snowpack conditions. A snowmelt event occurred across the study area on 10 April 2010 (Figure 2.2a) that caused considerable snowmelt at stations below an elevation of 3000 m and a loss of 10% of peak *SWE* on average at stations above 3000 m. Following this snowmelt event, substantial snow accumulation continued at SNOTEL stations above 3000 m until 17 May 2010, when the onset of snowmelt began (Figure 2.2a). A plot of σ_{ds} versus mean d_s among the SNOTEL stations highlights the hysteretic dynamics of accumulation and melt across the region [*Egli and Jonas*, 2009], and confirms that the lidar data were collected prior to and at the beginning of snowmelt across the study area (Figure 2.2b). Additionally, the statistical distributions of snow depth on 05 May 2010 and 20 May 2010 within the areas that were overlapped by both lidar campaigns (7.92 km^2; Figure 2.1) are shown to be similar and have a CV_{ds} of 1.01 and 1.10, respectively (Figure 2.3). Given that the lidar-derived snow depths were collected before substantial snowmelt had occurred within the persistent snow zone and the distributions of d_s from both dates exhibit similar characteristics, we are confident that the subgrid CV_{ds} evaluated in this study is representative of

snow variability at peak snow accumulation and was not significant influenced by the data collection to two separate dates.

2.4.2 Subgrid snow depth variability

Snow depth *CV* (CV_{ds}) and σ_{ds} were consistently greater in the alpine versus subalpine at each of the varying grid resolutions (Figure 2.4). The mean CV_{ds} across the study grids was generally consistent with changes in grid resolution; however, the standard deviation of CV_{ds} decreased with increasing grid resolution and stabilized around a 500 m grid size. The mean σ_{ds} across the study grids tended to increase with increasing grid size for all study grids, but stabilized around 400 m for subalpine study grids only. The 500 m resolution study grids (n = 642) were chosen for analysis in this study (Figure 2.1) and is believed to be representative of the subgrid snow variability at the 1000 m resolution.

The median d_s, σ_{ds}, and CV_{ds} across all study grids (500 m resolution) was equal to 1.27 m, 0.88 m, and 0.74, respectively, and subgrid CV_{ds} ranged from 0.15 to 2.74 across the study area. The variability of CV_{ds} collected on 05 May 2010 (n = 219 study grids) and 20 May 2010 (n = 423 study grids) (Figure 2.1) was similar, with the 05 May grids exhibiting a slightly smaller CV_{ds} (median = 0.64) than the 20 May grids (median = 0.81). Statistically significant differences (p value < 0.001) between the alpine and subalpine study grids were observed for d_s, σ_{ds}, and CV_{ds} by the nonparametric Mann-Whitney test (Figure 2.5). The alpine study grids exhibited a greater mean and range of snow accumulation and variability than the subalpine study grids. The range of CV_{ds} from the 10^{th} to the 90^{th} percentiles within the alpine and subalpine study grids was equal to 0.61 to 1.57 and 0.30 to 0.98, respectively. Figure 2.6 highlights the abrupt change of subgrid snow depth variability characteristics observed in a transition from the subalpine to

alpine ecosystem; the forest structure and topography characteristics appear to exert a strong influence on subgrid CV_{ds} and these relations were investigated further.

2.4.3 Relation of subgrid snow depth variability with topography and forest characteristics

A statistically significant linear correlation (Pearson's r coefficient; p value < 0.05) between CV_{ds} and d_s was observed to be -0.60 and -0.45 for the alpine and subalpine study grids, respectively (Table 2.1). However, further evaluation showed this relation to be nonlinear and best described by a power function (Figure 2.7). This function suggests that CV_{ds} exhibits a systematic decrease with increasing d_s and suggests that relative subgrid snow variability is importantly related to the total snow accumulation of a given year. The power relation between CV_{ds} and d_s was greatly improved when split between alpine and subalpine study grids, as a CV_{ds} for a corresponding d_s tended to be greater for alpine versus subalpine study grids (Figure 2.7). The power functions (CV_{ds} versus d_s) were detrended (i.e. removing the influence d_s on CV_{ds}) and the residuals of the functions were compared to topography and forest characteristics (Table 2.2). The alpine study grids were most positively correlated with σ_{Sx} suggesting that the variability of wind exposure and sheltering and thus wind redistribution within a study grid is a strong control on CV_{ds}. The σ_S, σ_{TPI}, σ_z were also closely related to CV_{ds} in both alpine and subalpine areas highlighting the overall importance of topographic roughness on subgrid snow variability. The subalpine study grids were negatively correlated with the *VH*, *NDVI*, and *CD* variables and also positively correlated with the variability of these vegetation metrics (CV_{VH}, σ_{NDVI}, σ_{CD}), suggesting that forest structure is important driver of subalpine subgrid variability.

2.4.4 Statistical models

The multiple linear regression models developed for predicting CV_{ds} in both alpine and subalpine seasonal snowpacks are presented in Table 2.2. Variable transformations were

necessary to CV_{ds} and d_s in both models and to σ_{Sx} in the alpine model and *CD* in the subalpine model to account for the nonlinearity of these datasets (Table 2.2). Snow depth exhibited the greatest explanatory ability within both the alpine and subalpine models, with standardized regression coefficients equal to -0.92 and -0.95, respectively (not shown). Standardized regression coefficients of σ_{Sx} and *CD* were equal to 0.50 and -0.72 for the alpine and subalpine models, respectively, and both showed the second strongest explanatory power in their respective models. The alpine model had a NSE of 0.66 (0.65) and RMSE of 0.24 (0.24) while the subalpine model had an NSE of 0.79 (0.78) and RMSE of 0.12 (0.13) for the model calibration (10-fold cross-verification) dataset (Figure 2.8). A total NSE of 0.81 was calculated for the entire dataset based on predictions from both models. These performance statistics suggest that the models perform reasonably well predicting CV_{ds} and cross-verification suggests the model may be transferable to independent data within the bounds of the original dataset.

2.5 Discussion

Based on an evaluation of CV_{ds} at a 500 m grid resolution, subgrid snow variability across a mountainous subalpine and alpine study area is shown to exhibit a wide range of spatial variation and be well correlated with ecosystem type, snow amount, as well as topographic characteristics and forest structure. Alpine CV_{ds} was most correlated with mean snow depth and the variability of exposure to wind while mean snow depth and canopy height and density were most correlated with CV_{ds} in subalpine areas. A simple statistical model for both alpine and subalpine ecosystems was able to reasonably predict subgrid CV_{ds} based on these relations and could be used as a methodology for improving model parameterizations of subgrid snow variability in mountainous terrain.

The range of CV_{ds} observed over relatively small distances in this study (Figure 2.6) highlights the importance of further characterizing the spatial variability of this parameter within mountainous terrain. The global classification of CV_{SWE} defined by *Liston* [2004] performed well predicting the average conditions observed in this study. *Liston* [2004] define the CV_{SWE} of mid-latitude mountainous forest (i.e. subalpine) as 0.60 and of mid-latitude treeless mountains (i.e. alpine) as 0.85, whereas this study found a median CV_{ds} of 0.55 for subalpine study grids and 1.05 for alpine study grids. However, the global classification was unable to adequately represent the range and variability of CV_{ds} across the study area (Figure 2.5c), and the results presented herein suggests promise for an improved parameterization of CV_{ds} in mountainous terrain.

Mean snow depth was well correlated with CV_{ds} variability across alpine and subalpine areas within the study area. As subgrid d_s increased, the CV_{ds} decreased, which is a result that is consistent with previous studies at various spatial scales [e.g., *Fassnacht and Deems*, 2006; *Fassnacht and Hultstrand*, 2015; *López-Moreno et al.*, 2015]. A positive correlation was observed between σ_{ds} and d_s in alpine and subalpine areas, which had a dampening effect on this overall negative correlation between the relative subgrid variability (CV_{ds}) with d_s. The relative subgrid variability of d_s likely decreases with increasing snow accumulation because of the consistent size of the roughness elements of topography and canopy that drive snow variability; as d_s increases, the relative influence of these topography and canopy features tends to decrease [e.g., *Fassnacht and Deems*, 2006; *López-Moreno et al.*, 2011; *López-Moreno et al.*, 2015]. The range of CV_{ds} observed in this study (Figure 2.5) is similar to previous studies conducted in mountainous mid-latitude forested and alpine areas [refer to Figure 2 from *Clark et al.*, 2011 and references therein]. Future research could further investigate CV_{ds} and d_s across different geographic regions and snow regimes as well as across multiple snow seasons and compare

results to the functions presented in Figure 2.7 to better understand the dynamics and consistency of this relation. An understanding of how the subgrid variability of snow depth for a given set of topography and canopy elements scales between low and high snow years could be particularly important.

Within the alpine study grids, the variability of the exposure/sheltering from wind (σ_{Sx}) was an important driver of CV_{ds}. Study grids with the greatest σ_{Sx} were generally positioned over large breaks in topography. For example, a given study grid with a large σ_{Sx} likely contained areas with both wind exposure ($Sx < 0°$) where snow accumulation is scoured by wind and sheltering from wind ($Sx > 0°$) where preferential deposition of wind transported snow occurs. Study grids with a consistent *Sx* showed a lower CV_{ds} with greater variability observed in sheltered grids than in exposed grids. *Winstral et al*. [2002] and many subsequent studies [e.g., *Erickson et al.*, 2005; *Molotch et al.*, 2005; *Revuelto et al.*, 2014; *McGrath et al.*, 2015] have highlighted this control of wind exposure on snow depth distribution in tree-less areas. The degree of importance of σ_{Sx} for describing CV_{ds} is likely variable from year-to-year, and would be expected to be well correlated with observed wind speeds [*Winstral and Marks*, 2014]. However, in alpine areas where high wind speeds are ubiquitous, σ_{Sx} is expected to be a consistently important driver of subgrid snow variability.

Subgrid snow variability within subalpine study grids was well correlated with the *VH*, *NDVI*, and *CD* vegetation metrics. As mean study grid *VH*, *NDVI*, and *CD* increased, CV_{ds} tended to decrease, but was also shown to be positively correlated with the variability of these metrics (CV_{VH}, σ_{NDVI}, σ_{CD}). Forest structure has been shown by various studies to exert a strong influence on snow variability because of a variety of physical process interactions. Interception of snow [e.g., *Hedstrom and Pomeroy*, 1998] and subsequent canopy sublimation [e.g., *Montesi*

et al., 2004; *Molotch et al.*, 2007], influences of trees on shortwave [e.g., *Ellis and Pomeroy*, 2007; *Musselman et al.*, 2012] and longwave [e.g., *Pomeroy et al.*, 2009] radiation dynamics, and the effect of trees on wind redistribution of snow [e.g., *Hiemstra et al.*, 2006] can each drive snow accumulation and evolution in forested areas. *Broxton et al.* [2015] utilized lidar-derived snow depth datasets and showed that the variability of snow depth in subalpine forests tended to be greatest beneath the forest canopy and near the forest canopy edge and the least snow depth variability occurred in forested openings that were distant from the forest edge. Also, substantial differences in accumulated d_s were observed between subcanopy areas and forest openings. The increased CV_{ds} with decreasing *VH*, *NDVI*, and *CD* observed in this study can be explained by a greater occurrence of transitional areas between subcanopy areas and forest openings (i.e., forest edges) occurring in study grids with smaller mean *VH* and *CD*. Across the study area, subalpine forest openings that spanned an entire study grid were not present; therefore, study grids with consistent forest cover tended to exhibit the least subgrid snow variability.

This study was limited by the spatial and temporal coverage of the lidar-derived snow datasets that were used (Figure 2.1). Although the alpine and subalpine areas evaluated are representative of mountainous terrain in the region and snowpacks in this area are representative of the continental snow regime [*Trujillo and Molotch*, 2014], further analysis of subgrid snow variability across a greater geographic area and across other regions with differing snow regimes could improve the applicability of a CV_{ds} parameterization for snow distributions in mountainous areas in general. Additionally, spatial patterns of snow variability have been shown to be temporally consistent from year-to-year [e.g., *Erickson et al.*, 2005; *Deems et al.*, 2008; *Sturm and Wagner*, 2010], but future studies with multiple years of lidar collection could help understand the inter-annual variability of CV_{ds} and the consistency of its driving variables [e.g.,

Fassnacht et al., 2012]. Of particular interest would be the temporal consistency of the relation between CV_{ds} and d_s.

This study evaluates the subgrid variability of d_s, but *SWE* is the most fundamental snowpack variable of interest in land surface processes [e.g., *Sturm et al.*, 2010]. Snow depth and *SWE* have been shown by many studies to be well correlated [e.g., *Jonas et al.*, 2009; *Sturm et al.*, 2010; *Sexstone and Fassnacht*, 2014], and the subgrid *CV* of these variables is expected to exhibit similar characteristics [e.g., *Fassnacht and Hultstrand*, 2015]. We suggest that a parameterization of CV_{ds} could be sufficient for representing subgrid *SWE* variability, but further investigation into this hypothesis is needed. In order to directly investigate CV_{SWE} from lidar-derived snow data in future studies, an estimation of snow density would be needed. Statistically-derived snow density models have been successfully developed over varying domain sizes for estimating *SWE* from d_s [e.g., *Jonas et al.*, 2009; *Sturm et al.*, 2010; *Sexstone and Fassnacht*, 2014], and these models make use of the fact that *SWE* and d_s variability is much greater than the variability of snow density [e.g., *Mizukami and Perica*, 2008; *Lopez-Moreno et al.*, 2013].

The snow distributions and variability characteristics evaluated in this study were likely somewhat influenced by the occurrence of snowmelt conditions within the study area. Although substantial snowmelt had not occurred prior to data collection within the study grids (Figure 2.2), the mid-season melt events and onset of snowmelt may have caused an increase in CV_{ds} (Figure 2.3) and this effect may have differed between the two dates of lidar-derived d_s. *López-Moreno et al.* [2015] observed a sharp increase in CV_{ds} just following the onset of snowmelt yet a fairly consistent CV_{ds} for the remainder of snowmelt season. Future studies evaluating subgrid snow variability should investigate the intra-annual variability CV_{ds} to further understand the seasonal evolution of this parameter.

The development of high resolution snow depth mapping from lidar has provided a unique ability for detailed snapshot views of the spatial distribution of snow in complex mountains areas. Although some key advantages of these datasets are related to validating satellite-based remote sensing products and direct use within water resources forecasting, this study also suggests that lidar-derived snow datasets can be an important tool for the improvement of snow representations within modeling applications. Future research should utilize lidar-derived snow datasets to directly evaluate the ability of physically-based models to represent snow distributions as well as to continue to improve the representation of subgrid variability of snow. Additionally, other key snow modeling questions such as how representative snow monitoring stations are of surrounding areas [e.g., *Molotch and Bales*, 2005; *Meromy et al.*, 2013] could also be investigated further by lidar-derived snow datasets. Lastly, the analyses that have been developed in this study may also be useful in future studies for characterizing the subgrid variability of other variables that can be measured remotely at a fine scale through lidar or other techniques.

2.6 Conclusions

This study outlines a methodology for utilizing lidar-derived snow datasets for investigating subgrid snow depth (d_s) variability and potentially improving its representation within physically-based modeling applications. At fine grid resolutions, subgrid snow depth coefficient of variation (CV_{ds}) generally increased and its variability decreased with increasing grid resolution, while study grid CV_{ds} characteristics were similar among a range of coarser resolutions (from 500 m to 1000 m). Study grids (500 m resolution) exhibited a wide range of CV_{ds} across the study area (0.15 to 2.74) and subgrid d_s variability was found to be greater in alpine areas than subalpine areas. Snow depth was the most important driver of CV_{ds} variability

in both alpine and subalpine areas and a systematic nonlinear decrease in CV_{ds} with increasing d_s was observed; the negative correlation between CV_{ds} and d_s is attributed to the static size of roughness elements (topography and canopy) that strongly influence seasonal snow variability. The variability of wind exposure in alpine areas as well as vegetation metrics in subalpine areas were also found to be important drivers of study grid CV_{ds}. Two simple statistical models were developed (alpine and subalpine) for predicting subgrid CV_{ds} from mean d_s and topography/canopy features that show reasonable performance statistics and suggest this methodology can be used for parameterizing CV_{ds} in snow-dominated mountainous areas. This research highlights the utility of using lidar-derived snow datasets for improving model representations of subgrid snow variability.

Table 2.1. Bivariate correlations (Pearson's *r* coefficient) between snow depth coefficient of variation (CV_{ds}) and the mean and standard deviation (σ) of snow depth (d_s), vegetation height (*VH*) and coefficient of variation of vegetation height (CV_{VH}), Normalized Difference Vegetation Index (*NDVI*), canopy density (*CD*), elevation (*z*), slope (*S*), winter clear-sky incoming solar radiation ($Q_{sw\downarrow}$), maximum upwind slope (*Sx*), and topographic position index (*TPI*) for both alpine and subalpine study grids. Correlations are also shown for the residuals from the detrended nonlinear relation of CVd_s and d_s. Bold values represent statistical significance (*p* value < 0.05).

	CV_{ds} *(alpine)*	CV_{ds} *(subalpine)*	CV_{ds} (alpine) d_s residuals	CV_{ds} (subalpine) d_s residuals
d_s	**-0.60**	**-0.45**	**---**	**---**
σ_{ds}	-0.06	**0.25**	**---**	**---**
VH	**-0.38**	**-0.48**	**-0.28**	**-0.71**
σ_{VH}	**-0.38**	**-0.57**	**-0.24**	**-0.59**
CV_{VH}	**0.16**	**0.28**	-0.08	**0.61**
NDVI	**0.2**	-0.10	**-0.13**	**-0.42**
σ_{NDVI}	**-0.12**	**0.25**	-0.01	**0.55**
CD	-0.06	**-0.32**	**-0.21**	**-0.64**
σ_{CD}	-0.06	**0.30**	**-0.26**	**0.50**
z	**0.17**	**-0.22**	**0.32**	**0.18**
σ_z	-0.07	0.09	**0.16**	**0.29**
S	-0.03	0.06	**0.25**	**0.28**
σ_S	-0.06	0.13	**0.37**	**0.38**
$Q_{sw\downarrow}$	0.10	-0.02	-0.07	**-0.17**
$\sigma_{Qsw\downarrow}$	-0.07	-0.03	**0.21**	**0.21**
Sx	0.02	0.08	**0.29**	0.09
σ_{Sx}	0.07	0.10	**0.43**	**0.28**
TPI	**0.28**	**0.11**	**0.15**	0.04
σ_{TPI}	-0.09	0.09	**0.29**	**0.33**

Table 2.2. Multiple linear regression equation variables and coefficients of the alpine and subalpine CV_{ds} models. The multiple linear regression is of the form: $y = \beta_0 + \beta_1 x_1 + \beta_2 x_2 + ... + \beta_n x_n$ where y is the dependent variable, x_1 through x_n are n independent variables, β_0 is the regression intercept, and β_1 through β_n are n regression coefficients. Units of the model variabiles area as following: snow depth (m), maximum upwind slope (°), clear-sky solar radiation (W m^{-2}), canopy density (%), surface slope (°).

	Alpine model	Subalpine model
Y	$\log(CV_{ds})$	$CV_{ds}^{0.5}$
β_0	9.00E-03	8.45E-01
β_1	-1.02E+00	-2.84E-01
x_1	$d_s^{0.5}$	$\log(d_s)$
β_2	1.00E-02	-9.79E-05
x_2	Sx	CD^2
β_3	3.42E-01	1.12E-02
x_3	$\log(\sigma_{Sx})$	σ_S
β_4	1.84E-03	---
x_4	$Q_{SW\downarrow}$	---

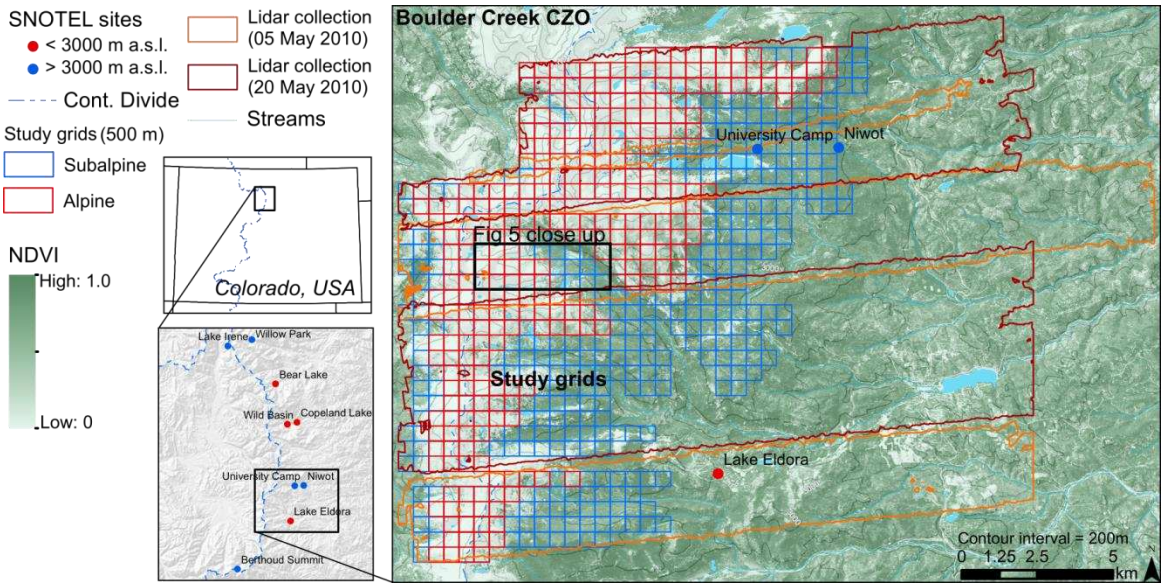

Figure 2.1. Map of the Boulder Creek CZO study area located within the Front Range Mountains of northern Colorado, USA. NRCS SNOTEL sites in the region are shown in blue (sites greater than 3000 m elevation) and red (sites less than 3000 m elevation). The extent of the snow-covered lidar collection on 05 May 2010 (20 May 2010) is shown in orange (dark red). The 500 m resolution study grids (n = 650) are shown in blue (subalpine) and red (alpine). The black rectangle highlights the area of close up shown in Figure 2.6.

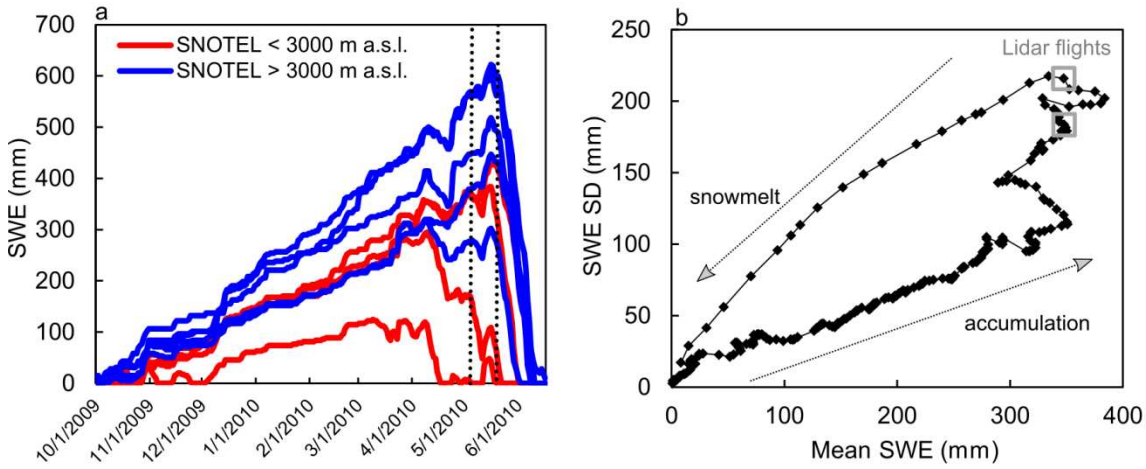

Figure 2.2. Snow water equivalent (*SWE*) data from nine NRCS SNOTEL sites within the region of the study area displayed as (a) niveographs showing snow accumulation and snowmelt throughout water year 2010 with the timing of 05 May 2010 and 20 May 2010 lidar flights plotted as vertical dashed lines and (b) a scatter plot of the standard deviation of SWE versus mean SWE from the SNOTEL sites highlighting the hysteretic dynamics of snow accumulation and snowmelt across the region based on nine SNOTEL stations [*Egli and Jonas*, 2009].

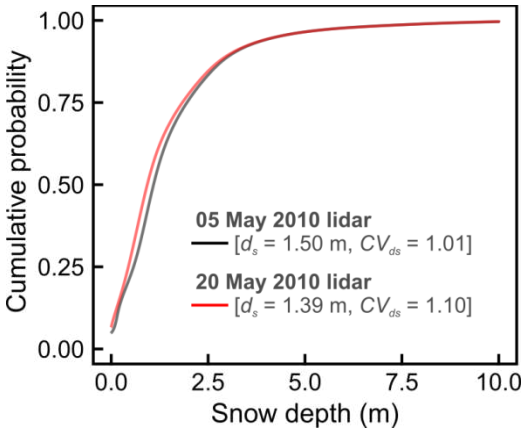

Figure 2.3. Statistical distributions of lidar-derived snow depth for the overlapping area (7.92 km^2) of the 05 May 2010 and 20 May 2010 lidar flights.

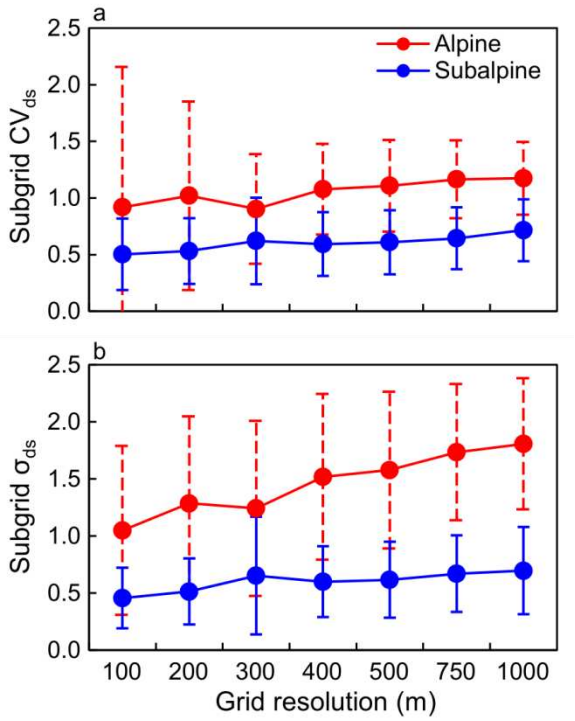

Figure 2.4. Mean subgrid (a) CV_{ds} and (b) σ_{ds} across the study area plotted versus study grid resolution for alpine (red) and subalpine (blue) study grids. Error bars represent the standard deviation of CV_{ds} and σ_{ds} across the study area.

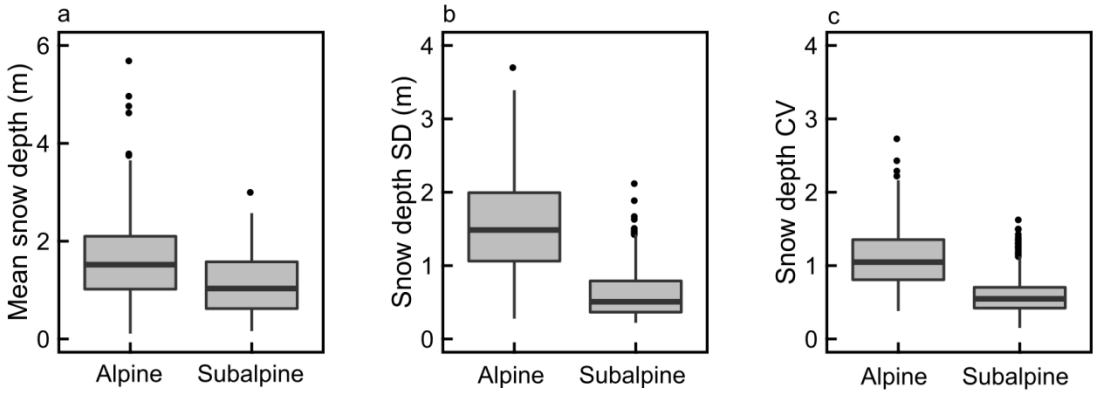

Figure 2.5. Boxplots showing the outliers (black circles), 10th and 90th percentiles (whiskers), 25th and 75th percentiles (box) and median (black horizontal line) for the (a) d_s, (b) σ_{ds}, and (c) CV_{ds} of the alpine and subalpine study grids (500 m resolution).

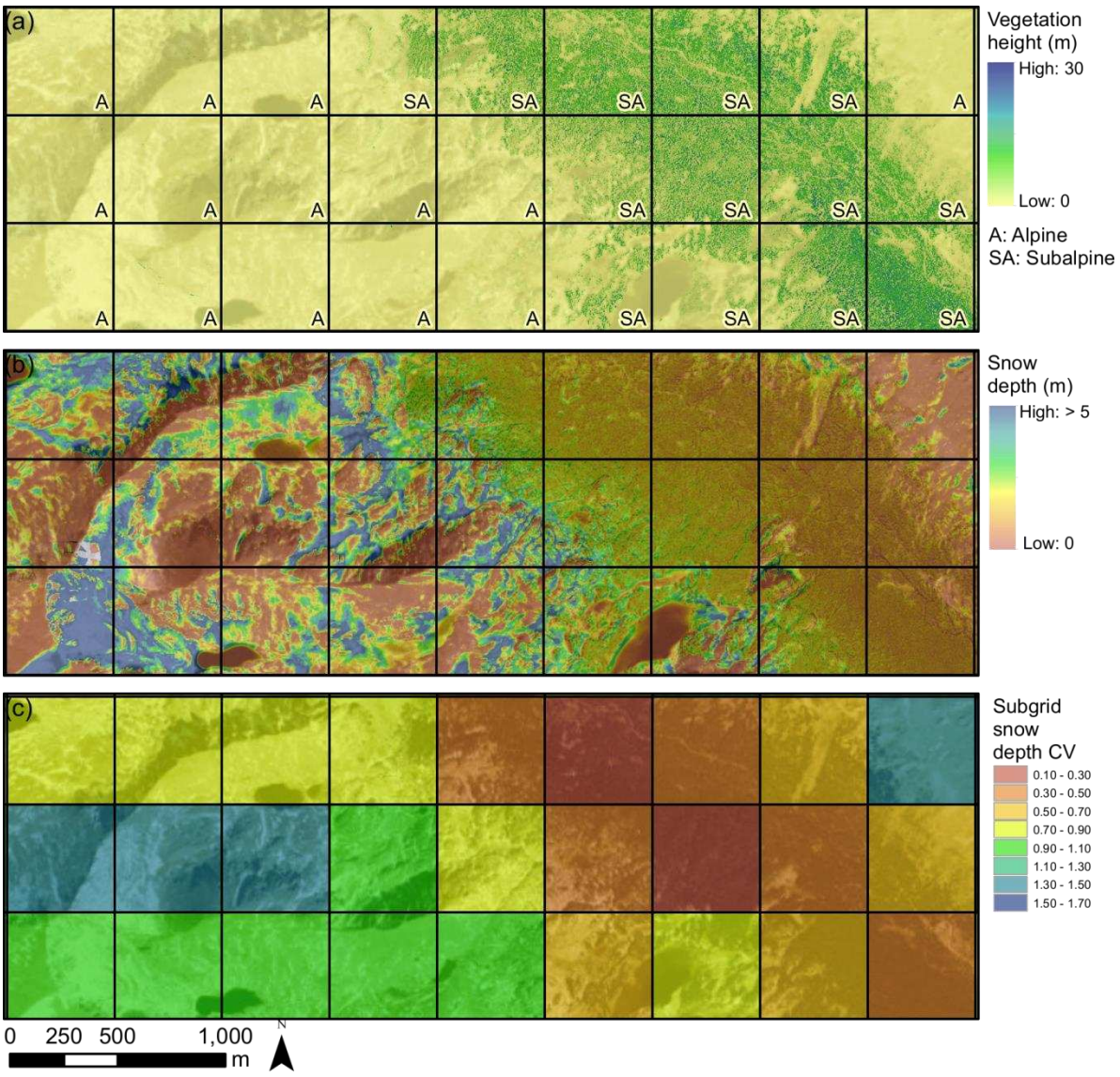

Figure 2.6. Close up map of selected study grids showing the distribution of (a) vegetation height and ecosystem type, (b) snow depth, and (c) subgrid CV_{ds} value. Area of close up is highlighted in Figure 2.1.

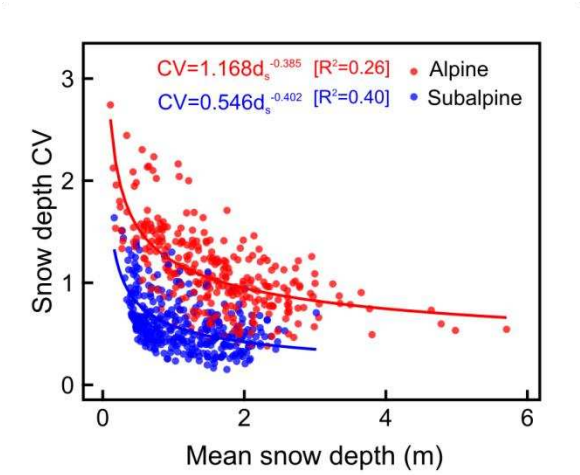

Figure 2.7. Nonlinear relation of CV_{ds} and d_s for alpine (red) and subalpine (blue) study grids (500 m resolution).

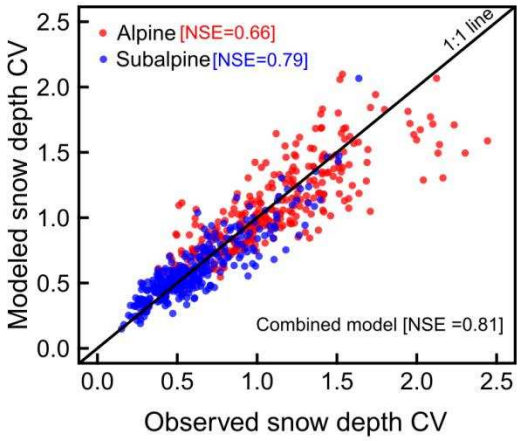

Figure 2.8. Modeled versus observed CV_{ds} for the alpine (red) and subalpine (blue) multiple linear regression models.

CHAPTER 3 – COMPARISON OF METHODS FOR QUANTIFYING SURFACE SUBLIMATION OVER SEASONALLY SNOW-COVERED TERRAIN[2]

3.1 Summary

Snow sublimation can be an important component of the snow-cover mass balance, and there is considerable interest in quantifying the role of this process within the water and energy balance of snow-covered regions. In recent years, robust eddy covariance (EC) instrumentation has been used to quantify snow sublimation over snow-covered surfaces in complex mountainous terrain. However, EC can be challenging for monitoring turbulent fluxes in snow-covered environments because of intensive data, power, and fetch requirements, and alternative methods of estimating snow sublimation are often relied upon. To evaluate the relative merits of methods for quantifying surface sublimation, fluxes calculated by the EC, Bowen ratio-energy balance (BR), bulk aerodynamic flux (BF), and aerodynamic profile (AP) methods and their associated uncertainty were compared at two forested openings in the Colorado Rocky Mountains. Biases between methods are evaluated over a range of environmental conditions and limitations of each method are discussed. Mean surface sublimation rates from both sites ranged from 0.33 to 0.36 mm day^{-1}, 0.14 to 0.37 mm day^{-1}, 0.10 to 0.17 mm day^{-1}, 0.03 to 0.10 mm day^{-1} for the EC, BR, BF, and AP methods, respectively. The EC and/or BF methods are concluded to be superior for estimating surface sublimation in snow-covered forested openings. The surface sublimation rates quantified in this study are generally smaller in magnitude compared to previously published studies in this region and help to refine sublimation estimates for forested openings in the Colorado Rocky Mountains.

[2] Chapter 3 has been published in early view of *Hydrological Processes* [doi:10.1002/hyp.10864] and is *in press*. Additional authors are D.W. Clow, D.I. Stannard, and S.R. Fassnacht.

3.2 Introduction

Snow sublimation is defined as the transfer of water directly between snow and the atmosphere through phase change. There is considerable interest in quantifying the seasonal amount of snow water equivalent (SWE) loss from snow sublimation and understanding how the equivalent energy flux (i.e. turbulent flux of latent heat) influences snowmelt dynamics [e.g., *Marks and Dozier*, 1992; *Cline*, 1997a; *Burns et al.*, 2014] because this process can represent an important component of the snow-cover mass balance [e.g., *Lang*, 1981; *Strasser et al.*, 2008; *MacDonald et al.*, 2010]. Turbulent fluxes of latent and sensible heat are particularly challenging to measure and model over a snowpack because the cold and smooth surface leads to a stable atmospheric surface layer and low levels of atmospheric turbulence [*Pomeroy et al.*, 1998]. Additionally, the spatial variability of snow sublimation in mountainous environments [e.g., *Strasser et al.*, 2008] is dependent on the spatial variability of the surface [e.g., *Hood et al.*, 1999], canopy [e.g., *Molotch et al.*, 2007], and blowing snow [e.g., *Pomeroy and Essery*, 1999] components of snow sublimation. Therefore, determining the importance of snow sublimation at the basin scale through measurements and modeling can be difficult [*Strasser et al.*, 2008; *Knowles et al.*, 2015b; *Svoma*, 2016].

A wide range of snow sublimation rates have been reported in the literature for both non-forested and forested seasonal snow covers [see Table VI from *Jackson and Prowse*, 2009]. Surface sublimation losses from the Colorado Rocky Mountains have been reported to account for about 15 percent of maximum snow accumulation [*Hood et al.*, 1999], and from about 1 to 4 percent of total ablation during the snowmelt period at an exposed alpine site [*Cline*, 1997a]. Additionally, simulation at a sheltered site beneath the forest canopy in this region showed surface sublimation accounting for a loss of about 6.5 percent of snow mass [*Marks et al.*, 2008],

whereas measurements of canopy sublimation from intercepted snow indicate canopy sublimation may account for as much as 30 to 68 percent of precipitation [*Montesi et al.,* 2004; *Molotch et al.,* 2007]. Surface sublimation from forested openings in the Colorado Rocky Mountains has not commonly been evaluated, but *Meiman and Grant* [1974] have estimated surface sublimation from a forested opening as 45 percent of winter precipitation. Automated snowpack and meteorological monitoring stations are most often sited in forested openings and improving measurement techniques of surface sublimation from these sites could provide insight into the hydrologic importance of surface sublimation from these environments. A better understanding of the hydrologic importance of surface sublimation from forested openings is increasingly important because of recent forest disturbances from wildfire and mountain pine beetle in this region [*Westerling et al.,* 2006; USDA Forest Service, 2011]. Previous research has often shown that snow accumulation will increase with decreasing canopy cover in a post-disturbance landscape because of decreased canopy interception and sublimation [e.g., *Boon,* 2012; *Pugh and Small,* 2012]. However, recent studies have shown that increased surface sublimation in forest-disturbance openings can compensate for decreased interception resulting in no difference in peak SWE [*Biederman et al.,* 2014] or even result in a decrease of peak SWE in open areas compared to subcanopy areas [*Harpold et al.,* 2014a].

Snow sublimation rates have been obtained using gravimetric methods [e.g., *Dewalle and Meiman,* 1971; *Schmidt et al.,* 1998; *Jackson and Prowse,* 2009; *Zhou et al.,* 2012], various formulations of either the bulk aerodynamic flux (BF) [e.g., *Marks and Dozier,* 1992; *Andreas,* 2002; *Arck and Scherer,* 2002; *Fassnacht,* 2004; *Andreas et al.,* 2010; *Reba et al.,* 2012] or aerodynamic profile (AP) methods [e.g., *Cline,* 1997a; *Hood et al.,* 1999; *Box and Steffen,* 2001; *Zhang et al.,* 2008], and more recently the eddy covariance (EC) method [e.g., *Pomeroy and*

Essery, 1999; *Arck and Scherer*, 2002; *Lee and Mahrt*, 2004; *Molotch et al.*, 2007; *Marks et al.*, 2008; *Reba et al.*, 2009; *Helgason and Pomeroy*, 2012b; *Knowles et al.*, 2012]. Although the Bowen ratio-energy balance (BR) method has commonly been used for calculating evapotranspiration [e.g., *Blad and Rosenberg*, 1974; *Brotzge and Crawford*, 2003; *Drexler et al.*, 2004], this method has seldom been used over a snow-covered surface for estimating snow sublimation. Eddy covariance is often considered the most direct and reliable method for measuring turbulent energy fluxes [e.g., *Arya*, 1988; *Kaimal and Finnigan*, 1994], and is becoming more commonly used in complex alpine and forested mountainous terrain [e.g., *Pomeroy et al.*, 2003; *Turnipseed et al.*, 2003; *Molotch et al.*, 2007; *Hiller et al.*, 2008; *Blanken et al.*, 2009; *Mott et al.*, 2011; *Helgason and Pomeroy*, 2012a; *Knowles et al.*, 2015a]. However, the EC method can be challenging for monitoring turbulent energy fluxes in snow-covered environments because of its intensive data, power, and fetch requirements. For this reason, there is often a need to rely on alternative methods for providing estimates of snow sublimation in complex mountainous terrain.

In this study, a field experiment is conducted to simultaneously evaluate the BF, AP, EC, and BR methods for quantifying surface sublimation at two sites within forested openings through three winters in the Colorado Rocky Mountains. Gravimetric estimates of surface sublimation could not be made because precipitation was not directly measured at each site and because of challenges related to wind redistribution of snow [*Meyer et al.*, 2012]. The objectives of this research were to (1) evaluate the strengths and weaknesses of each method for determining surface sublimation, (2) determine which method may provide the best performance for estimating surface sublimation within a range of environmental conditions, and (3) quantify a range of surface sublimation estimates from the two sites.

3.3 Methods

3.3.1 Study area

This research was conducted in the upper Colorado River Basin, Colorado, located in the western United States (Figure 3.1). Measurements were made upstream from Granby, Colorado, in an area characterized by terrain varying from the relatively low relief around the Fraser River valley to the steep complex terrain of the Colorado Front Range Mountains along the Continental Divide. Approximately 28 percent of the study area (Figure 3.1) is located above treeline, 35 percent is classified as forested area, 21 percent is classified as open areas below treeline (i.e forested openings), and 16 percent is developed (land cover and canopy density information accessed at <http://www.mrlc.gov/nlcd2011.php>). Measurements were collected at two micrometeorological stations, the Cabin site and the Arrow site, which are located at elevations of 2810 m and 2955 m, respectively (Figure 3.1). The Cabin site is located in a small clearing (approximately 100 m in diameter) surrounded by sparse lodgepole pine (*Pinus contorta*) forest with a canopy density of about 35 percent. The Cabin site is positioned approximately 60 m from the forest edge, and the mean slope of the clearing is 8 percent. The Arrow site is located on moderately sloping terrain with an aspect and predominant upslope wind direction of 290 degrees. Wind directions at the Arrow site were measured as upslope between 260 and 340 degrees (52 percent of all measured wind) during the day and downslope between 70 and 150 degrees (29 percent of all measured wind) at night. The site is characterized by an open upwind fetch of approximately 500 m and a mean slope of 20 percent (Figure 3.1, Figure 3.2). Both micrometeorological sites were operated during the snow-covered period (i.e. period of time with snow cover on ground at each site often lasting from November through May) of water years (i.e.

period beginning 1 October and ending 30 September of the given year) 2013 and 2014. The Arrow site was also operated during water year 2015.

3.3.2 Study instrumentation

The instrumentation setup at the Arrow and Cabin sites, measurements collected as part of this field experiment, and measurement uncertainties are summarized in Table 3.1. Photographs of the site instrumentation are shown in Figure 3.2. Air temperature (T) and relative humidity (RH) were measured by aspirated sensors at approximately 0.1 m and 1.1 m above the snow surface (Figure 3.2d), and vapor pressure (e) was calculated at both heights from T and RH. The aspirated sensors were raised or lowered every 1 to 2 weeks to maintain constant heights above the snowpack. Additionally, any biases between the upper and lower sensor measurements were removed by automatically exchanging the vertical position of the two sets of sensors every 15 minutes and averaging the measurements over a 30-minute interval [*Tanner*, 1960]. Wind speed (u), net radiation (Q^*), snow surface temperature (T_{srf}), and snow depth (d_s) were all measured from sensors located at a height of 3 m above the soil surface that were statically affixed to a tripod. The profile of snow temperature was measured every 0.1 m along a vertical array of 24 gauge (0.511 mm diameter) type-E thermocouple wires distributed through the entire depth of the snowpack (from 0 m to 2.0 m above the soil surface) (Figure 3.2c). Horizontal and vertical wind speed and direction, sonic temperature, and atmospheric water vapor density were measured at the Arrow site with a fast response (10 Hz) 3-dimensional sonic anemometer and infrared gas analyzer (EC instrumentation). These sensors were raised or lowered every 1 – 2 weeks to maintain a height of 1.5 m above the snow surface throughout the measurement period. The heights of all sensors above the snow surface were calculated using the snow depth sensor

throughout the measurement period. Manual snow density measurements were collected every 2 to 4 weeks at both sites (see Appendix A).

3.3.3 Snow-cover energy balance

The snow-cover energy balance can be expressed as

$$dU\ dt^{-1} = Q^* + Q_G + Q_A - Q_E - Q_H \quad (3.1)$$

where $dU\ dt^{-1}$ is the net rate change of internal energy within the snowpack, Q^* is net radiation, Q_G is ground heat flux, Q_A is advective energy flux (i.e. energy from precipitation onto the snowpack), and Q_E and Q_H are the turbulent fluxes of latent and sensible heat, respectively. Here the turbulent flux terms Q_E and Q_H are positive when the flux is directed from the snowpack to the atmosphere, while all other energy terms are positive when directed into the snowpack. Snowpack sublimation is represented within the snow-cover energy balance by Q_E and is calculated by dividing Q_E by the latent heat of sublimation (L_s), which is determined as a function of the temperature of the snow surface [*Oke*, 1987]. Sublimation losses away from the snowpack are represented by positive values in this study, and sublimation gains (water vapor depositing on the snow directly as ice) are represented by negative values and hereinafter referred to as deposition.

3.3.4 Available energy for turbulent flux

The non-turbulent flux terms of the snow-cover energy balance in Eq. 3.1 were measured in this study to (1) evaluate the energy balance closure (i.e. the degree to which the sum of the turbulent fluxes are equal to all other energy sinks and sources) of EC turbulent flux measurements [*Wilson et al.*, 2002] and (2) calculate turbulent fluxes of latent heat using the BR method. The measured available energy for turbulent flux over these snow-covered sites can be expressed as $Q^* - dU\ dt^{-1}$. Ground heat flux (Q_G) below deep Colorado snowpacks is negligible

[*Cline*, 1997a] and was not considered in this study. Additionally, the advection term (Q_A) could not be considered because precipitation was not directly measured in this study. There was no rainfall onto the snowpack during the snow-accumulation periods and the advection energy from snowfall was not considered to be an important energy flux to the snowpack.

The rate of snowpack internal energy change is dependent on internal latent heat fluxes (melting and refreezing) and sensible heat fluxes (warming and cooling) within the snowpack. Prior to the snowmelt period, when the snowpack is cold with negligible liquid water content, $dU\ dt^{-1}$ can be calculated as the change with time of the snowpack cold content (the energy required to bring the snowpack to an isothermal temperature of 0.0°C):

$$dU\ dt^{-1} = \int_{z=0}^{d_s} \left[\frac{d}{dt} \left(\rho_s(z) c_i T_S(z) \right) \right] dz \tag{3.2}$$

where z is the height above the soil surface, d_s is the snow depth, ρ_s is the snow density, c_i is the specific heat of ice, and T_S is the snowpack temperature. See the Appendix A for details on the calculation of $dU\ dt^{-1}$. *Helgason and Pomeroy* [2012b] estimated the uncertainty in $dU\ dt^{-1}$ as ±10 to 15 percent. This study estimates the uncertainty in $dU\ dt^{-1}$ to be ±15 percent.

3.3.5 Aerodynamic formulation turbulent flux calculations

The BF method uses measurements of barometric pressure, wind speed, air temperature, and relative humidity at any height, and snow surface temperature, to calculate latent heat flux ($Q_{E\text{-}BF}$):

$$Q_{E-BF} = \rho L_s C_E u_r (q_s - q_r) \tag{3.3}$$

where ρ is air density, C_E is the transfer coefficient for latent heat, u_r is the wind speed at reference height, and q_s and q_r are the specific humidity at the snow surface and reference height, respectively. Specific humidity is calculated based on vapor pressure and atmospheric pressure and the specific humidity at the snow surface is calculated based on saturation vapor pressure of

the snow surface. The transfer coefficient for latent heat (C_E) (see the Appendix A) is computed based on the roughness lengths for wind speed (z_0) and humidity (z_q) and the atmospheric stability parameter (ζ):

$$\zeta = \frac{-kzgQ_H}{\rho c_p T u^{*3}} \tag{3.4}$$

where k is von Karman's constant (0.41), z is the measurement height, g is acceleration due to gravity (9.81 m s^{-2}), c_p is the specific heat of dry air, T is air temperature, and u^* is the friction velocity. Positive (negative) values of ζ represent stable (unstable) atmospheric conditions and values close to zero represent neutral conditions. *Andreas et al.* [2010] developed a BF method algorithm that was used in this study. The parameterization of the roughness lengths used by this algorithm were developed from EC measurements made over the Arctic Ocean during the winter period when sea ice was compact and snow covered (see *Andreas et al.* [2010], for specifics of the algorithm).

An iterative procedure of the AP method adapted from *Arya* [1988] was developed for calculating the latent heat flux ($Q_{E\text{-}AP}$) from measurements of ΔT and Δq as well as wind speed (u) at any height:

$$Q_{E-AP} = -\rho L_s C_E \Delta u \Delta q \tag{3.5}$$

where Δu is the wind speed gradient between measurements heights, and Δq is the specific humidity gradient between measurements heights (see the Appendix A for details on these iterative calculations). Although measurements of ΔT and Δq made in this study are vertical differences between values at two measurement heights (i.e. approximations of gradients), they are hereinafter referred to as gradients.

The greatest uncertainty associated with latent heat fluxes calculated by the aerodynamic (BF and AP) methods is from the transfer coefficient for latent heat (C_E). The uncertainty in C_E

has been estimated to be ±20 percent in neutral and unstable conditions [*DeCosmo et al.*, 1996; *Andreas et al.*, 2005] and suggested to have greater uncertainty in stable conditions [*Andreas*, 2002; *Grachev et al.*, 2007]. Given that stable atmospheric conditions are often observed over snow-covered surfaces, this study estimates the uncertainty in C_E to be ±40 percent.

3.3.6 Eddy covariance turbulent flux calculations

The latent ($Q_{E\text{-}EC}$) and sensible ($Q_{H\text{-}EC}$) heat fluxes as calculated by the EC method are

$$Q_{E-EC} = \rho L_s \overline{w'q'} \tag{3.6a}$$

$$Q_{H-EC} = \rho c_p \overline{w'T'} \tag{3.6b}$$

where w is the vertical wind speed and overbars denote mean values and primes denote deviations from the mean. *Reba et al.* [2009] provides a detailed overview of the theory and data processing steps for collection of EC data over snow. The raw 10 Hz data collected in this study were corrected and post processed using the LI-COR EddyPro software (available online at <http://www.licor.com>) to account for systematic errors. Sonic temperature data were corrected for humidity and momentum fluctuations [*Schotanus et al.*, 1983], the covariance between water vapor density and vertical wind speed was corrected for air density [*Webb et al.*, 1980], and the double rotation scheme was used to adjust preferential vertical motion in mean vertical wind velocity [*Kaimal and Finnigan*, 1994]. The statistical-screening analysis described by *Vickers and Mahrt* [1997] was followed. Wind direction was not filtered [e.g., *Stannard et al.*, 1994; *Moreo et al.*, 2007], as downsloping winds often occurred from behind the sensor supports. Finally, the quality check described by *Mauder and Foken* [2004] was used to test for the assumptions of steady state and fully developed turbulence. Fluxes rated as low quality [*Mauder and Foken*, 2004] because of under-developed turbulence or non-stationarity in the data were flagged as faulty, while fluxes deemed as moderate to high quality [*Mauder and Foken*, 2004]

were considered valid (Table 3.3). All covariances and thus turbulent fluxes were calculated using a 10-minute interval and subsequently averaged over a 1-hour interval to reduce sampling errors [*Vickers and Mahrt*, 1997]. The flux footprint was calculated to quantify the upwind distance over the snow surface contributing to the EC fluxes using the method developed by *Schuepp et al.* [1990].

Although rigorous and well documented data screening techniques and corrections are applied to EC measurements [*Reba et al.*, 2009], these measurements tend to have a high degree of scatter and uncertainty. Uncertainty in turbulent fluxes of latent and sensible heat measured by the EC method over snow have been estimated on the order of ±10 percent [*Knowles et al.*, 2015b] to ±20 percent [*Andreas et al.*, 2010]. This study estimates the uncertainty in both $Q_{E\text{-}EC}$ and $Q_{H\text{-}EC}$ to be ±20 percent.

3.3.7 Bowen ratio-energy balance method turbulent flux calculations

The Bowen ratio (β) is defined as the ratio of sensible heat flux and latent heat flux and is commonly expressed as the ratio of vertical gradients of temperature and specific humidity [*Bowen*, 1926]. The Bowen ratio is calculated as

$$\beta = \frac{c_p K_h \Delta T}{L_s K_v \Delta q} = \frac{Q_H}{Q_E} \tag{3.7}$$

where ΔT is the air temperature gradient between measurements heights and K_h and K_v are the eddy diffusivities for temperature and water vapor, respectively, which are assumed to be equal. If the Bowen ratio is calculated along with the non-turbulent flux terms of the snowpack energy balance, Eq. 3.1 can be rewritten as

$$Q_{E-BR} = \frac{Q* - dU\ dt^{-1}}{1+\beta} \tag{3.8}$$

where $Q_{E\text{-}BR}$ is the latent heat flux calculated by the BR method. The flux footprint was calculated for the BR fluxes based on the geometric mean of the measurement heights ([*Stannard*, 1997]; see Appendix A) using the method developed by *Schuepp et al.* [1990].

The latent heat fluxes calculated by the BR method in this study were evaluated based on the method described by *Ohmura* [1982] to identify erroneous or faulty turbulent flux values. Values of Bowen ratios close to -1, calculated in the range $-0.5 > \beta > -1.5$, can lead to very large and extremely inaccurate flux values and were flagged as faulty [*Tanner et al.*, 1987]. Bowen ratios close to -1 often occur when $(Q^* - dU\ dt^{-1}) \approx 0$. Additionally, data were flagged if a counter-gradient flux (i.e. fluxes with a sign opposite to that indicated by the measured temperature or vapor pressure gradient) was indicated, which did not meet the following inequalities [*Payero et al.*, 2003]:

$$\text{If } (Q^* - dU\ dt^{-1}) > 0, \text{ then } L_s(\Delta e + \gamma \Delta T) < 0 \text{ or } \Delta T < \frac{-\Delta e}{\gamma} \tag{3.9a}$$

$$\text{If } (Q^* - dU\ dt^{-1}) < 0, \text{ then } L_s(\Delta e + \gamma \Delta T) > 0 \text{ or } \Delta T > \frac{-\Delta e}{\gamma} \tag{3.9b}$$

where γ is the psychrometric constant (≈ 0.04 kPa °C^{-1}), Δe is the vapor pressure gradient between measurements heights, and the direction of the gradients are measured as the upper height minus the lower height. The cumulative errors in the measurements of Q^*, $dU\ dt^{-1}$, ΔT, and Δe, or problems with the development or stationarity of the surface layer, are likely responsible for these problematic BR fluxes [*Ohmura*, 1982]. Lastly, the BR method was not used during snowmelt periods, when accurate calculation of internal snowpack energy storage was not feasible because of the difficulty measuring the internal melting and refreezing rate within the snowpack as well as the snowmelt outflow from the snowpack.

3.3.8 Measurement uncertainty

The systematic uncertainties of field measurements collected in this study were determined using either manufacturer calibration or expert opinion (Table 3.3). To transfer measurement uncertainty through the nonlinear equations [*Graham et al.*, 2010; *Knowles et al.*, 2015b] used for turbulent flux calculations, uncertainty was propagated using the standard error propagation formula [*Taylor*, 1997]:

$$\delta_s y = \sqrt{\sum_{n=1}^{N}\left(\frac{\partial y}{\partial x_n}\delta_s x_n\right)^2} \tag{3.10}$$

where y is a function with N variables (x), $\delta_s x$ is the uncertainty in variable x, and $\delta_s y$ is the propagated systematic error through y. Hourly systematic uncertainties were aggregated to longer time scales in an additive manner as the square of the sum [*Moncrieff et al.*, 1996]:

$$\eta = \sqrt{\left(\sum_{t=1}^{T}\frac{\partial y}{\partial x_n}\delta_s x_t\right)^2} \tag{3.11}$$

from time 1:T where η is the aggregated systematic error. Random uncertainties were not considered in this study because these evenly distributed errors diminish with increasing size of the dataset according to $1/\sqrt{T}$ [*Barlow*, 1989] and were assumed to cancel out over longer time scales [*Knowles et al.*, 2015b].

3.3.9 Gap filling

Each of the methods for calculating turbulent fluxes of latent heat in this study were not serially complete, and data gaps were filled to quantify the importance of snow sublimation over a given snow-covered period. The "look-up tables" gap-filling method as defined in *Falge et al.* [2001] was used in this study. Tables were developed for each of the latent heat flux calculation methods at each site during each snow-covered period so that missing or flagged fluxes could be

gap filled based on environmental conditions. Look-up tables were developed based on 18 net radiation (Q^*) classes x 16 wind speed (u) classes that were selected based on the distribution of Q^* and u observed at the Arrow and Cabin sites. The mean turbulent flux of latent heat and associated mean uncertainty within each class was used as a look-up table for gap-fill fluxes based on Q^* and u associated with the missing value. In cases where Q^* or u were not available at a site because of power loss or instrument malfunction, a simple linear regression between these variables at the Arrow and Cabin sites was used to model the missing values. The uncertainty associated with the gap-filling method was accounted for by adding an additional of 10 percent to look-up table uncertainty for gap-filled fluxes.

3.4 Results

3.4.1 Snowpack and meteorological conditions

The Arrow site received more winter precipitation (total precipitation during the snow-covered period), had a greater peak SWE, and had a longer snow-covered period than the Cabin site each year of the field experiment (Table 3.2). Snow-accumulation periods (i.e. period of time with snow cover on ground prior to the onset of snowmelt) and snowmelt periods (i.e. period of time during active snowmelt before snow cover completely melts) are also presented in Table 3.2. The Arrow site generally exhibited lower T, lower e, and higher u than the Cabin site, however, the later spring snowmelt (i.e. higher T) at the Arrow site led to similar mean T and e at the two sites during the snow-covered period (Table 3.2). Mean-hourly ΔT (upper height minus lower height) observed at the Cabin and Arrow sites was consistently directed from the atmosphere to the snowpack during the snow-covered period, suggesting persistent stable atmospheric conditions over the snowpack. The mean-hourly Δe was directed from the atmosphere to the snowpack (promoting deposition) during nighttime and from the snowpack to

the atmosphere (promoting sublimation) during daytime (Figure 3.3). The atmospheric surface layer became less stable (based on the atmospheric stability parameter ζ) during the daytime, at times approaching neutral stability conditions. The duration of Δe directed from the snowpack to the atmosphere increased during the snowmelt period as day length increased and the snow surface warmed (Figure 3.3). Mean Q^* flux was generally small at both sites during the snow-accumulation period (Table 3.2) because of a balance of incoming and outgoing shortwave and longwave radiation over the day. Net radiation was dominated by outgoing longwave radiation during nighttime and by the net shortwave radiation during the day, which was small because the high albedo of the snow surface (Figure 3.4). The internal snowpack energy change, $dU\ dt^{-1}$, of the snowpack was approximately equal to zero on average throughout the snow-accumulation period at each site (Table 3.2). The diurnal pattern of $dU\ dt^{-1}$ driven by changes to internal snowpack temperature was similar to Q^* although it peaked earlier in the day (Figure 3.4).

3.4.2 Evaluation of turbulent fluxes

The percentage of flagged or faulty hourly turbulent fluxes by each method in this study is presented in Table 3.3. Turbulent fluxes were flagged because of power loss, instrumentation malfunction, or the specific criteria outlined in the methods section. Hourly fluxes that were not flagged as faulty are hereinafter referred to as valid fluxes. Both sites were run continuously through the snow-covered periods with the exception of a loss of power during 23 February 2014 through 20 March 2014 at the Arrow site. Aerodynamic (BF and AP) method fluxes were only flagged because of power loss, a malfunction of the sensor exchanging mechanism, or the sensor intakes becoming clogged with snow (Table 3.3) and these flagged values were not related to specific environmental conditions or temporal patterns. Eddy covariance turbulent fluxes from the Arrow site that were both serially complete (from beginning to end of the hour) and rated as

moderate to high quality based on tests for steady-state conditions and turbulence development [*Mauder and Foken*, 2004] were considered valid while all others were flagged. A total of 42 and 44 percent of the hourly WY 2014 and WY 2015, respectively, EC turbulent fluxes were flagged (Table 3.3), with approximately 67 percent of the flagged values occurring at night. Bowen ratio-energy balance turbulent fluxes that did not meet the criteria outlined in the methods section, and were flagged as faulty, included between 38 and 59 percent of the values in each of the snow-accumulation period datasets (Table 3.3). Most faulty BR fluxes were flagged because of a counter-gradient flux (approximately 70 percent of flagged values), because the inequalities presented in Eq. 3.9 were not satisfied. Bowen ratios between -1.5 and -0.5 occurred when the available energy ($Q^* - dU\,dt^{-1}$) is very close to zero [*Ohmura*, 1982] and accounted for approximately 16 percent of flagged values. Fluxes were not calculated by the BR method during the snowmelt period.

Eddy covariance turbulent flux measurements at the Arrow site during the snow-accumulation periods of WY 2014 and WY 2015 were also evaluated by assessing the energy balance closure [*Wilson et al.*, 2002] for 24-hour periods with valid measurements or "complete days." Complete days are defined in this study as periods with 24 hours of serially complete eddy covariance data beginning and ending at midnight in which at least 80 percent of the hourly fluxes are rated as moderate to high quality. The hourly fluxes with under-developed turbulence (less than 20 percent of the day) were included in the daily means. The sum of measured turbulent fluxes ($Q_{E\text{-}EC} + Q_{H\text{-}EC}$) were compared to the measured available energy ($Q^* - dU\,dt^{-1}$) to assess energy balance closure for complete days (Figure 3.5). The energy balance closure ratio (i.e. the sum of the turbulent flux terms divided by the sum of the available energy terms) was

equal to 0.71 and 0.60 and the mean-residual value ($Q^* - dU\,dt^{-1} - Q_{E\text{-}EC} - Q_{H\text{-}EC}$) was -3.3 ± 4.6 W m^{-2} and -5.7 ± 4.6 W m^{-2} during WY 2014 and WY 2015, respectively.

The flux footprints of the EC and BR turbulent fluxes were relatively short distances because the micrometeorological measurements in this study were made close to the snow surface. The footprint calculations indicate that greater than 80 percent of the measured EC fluxes at the Arrow site were contained within 164 m of the upwind area. Greater than 80 percent of the measured BR fluxes were contained within 130 m (59 m) of the upwind area at the Arrow (Cabin) site. This study assumes that the flux footprint calculations for the BR method are applicable for the AP and BF methods considering they are based on the same environmental variables and measurement heights. The calculated flux footprint for each method was within the open fetch at both sites suggesting the turbulent fluxes calculated in this study were from the forested openings and not the adjacent forest at each site.

3.4.3 Comparison of valid turbulent fluxes of latent heat

Mean differences calculated for matched pairs of valid hourly latent heat flux calculations were evaluated at each site during the snow-accumulation and snowmelt periods using the Wilcoxon signed-rank test (Table 3.4). All differences were statistically significant (p value < 0.05). Mean differences between hourly fluxes calculated by the BF, AP, and BR methods were biased low when compared to the EC method. The AP method was biased low when compared to the BF method at both sites during the snow-accumulation and snowmelt periods. When compared to the BF and AP methods, the BR method was biased low at the Arrow site and biased high at the Cabin site during the snow-accumulation period. Differences between methods and associated propagated uncertainties were greater during the snowmelt period than the snow-accumulation period (Table 3.4).

A comparison was made between simultaneous valid hourly latent heat flux calculations from the EC, BR, BF, and AP methods (Figure 3.6). The diurnal patterns of valid EC, BR, AP, and BF fluxes at the Arrow site (Figure 3.6a) during the WY 2014 snow-accumulation period were similar to the Cabin site (Figure 3.6b). The BR fluxes were biased low during the night (showing deposition) and biased high (showing greater sublimation) during midday when compared to all other methods. These midday biases were greater at the Cabin site (Figure 3.6b) compared to the Arrow site (Figure 3.6a). The AP fluxes were similar to the BF fluxes during the night but were biased low when compared to the BF fluxes during the day at both sites. The EC fluxes at the Arrow site were biased high when compared to all other methods except the BR method during midday. Latent heat fluxes calculated by all methods were well correlated with each other, with the strongest correlations between the BF and AP methods (r = 0.85 and 0.83; p value < 0.05) at the Arrow and Cabin sites, and between the EC and BF methods at the Arrow site (r = 0.83; p value < 0.05) (Table 3.5). The diurnal pattern of when fluxes were flagged by each method was compared to determine which flagged values were controlling when simultaneously valid hourly fluxes were available (Figure 3.6c and 3.6d). The majority of flagged EC fluxes occurred during the night when u was lowest and ζ was greatest (most stable) (Figure 3.3), while the majority of flagged BR fluxes occurred midday when Q^* and $dU\ dt^{-1}$ were greatest (Figure 3.4).

Bivariate correlations between valid latent heat fluxes and environmental variables exhibit that fluxes from each method are positively correlated with Q^*, u, T, and T_{srf} and negatively correlated with ζ and q (Table 3.5; Figure 3.7). The EC and BR methods are most correlated with Q^*, and the AP and BF methods are most correlated with u at the Arrow site and Q^* at the Cabin site. The percentages of latent heat fluxes flagged for all methods were evaluated

as a function of these well-correlated environmental variables (Figure 3.7). As Q^* and u increased the percentage of EC fluxes that were flagged decreased, whereas the percentage of BR and AP fluxes increased (Figure 3.7e and 3.7f). The percentage of flagged EC and AP fluxes decreased with increasing T, while the percentage of flagged BR fluxes was lowest between T of -5°C to 0°C. As ζ increased (increasing stable conditions), the percentage of flagged BR fluxes decreased, while the percentage of flagged EC fluxes was lowest in near-neutral to slightly stable conditions ($0 < \zeta < 0.5$).

3.4.4 Comparison of estimated seasonal sublimation

Mean and net surface sublimation as well as propagated uncertainty was quantified for the entire snow-covered period for each method at both the Arrow and Cabin sites during WY 2013 and WY 2014 and at the Arrow site only during WY 2015 (Figure 3.8, Table A1). Seasonal surface sublimation rates and totals were computed using valid hourly fluxes for each method as well as gap-filled values for hours of flagged data. Amongst all methods, the mean-daily surface sublimation rates ranged from 0.09 ± 0.09 mm day^{-1} to 0.36 ± 0.08 mm day^{-1} at the Arrow site and from 0.03 ± 0.03 mm day^{-1} to 0.37 ± 0.13 mm day^{-1} at the Cabin site. However, the range of mean surface sublimation rates amongst individual methods was much more consistent from year to year (Figure 3.8a). For example, the mean BF surface sublimation rates at the Arrow site from WY 2013 – WY 2015 ranged only from 0.15 ± 0.06 to 0.17 ± 0.07 mm day^{-1}. For each method, the surface sublimation rates at the Arrow and Cabin sites increased throughout the snow-covered period, with greater surface sublimation rates during the snowmelt period than the snow-accumulation period (Figure 3.8a).

Net surface sublimation calculated by the BR, BF, and AP methods at the Arrow site was comparable within the range of uncertainty of each method [*Taylor*, 1997] but were each

significantly (based on the bounds of uncertainty) biased low when compared to the EC method. Eddy covariance exhibited a net surface sublimation of 55.3 ± 13.9 mm and 58.6 ± 13.3 mm equal to 13 and 17 percent of winter precipitation during WY 2014 and WY 2015, respectively (Figure 3.8b and Figure 3.8c). Net surface sublimation calculated by the aerodynamic methods (BF and AP) were comparable within the range of uncertainty at the Cabin site, but the BR method was significantly biased high compared to the aerodynamic methods. A comparison between the Arrow and Cabin sites during WY 2013 and WY 2014 shows that the aerodynamic methods (BF and AP) are comparable within the range of uncertainty of each method, but the calculated surface sublimation was greater at the Arrow site than the Cabin site. The BR method was significantly different between sites with greater surface sublimation calculated for the Cabin site. The mean propagated uncertainty calculated for each method in this study was equal to 24 percent (η = 13.6 mm), 46 percent (η = 10.2 mm), 94 percent (η = 10.3 mm), and 46 percent (η = 17.4 mm) for the EC, BF, AP, and BR methods, respectively.

3.5 Discussion

Based on method comparisons, propagated uncertainty calculations, as well as instrumentation requirements, this study suggests that the EC and/or BF methods are preferable for estimating surface sublimation in snow-covered forested openings. The EC method provided reliable estimates of sublimation during periods of well-developed turbulence, but often required gap filling during periods of low turbulence and high atmospheric stability which was biased high compared to other methods. The BF and AP methods required the least gap filling amongst methods, but were generally biased low when compared to EC estimates with the BF method exhibiting a stronger correlation and smaller mean difference than the AP method. The BR method often required gap filling during daytime periods when sublimation rates were highest

and during the entire snowmelt period, and exhibited strong diurnal biases compared to other methods. Researchers seeking to use the EC method to quantify surface sublimation should take special care to evaluate conditions during under-developed turbulence (often at night) when fluxes may be overestimated (or of opposite signs to near-surface gradients) by gap filling techniques and better represented by the BF method. Alternatively, if the BF method is used, special care should be paid to evaluating the highly uncertain transfer coefficient (C_E) that represents site conditions related to atmospheric stability and surface roughness. The BF method was often biased low from the EC method during well-developed turbulence conditions in this study when the EC method was not likely to overmeasure turbulent fluxes, and these biases may have been related to uncertainty in C_E. Research design using the EC and/or BF method to quantify surface sublimation from forested openings should also take special care to evaluate the size of the forest opening compared to the measurement footprint to ensure these techniques are sampling from the area of interest. If measurements are desired from a small forested opening where available fetch and turbulence development will not be adequate, the gravimetric method may be more applicable.

Results presented in this study differ from previous comparisons of methods of quantifying turbulent fluxes of latent heat. *Marks et al.* [2008] presented a comparison between the EC and BF methods and highlighted a positive bias in the BF method, while the EC and BF methods were shown to compare well using the same method in a subsequent study [*Reba et al.*, 2012]. *Box and Steffen* [2001] compared the AP, BF, and EC methods and reported that the AP method compared well with the EC method but the BF method was biased high. Comparisons of turbulent fluxes of latent heat over non-snow covered surfaces have often reported that the EC and BR methods are well correlated, but that the EC method is biased low when compared to the

BR method [e.g., *Brotzge and Crawford*, 2003]. The results of this study suggest that the different conclusions of relative biases between methods observed by previous studies and the present work are likely related to data quality based on time of day or environmental condition (Figure 3.6 and 3.7) or overall method uncertainty (Figure 3.8).

3.5.1 Limitations of methods for determining surface sublimation

The experimental design of this study highlighted important limitations and challenges with each method for determining surface sublimation. Eddy covariance measurements were collected at a site with a moderate slope and non-uniform terrain and likely experiences non-uniform flow which challenges the assumptions of the EC method. Also, the study site experienced drainage of cold, dense air at night along with a vapor pressure gradient from the atmosphere to the snowpack (shown by the exchanging aspirated sensors) that was not often captured by the EC sensors at 1.5 m height. This, along with the majority of nighttime EC fluxes flagged because of turbulence development, suggests that EC was not the best method for quantifying nighttime sublimation or deposition at the Arrow site. The EC method fluxes exhibited an energy balance closure ratio ranging from 0.60 to 0.71 that is slightly low compared to observations made over non-snow covered surfaces. Non-closure is a common problem with eddy covariance measurements [*Foken*, 2008] and energy balance closure discrepancies are often on the order of 10 to 30 percent at long-term eddy covariance (FLUXNET) measurement sites [*Wilson et al.*, 2002]. However, energy balance closure over a snow-covered surface has not often been measured, and *Helgason and Pomeroy* [2012b] report a large energy imbalance (energy balance closure discrepancies from 45 to 100 percent) over the snow cover. Underestimations of the EC turbulent energy fluxes compared to the measured available energy may be related to a systematic instrumentation bias, difference in observation scale between the

available energy (measured at a point) and turbulent flux (measured over the flux footprint of 164 m) [*Wilson et al.*, 2002], or because of cold air drainage and its unmeasured advection. An under measurement of sensible heat flux towards the snowpack and/or latent heat flux towards the snowpack (deposition), both of which warm the snowpack, may have been responsible for the closure discrepancy observed in this study [*Helgason and Pomeroy*, 2012b; *Burns et al.*, 2014].

A potential limitation of the aerodynamic (BF and AP) methods and the BR method is that the measurement heights of the near-surface *T* and *RH* measurements may have been collected so close to the snow surface that they did not represent sampling from a constant-flux layer, which could explain biases from the EC method in conditions with fully developed turbulence. Future research should evaluate the best measurement heights for aerodynamic methods in order to ensure measurement from a constant flux layer but also measure important near-snow surface processes such as cold air drainage. Biases observed in the aerodynamic methods may also be improved through calibrating the aerodynamic methods to site-specific conditions. *Reba et al.* [2014] showed that turbulent fluxes calculated by the BF method were particularly sensitive to the snow surface roughness length (z_0). Specifically calibrating the aerodynamic methods to EC measurements was outside of the scope of this study, but future research could focus on calibrating the BF method for site-specific conditions and evaluating biases between BF and EC methods in various site conditions of complex mountainous terrain.

The BR method exhibited strong biases (negative during nighttime and positive during daytime conditions) when compared to hourly measurements made by all other methods (Figure 3.6). It is possible that the large biases observed in the BR method could be related to the inequality of the eddy diffusivities for temperature (K_H) and water vapor (K_V) that have been

suggested by various studies [e.g., *Blad and Rosenberg*, 1974; *Irmak et al.*, 2014], but evaluation of this hypothesis was outside of the scope of this study. The BR method has the benefit of providing turbulent fluxes without the need for making turbulence measurements or estimating the atmospheric stability and snow surface roughness. Additionally, the fluxes estimated by this method are constrained by energy balance measurements. However, this can also be problematic, as a propagated uncertainty of 46 percent was calculated in the seasonal BR method surface sublimation estimates because of uncertainty in Q^*, $dU\ dt^{-1}$, ΔT, and Δq. *McKay and Thurtell* [1978] suggest that the BR method should be considered inadequate for winter-time energy balance calculations because of the size of the measurement errors relative to the magnitude of the fluxes. The data screening and removal procedures implemented by this study likely eliminated some of the most serious measurement errors, but also resulted in flagging a substantial percentage of the estimated fluxes (Table 3.3) and often flagging values in the middle of the day when net radiation and wind speed are highest. Additionally, the BR method over snow cannot be used with confidence over a melting snowpack [*Storr and Ferguson*, 1974]. This limitation is underscored by the increased importance of sublimation during the snowmelt period (Figure 3.8).

Gravimetric estimations of surface sublimation could not be made with confidence in this study because (1) precipitation was estimated from a spatial climate dataset (Table 3.2) rather than measured directly, and (2) the measurement sites were positioned such that wind redistribution may have contributed to the difference between estimated winter precipitation prior to peak SWE and measured peak SWE [e.g., *Meyer et al.*, 2012]. These sources of uncertainty are highlighted in Table 3.2, where peak SWE often exceeds winter precipitation, while all other methods for estimating surface sublimation show a net loss of water away from

the snowpack. Future studies that attempt to quantify surface sublimation using gravimetric methods should take particular care to directly measure precipitation and account for gage undercatch [e.g., *Fassnacht*, 2004] while also measuring SWE from areas that are not subjected to wind redistribution of snow.

3.5.2 Meteorological drivers of surface sublimation

The meteorological conditions that promote surface sublimation from forested openings at both the Arrow and Cabin included high wind speeds (increasing surface layer turbulence) and net radiation, warm snow surface temperatures and low relative humidity (promoting a vapor pressure gradient directed from the snowpack to the atmosphere), and a reduction in surface layer stability toward neutral conditions (Table 3.5). These conditions are generally dominant during midday periods and peak in the early afternoon, which coincides with the timing of the greatest surface sublimation rates observed in this study. Because of these radiative and meteorological drivers, surface sublimation showed a strong diurnal pattern at both sites (Figure 3.6) consistent with observations of previous studies [e.g., *Meiman and Grant*, 1974; *Box and Steffen*, 2001; *Molotch et al.*, 2007; *Reba et al.*, 2012]. A vapor pressure gradient directed from the atmosphere to the snowpack was often measured at night (which drives deposition), but strong stable atmospheric conditions limited deposition rates and allowed for surface sublimation to be the dominant water flux between the snow and atmosphere. Surface sublimation rates generally increased throughout the snow season at each site and the greatest rates were often observed during the snowmelt period (Figure 3.8).

3.5.3 Hydrological importance of surface sublimation in the Colorado Rocky Mountains

The year-to-year surface sublimation rates amongst individual methods in this study displayed little variability (Figure 3.8a). This is a result that was also observed by *Reba et al.*

[2012] and suggests that the importance of snow sublimation in the region is largely dependent on the amount of snowfall in a given year (Figure 3.8c). In other words, the role of snow sublimation will likely have a greater effect on the overall water balance during low snow years. Snow sublimation rates are not expected to scale with snowpack depth or SWE, as a given set of meteorological conditions would be expected to sustain virtually the same sublimation rate for any depth of snow on the ground. Furthermore, years with deeper snowpacks tend to have greater occurrence of snowfall coinciding with conditions that repress surface sublimation, suggesting a potential negative correlation between seasonal snow sublimation rates and total winter precipitation. This result has important implications for water management decision making and future long-term studies of snow sublimation measurements could provide greater insight into the relation between snowfall amounts, occurrence of snowfall, snow-cover duration, and snow sublimation totals.

The surface sublimation rates quantified in this study are generally smaller in magnitude compared to previously published surface sublimation rates for the Rocky Mountain region of the USA. *Meiman and Grant* [1974] found surface sublimation rates of 0.58 mm day^{-1} and 0.64 mm day^{-1} using evaporation pans in a forested and open site at Pingree Park, Colorado. *Hood et al.* [1999] found an average seasonal surface sublimation rate of 0.67 mm day^{-1} with greater rates (approximately 1.0 mm day^{-1}) during the snow-accumulation period using the AP method at an alpine site on Niwot Ridge, Colorado. EC measurements of surface sublimation below the forest canopy in the Front Range of Colorado have been reported as 0.41 mm day^{-1} by *Molotch et al.* [2007] and 0.17 mm day^{-1} by *Marks et al.* [2008]. Additionally, *Reba et al.* [2012] found an average surface sublimation rate of 0.39 mm day^{-1} at an exposed forested opening and 0.15 mm day^{-1} at a sheltered site beneath an aspen canopy at Reynolds Creek Experimental Watershed,

Idaho. The range of BF and EC seasonal surface sublimation reported in this study at both sites, 0.10 ± 0.05 mm day^{-1} to 0.36 ± 0.08 mm day^{-1}, is most comparable to the rates reported in the subcanopy by *Marks et al.* [2008] and *Reba et al.* [2012] and in an exposed forested opening by *Reba et al.* [2012]. Previously published results of canopy sublimation in this region [e.g., *Montesi et al.*, 2004; *Molotch et al.*, 2007] are also greater than the surface sublimation rates quantified in this study, suggesting that estimations of surface sublimation from forested openings may represent the lower bound, or a conservative estimate, of basin-wide snow sublimation losses. Future research design including simultaneous measurements of surface sublimation from forested openings and surface and canopy sublimation from forested areas in this region could provide more confidence in understanding the hydrologic importance of snow sublimation from land covers below treeline. Across the entire study area, it is hypothesized that snow sublimation (including surface and canopy sublimation) from forested areas (35 percent of study area) accounts for a greater contribution to the winter water balance than surface sublimation from forested openings (21 percent of study area), but that snow sublimation from forested openings also has a substantial relative contribution to the winter water balance [e.g., *Strasser et al.*, 2008]. Measurements made in this study help to refine surface sublimation estimates for forested openings in the Colorado Rocky Mountains.

3.6 Conclusions

In this study, surface sublimation is evaluated within two forested openings using the eddy covariance (EC), Bowen ratio-energy balance (BR), bulk aerodynamic flux (BF), and aerodynamic profile (AP) methods. Results from all methods are evaluated over a range of environmental conditions and show considerable propagated uncertainty. The EC and BF methods are concluded to be preferable for estimating surface sublimation in snow-covered

forested openings, and potential limitations and biases in each of these methods are highlighted to guide future research design. Mean surface sublimation rates calculated for the Arrow site ranged from 0.33 ± 0.08 mm day^{-1} to 0.38 ± 0.08 mm day^{-1} by the EC method and from 0.15 ± 0.07 mm day^{-1} to 0.17 ± 0.06 mm day^{-1} by the BF method. Mean surface sublimation calculated by the BF method at the more sheltered Cabin site ranged from from 0.10 ± 0.05 mm day^{-1} to 0.13 ± 0.07 mm day^{-1}. Surface sublimation rates quantified in this study are generally smaller in magnitude than snow sublimation rates reported for this region and help to refine surface sublimation estimates for forested openings in the Colorado Rocky Mountains.

Table 3.1. Field-experiment instrumentation. [(1)]Denotes sensor specific to Cabin site, [(2)]denotes sensor specific to Arrow site,[(*)]denotes sensor instrument height adjusted with snow accumulation to remain a constant height above snow surface, and [(#)]denotes estimated uncertainty (manufacturer accuracy not stated).

Measured variable	Manufacturer and model number	Instrument height above soil surface (m)	Instrument uncertainty
Air temperature and relative humidity	REBS exchanging aspirated temperature humidity profile sensors (THP-1)	0.1*, 1.1*	±0.2°C, ±2.0%
	Rotronic HC2S3 temperature and humidity probe[2]	3.0	±0.1°C to ±0.3°C, ±0.8% to ±3.0%
Wind speed	Met One 014A[1]	2.0[1]	±0.3 m s^{-1}
	R. M. Young 05103-45[2]	3.0[2]	
Net radiation	Campbell Scientific CNR2[1]	2.0[1]	±10%,
	Campbell Scientific NR-LITE2[2]	3.0[2]	±10%[#]
Snow temperature profile	Omega 24 AWG type E thermocouple wire	0 – 2.0 (0.1 m spacing)	±0.4%
Snow surface temperature	Apogee SI-111 infrared radiometer	2.0[1], 3.0[2]	±0.2°C to ±0.5°C
Snow depth	Campbell Scientific SR50A	2.0[1], 3.0[2]	±0.01 m
Vertical and horizontal wind speed and direction	Campbell Scientific IRGASON 3-D sonic anemometer[2]	1.5*	±2% to ±6%
Sonic temperature	Campbell Scientific IRGASON 3-D sonic anemometer[2]	1.5*	±0.025°C
Water vapor concentration	Campbell Scientific IRGASON gas analyzer[2]	1.5*	±2%
Datalogger	Campbell Scientific CR3000[2]	1.5	---
	Campbell Scientific CR1000	1.5	
	Campbell Scientific AM25T multiplexer	0	

Table 3.2. Snowpack and meteorological conditions during the snow-covered period. *P* is winter precipitation determined as the total precipitation during the snow-covered period derived from PRISM (PRISM Climate Group, Oregon State University, http://prism.oregonstate.edu), *peak SWE* is maximum snow water equivalent, *T* is mean air temperature, *e* is mean vapor pressure, *u* is mean wind speed, T_{srf} is mean snow surface temperature, ζ is mean atmospheric stability parameter, Q^* is mean net radiation, and $dU\ dt^{-1}$ is mean internal snowpack energy change. (#)The average wind speed and atmospheric stability parameter at Arrow excludes the period from 23 February 2014 through 20 March 2014 because of missing data. (&)Mean internal snowpack energy change only includes data from the snow-accumulation period.

	Arrow			**Cabin**	
	WY 2013	*WY 2014*	*WY 2015*	*WY 2013*	*WY 2014*
P (mm)	344	433	348	194	211
Peak SWE (mm)	305	566	360	124	286
Snow-covered period (days)	187	168	164	142	151
Snow-accumulation period (days)	167	138	120	85	131
Snowmelt period (days)	20	30	44	57	20
T (°C)	-5.46	-5.42	-2.53	-6.80	-5.28
e (kPa)	0.30	0.30	0.29	0.29	0.31
u (m s^{-1})	2.13	2.69[#]	1.99	1.62	2.03
T_{srf} (°C)	-9.96	-10.39	-9.27	-11.19	-9.96
ζ	2.26	2.29[#]	2.93	2.32	2.07
Q^* (W m^{-2})	-1.40	-6.26	-8.68	11.47	2.04
$dU\ dt^{-1}$ (W m^{-2})[&]	0.13	-0.16	-0.11	0.25	-0.01

Table 3.3. Percentage of flagged hourly turbulent fluxes of latent heat for the eddy covariance (EC), Bowen ratio-energy balance (BR), aerodynamic profile (AP), and bulk aerodynamic flux (BF) methods during the snow-covered period. (*)The percentage of values flagged for the BR method is based on the snow-accumulation period only. (&)Percentage from the Arrow site does not include time during a power outage from 23 February 2014 through 20 March 2014.

	Arrow			
	EC	*BR**	*AP*	*BF*
WY 2013	---	40%	4%	5%
WY 2014[&]	42%	59%	30%	2%
WY 2015	44%	---	---	0%
	Cabin			
	EC	*BR**	*AP*	*BF*
WY 2013	---	38%	6%	6%
WY 2014	---	54%	10%	11%

Table 3.4. Hourly latent heat flux mean differences (y-x) and propagated uncertainty (η) for matched pairs calculated by the eddy covariance ($Q_{E\text{-}EC}$), Bowen ratio-energy balance ($Q_{E\text{-}BR}$), aerodynamic profile ($Q_{E\text{-}AP}$), and bulk aerodynamic flux ($Q_{E\text{-}BF}$) methods from all years collected at the Arrow and Cabin sites during the snow-accumulation period $^{(SAP)}$ and snowmelt period $^{(SMP)}$. Bold values represent statistically significant differences (p value < 0.05) calculated by the Wilcoxon signed-rank test.

	Arrow^{SAP} mean difference (W m^{-2})		
	$Q_{E\text{-}EC}$	$Q_{E\text{-}BF}$	$Q_{E\text{-}AP}$
$Q_{E\text{-}BF}$	**-4.9** ± 3.3	---	---
$Q_{E\text{-}AP}$	**-8.6** ± 3.8	**-1.0** ± 2.9	---
$Q_{E\text{-}BR}$	**-7.8** ± 2.6	**-3.4** ± 2.1	**-2.1** ± 2.3
	Arrow^{SMP} mean difference (W m^{-2})		
	$Q_{E\text{-}EC}$	$Q_{E\text{-}BF}$	$Q_{E\text{-}AP}$
$Q_{E\text{-}BF}$	**-14.4** ± 8.9	---	---
$Q_{E\text{-}AP}$	**-17.1** ± 7.8	**-4.5** ± 5.4	---
$Q_{E\text{-}BR}$	---	---	---
	Cabin^{SAP} mean difference (W m^{-2})		
	$Q_{E\text{-}EC}$	$Q_{E\text{-}BF}$	$Q_{E\text{-}AP}$
$Q_{E\text{-}BF}$	---	---	---
$Q_{E\text{-}AP}$	---	**-1.8** ± 2.0	---
$Q_{E\text{-}BR}$	---	**1.1** ± 2.6	**2.2** ± 2.5
	Cabin^{SMP} mean difference (W m^{-2})		
	$Q_{E\text{-}EC}$	$Q_{E\text{-}BF}$	$Q_{E\text{-}AP}$
$Q_{E\text{-}BF}$	---	---	---
$Q_{E\text{-}AP}$	---	**-4.2** ± 3.5	---
$Q_{E\text{-}BR}$	---	---	---

Table 3.5. Bivariate correlations (Pearson's correlation coefficient) between hourly turbulent fluxes of latent heat by the eddy covariance ($Q_{E\text{-}EC}$), Bowen ratio-energy balance ($Q_{E\text{-}BR}$), aerodynamic profile ($Q_{E\text{-}AP}$), and bulk aerodynamic flux ($Q_{E\text{-}BF}$) methods and environmental conditions for all years at the Arrow and Cabin sites. Bold values represent statistical significance (p value < 0.05).

	Arrow				**Cabin**		
	$Q_{E\text{-}EC}$	$Q_{E\text{-}BR}$	$Q_{E\text{-}AP}$	$Q_{E\text{-}BF}$	$Q_{E\text{-}BR}$	$Q_{E\text{-}AP}$	$Q_{E\text{-}BF}$
$Q_{E\text{-}EC}$ (W m^{-2})	---	---	---	---	---	---	---
$Q_{E\text{-}BR}$ (W m^{-2})	**0.66**	---	---	---	---	---	---
$Q_{E\text{-}AP}$ (W m^{-2})	**0.81**	**0.71**	---	---	**0.71**	---	---
$Q_{E\text{-}BF}$ (W m^{-2})	**0.83**	**0.69**	**0.85**	---	**0.76**	**0.83**	---
T (°C)	**0.51**	**0.14**	**0.28**	**0.40**	**0.21**	**0.34**	**0.43**
q (kg kg^{-1})	**-0.09**	**-0.09**	**-0.08**	**-0.07**	**-0.12**	**-0.09**	**-0.07**
u (m s^{-1})	**0.45**	**0.34**	**0.48**	**0.51**	**0.32**	**0.42**	**0.48**
T_{srf} (°C)	**0.50**	**0.33**	**0.31**	**0.39**	**0.43**	**0.40**	**0.43**
ζ	**-0.33**	**-0.39**	**-0.31**	**-0.35**	**-0.43**	**-0.34**	**-0.31**
Q^* (W m^{-2})	**0.60**	**0.57**	**0.37**	**0.42**	**0.79**	**0.45**	**0.50**
$dU\ dt^{-1}$ (W m^{-2})	**0.14**	**0.13**	**0.14**	**0.07**	0.02	**0.11**	**0.16**

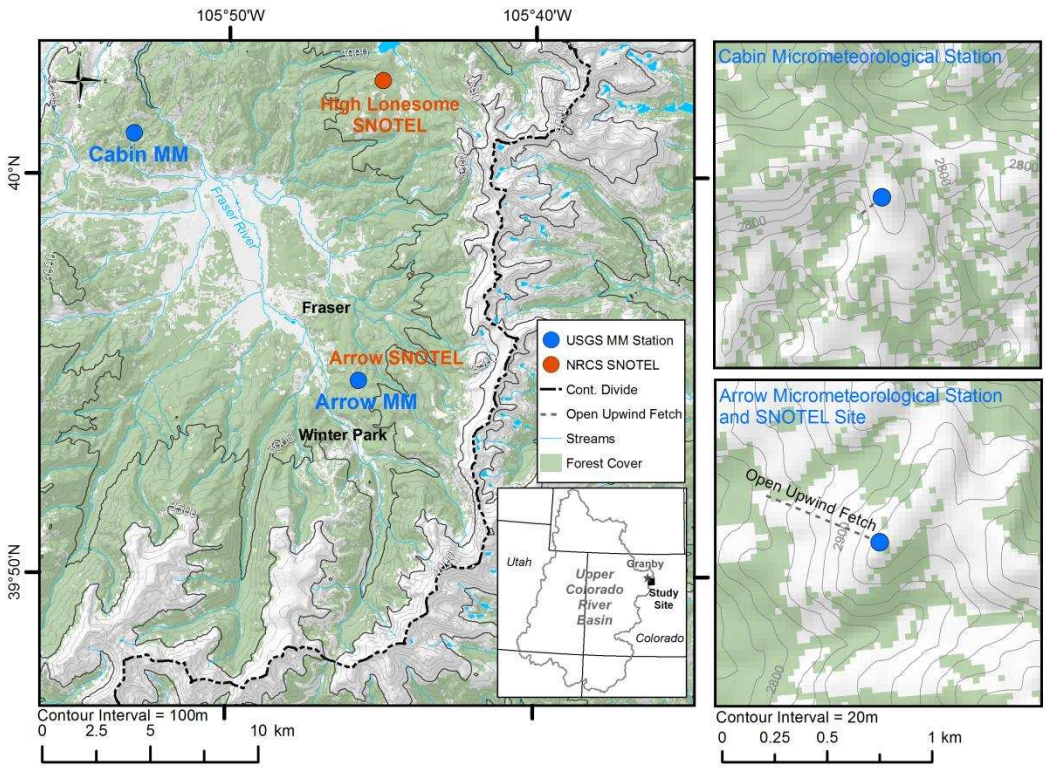

Figure 3.1. Map of study area located within the upper Colorado River Basin, Colorado, U.S.A. The locations of micrometeorological stations (MM) are shown in blue and the SNOTEL stations are shown in orange.

Figure 3.2. Photographs of the field instrumentation at (a) the Arrow site looking southwest, and (b) the Cabin site looking southwest. Close up photographs are shown for (c) the snowpack temperature thermocouple array, and (d) the exchanging aspirated temperature and relative humidity sensors.

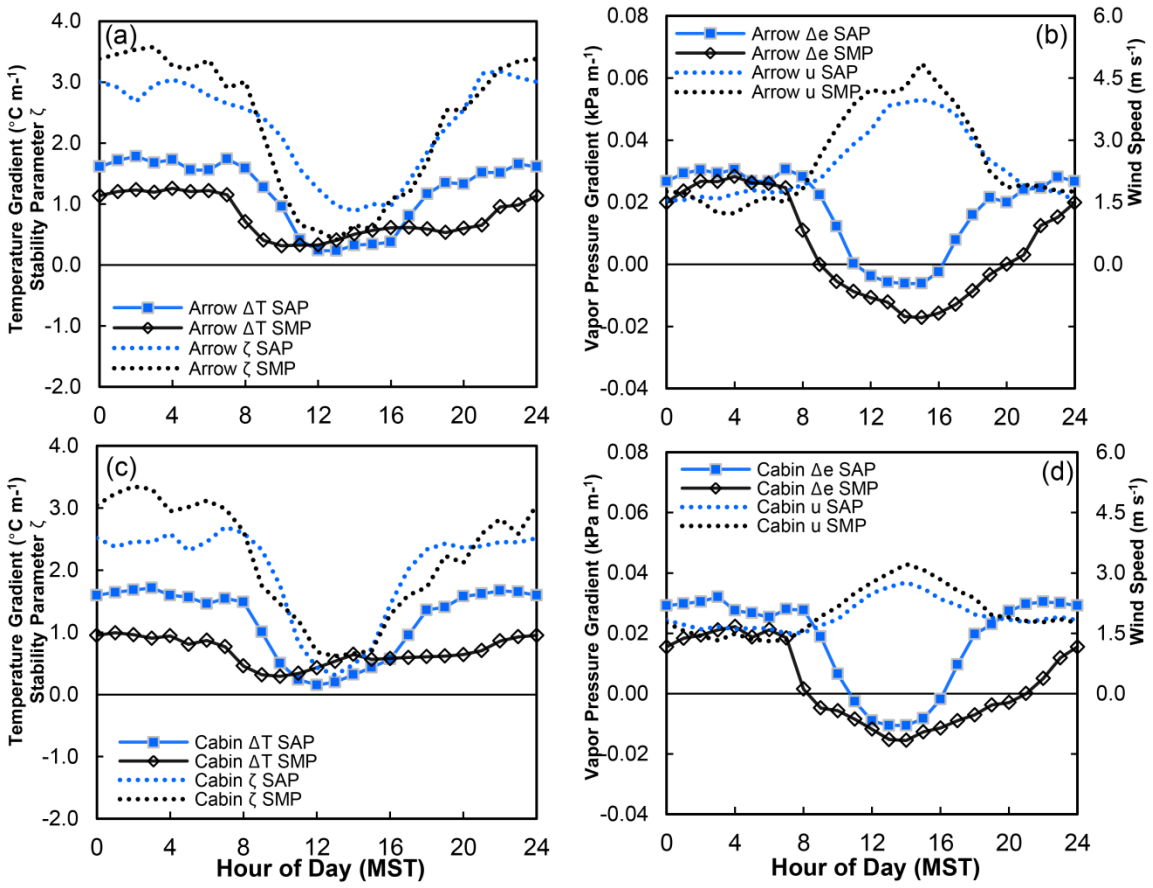

Figure 3.3. Mean-hourly air temperature gradient (ΔT) (upper height minus lower height), atmospheric stability parameter (ζ), vapor pressure gradient (Δe), and wind speed (u) during a selection of the snow-accumulation period (SAP; 01 December 2013 – 22 February 2014) and snowmelt period (SMP; 04 April 2014 – 24 April 2014) at the (a, b) Arrow site and (c, d) Cabin site.

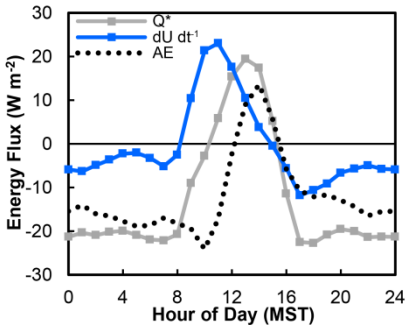

Figure 3.4. Mean-hourly net radiation (Q^*), internal snowpack energy change ($dU\ dt^{-1}$), and available energy for turbulent flux (AE) at the Arrow site during the snow-accumulation period (20 December 2013 – 20 February 2014).

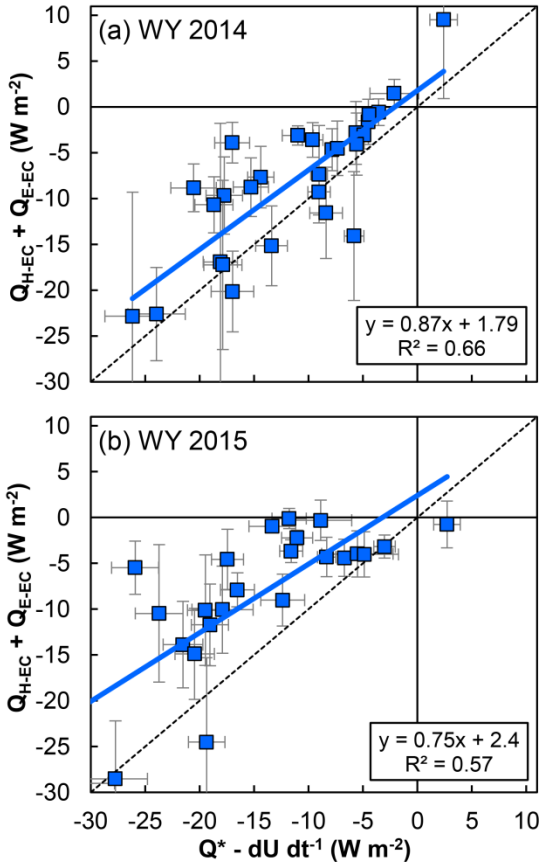

Figure 3.5. Eddy covariance energy balance closure (comparison between the sum of turbulent fluxes [$Q_H + Q_E$] and measured available energy [$Q^* - dU\ dt^{-1}$]) for valid complete days measured at the Arrow site during (a) WY 2014 (n = 28) and (b) WY 2015 (n = 23) snow-accumulation periods. Error bars represent the propagated uncertainty in both the sum of the turbulent fluxes and the measured available energy. Note the dotted 1:1 equivalence line.

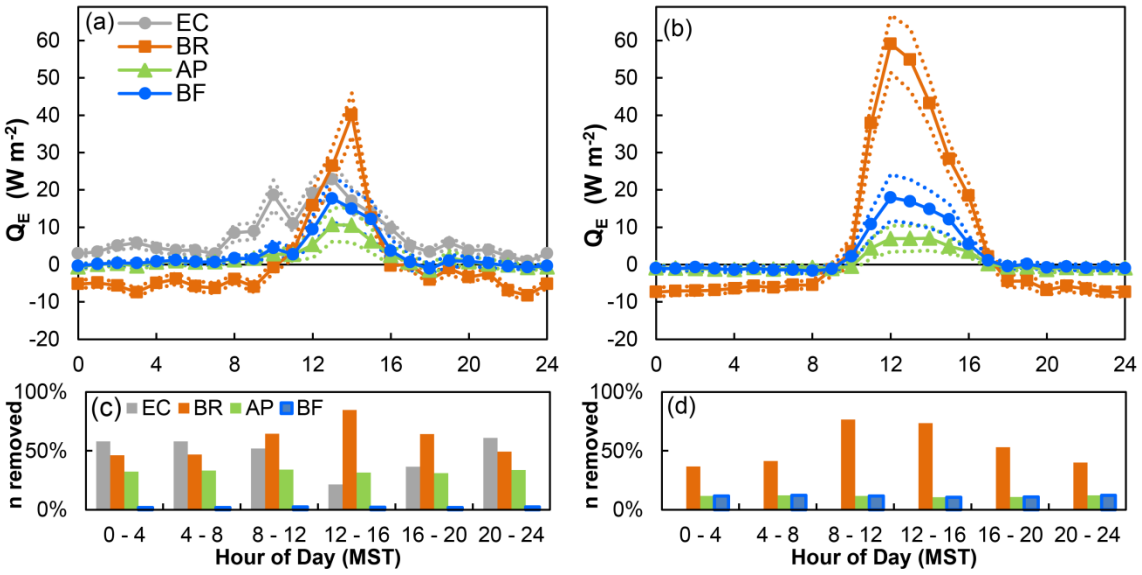

Figure 3.6. Simultaneous valid mean-hourly turbulent fluxes of latent heat from the eddy covariance (EC), Bowen ratio-energy balance (BR), aerodynamic profile (AP), and bulk aerodynamic flux (BF) methods during the WY 2014 snow-accumulation period at (a) the Arrow site and (b) the Cabin site, with the dotted lines representing the propagated measurement uncertainty for the sample mean of each method. EC was not available at the Cabin site. The percentage of hourly turbulent fluxes of latent heat removed for each method are shown for (c) the Arrow site and (d) the Cabin site.

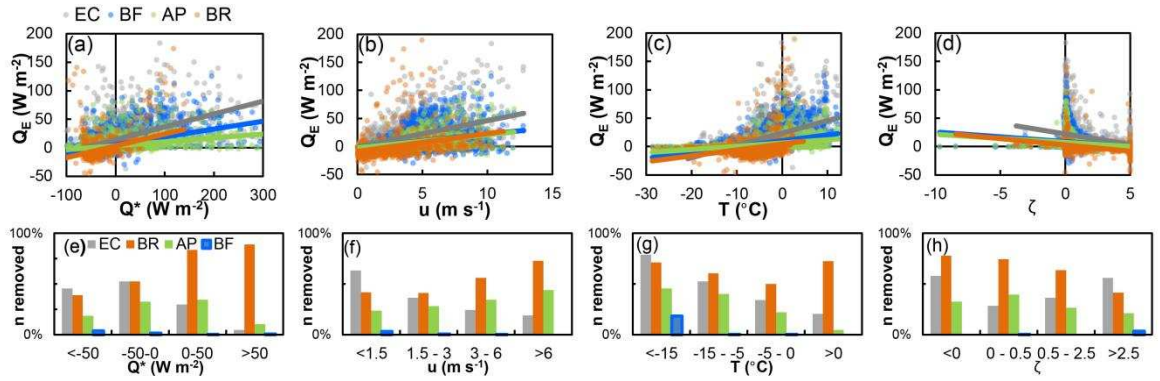

Figure 3.7. All Arrow WY 2014 valid hourly turbulent fluxes of latent heat from each method compared to (a) net radiation (Q^*), (b) wind speed (u), (c) air temperature (T), and (d) atmospheric stability parameter (ζ) with the linear trend of each relation displayed. The percentage of hourly turbulent fluxes of latent heat removed for each method are shown as a function of (e) Q^*, (f) u, (g) T, and (h) ζ.

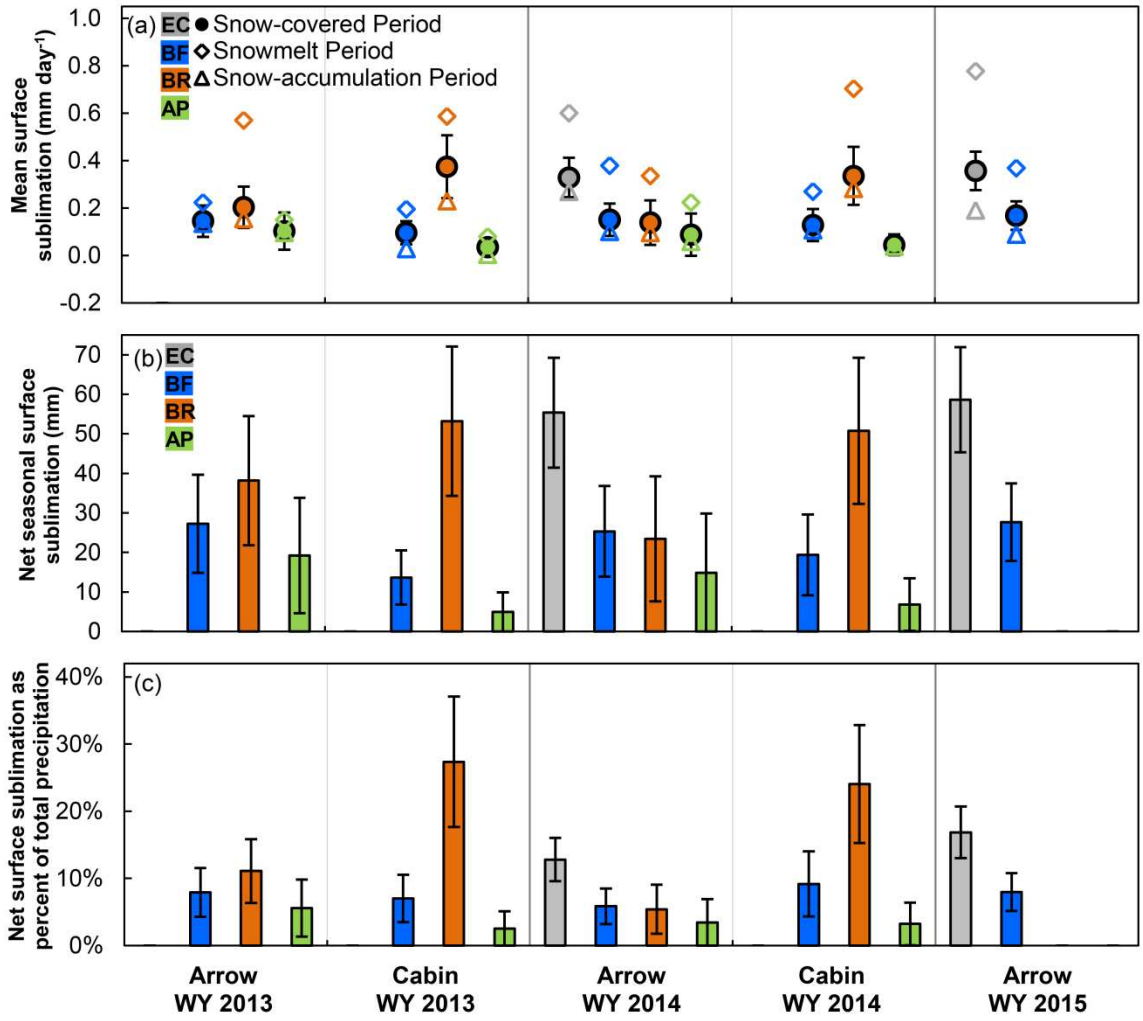

Figure 3.8. (a) Mean-seasonal surface sublimation rates, (b) total seasonal surface sublimation, and (c) surface sublimation losses as a percentage of total winter precipitation for the EC method (shown in gray), BF method (shown in blue), BR method (shown in orange), and AP method (shown in green). The propagated measurement uncertainty for each method is displayed by error bars on each panel.

CHAPTER 4 – MODELING THE VARIABILITY AND IMPORTANCE OF SNOW SUBLIMATION IN THE NORTH-CENTRAL COLORADO ROCKY MOUNTAINS[3]

4.1 Summary

In the western United States, where snowmelt from seasonal snow covers is a critical water resource for ecological and anthropological needs, snow sublimation has been suggested by many studies to be an important component of the snow cover mass balance. However, few studies have evaluated the spatial and temporal variability of this process, including surface, canopy, and blowing sublimation, in complex mountainous environments. In this study, we use a process-based snow model (SnowModel) and eddy covariance (EC) measurements to evaluate the variability and importance of snow sublimation across the north-central Colorado Rocky Mountains for five water years (WY 2011 – WY 2015). *In-situ* EC observations of snow sublimation compare well with modeled snow sublimation at sites dominated by surface and canopy sublimation, but model verification of blowing sublimation in alpine areas was not feasible as these fluxes often occur from blowing snow in turbulent suspension which cannot always be resolved by EC instrumentation. Model simulations showed substantial spatial and temporal variability of snow sublimation across the study domain. Snow sublimation rates increased from lower to higher elevations and differences between land cover types were evident. Additionally, the interannual differences in total snow sublimation were strongly linked with seasonal snowfall amounts. Land cover type was an important factor in snow sublimation variability, with substantial snow sublimation occurring in alpine and forested areas, and relatively lower snow sublimation occurring in open areas below treeline. Snow sublimation

[3] Chapter 4 is in preparation for submission to *Water Resources Research*. Additional authors are D.W. Clow, S.R. Fassnacht, G.E. Liston, C.A. Hiemstra, and J.F. Knowles.

from forested areas (canopy plus surface sublimation) accounted for the majority of modeled snow sublimation losses across the study domain and highlights the importance of sublimation from snow stored in the forest canopy in this region. Results from this study suggest that snow sublimation is a significant component of the winter water balance and is equivalent to 43 percent of seasonal snowfall on average, which has important implications for future water management and decision making.

4.2 Introduction

In the mountains of the western United States, snow water equivalent (SWE) stored in seasonal snowpacks provides a critical water resource for ecological and human needs. Considerable research has focused on characterizing and forecasting snow accumulation, snowmelt and runoff in this region [e.g., *Dozier*, 2011]. In the simplest terms, the snow cover mass balance for characterizing snowmelt water available for soil recharge, vegetation uptake, and runoff to streams each year can be described as total winter precipitation minus net snow sublimation [*Liston and Sturm*, 2004]. However, in reality, the seasonal snow cover is dynamic and exhibits considerable variability over space and time from wind-induced drifting and transport and interactions with topography and canopy features, thus is difficult to characterize across mountainous landscapes [e.g., *Elder et al.*, 1991]. Additionally, there is considerable uncertainty in measuring both precipitation [e.g., *Goodison et al.*, 1998] and snow sublimation [e.g., *Sexstone et al.*, 2016b] and reliable winter observations of these variables are sparse [*Bales et al.*, 2006]. In arid and semi-arid regions of the western U.S., snow sublimation has been suggested by various carefully executed studies to be an important component of the snow cover mass balance [e.g., *Meiman and Grant*, 1974; *Kattelmann and Elder*, 1991; *Marks and Dozier*, 1992; *Cline*, 1997b; *Hood et al.*, 1999; *Montesi et al.*, 2004; *Molotch et al.*, 2007; *Marks et al.*,

2008; *Gustafson et al.*, 2010; *Reba et al.*, 2012; *Knowles et al.*, 2015b; *Sexstone et al.*, 2016b]. However, these investigations are based on point measurements that have limited distribution in space and time and present a wide range of results, and little research has evaluated the spatial and temporal variability of snow sublimation within the complex mountainous terrain of this region. Given the importance of seasonal snow for water availability in the western United States as well as the potential significance of snow sublimation losses within the annual water balance, there is a need for a better understanding of the interannual importance of snow sublimation across mountainous environments in this region.

Snow sublimation is defined as the transfer of water directly between snow and the atmosphere through phase change, and encompasses water vapor fluxes between the atmosphere and the snowpack surface (surface sublimation), intercepted snow held within the forest canopy (canopy sublimation), and snow being transported by wind (blowing sublimation). Previous studies have reported a wide range of importance for surface sublimation in the snow cover mass balance, but in mountainous areas of the western United States, estimates of surface sublimation have often been on the order of 10 – 20 percent of annual snowfall in open areas [e.g, *Kattelmann and Elder*, 1991; *Marks and Dozier*, 1992; *Hood et al.*, 1999; *Reba et al.*, 2012; *Sexstone et al.*, 2016b] and less than 10 percent of annual snowfall in sheltered and subcanopy areas [e.g, *Marks et al.*, 2008; *Reba et al.*, 2012]. Canopy sublimation in various coniferous forest types has been suggested to be on the order of 30 – 40 percent of annual snowfall [*Pomeroy and Gray*, 1995], and in the Colorado Rocky Mountains, canopy sublimation measured by *Montesi et al.* [2004] accounted for 20 – 30 percent of total snowfall. Estimations of blowing sublimation from different environments vary greatly and have often been estimated to be a significant loss from the snow cover mass balance, ranging between 10 – 50 percent of

seasonal snowfall [*Pomeroy and Gray*, 1995; *Pomeroy and Essery*, 1999]. However, other studies have suggested that temperature and humidity feedbacks during blowing sublimation events limit this process [*Déry et al.*, 1998], and that blowing sublimation losses restricted by these feedbacks account for only 0.1 percent, and locally as much as 1.8 percent, of annual snowfall [*Groot Zwaaftink et al.*, 2013]. The spatial variability and importance of snow sublimation in mountainous environments is complex and likely driven by variations of land cover, topography, and meteorology [e.g., *Strasser et al.*, 2008]. Therefore, process-based snow modeling systems that can simulate important snowpack processes over space and time [e.g., *Lehning et al.*, 2006; *Liston and Elder*, 2006b; *Pomeroy et al.*, 2007] provide the opportunity to evaluate the role of snow sublimation across various snow and climate regimes that rely on snowmelt as an important water resource.

In this study, we use SnowModel [*Liston and Elder*, 2006b], a process-based snow evolution model, to simulate snowpack processes for five water years (WY) (i.e. period beginning 1 October and ending 30 September of the given year) over a model domain across the Front Range Mountains of north-central Colorado, U.S.A. Model simulations allow for quantification of surface, canopy, and blowing sublimation across the domain for each year of the study. The specific objectives of this modeling study were to (1) evaluate the performance of modeled snow sublimation compared to station measurements of winter period water vapor fluxes via eddy covariance, (2) determine the spatial and temporal variability of modeled snow sublimation across the domain, and (3) quantify the importance of the individual components and total of snow sublimation contributing to the seasonal ablation of the snowpack.

4.3 Methods

4.3.1 Study domain

The study domain is a 40 km x 90 km area (centered at 40.18°N, 105.71°W) and ranges in elevation from 2261 m to 4345 m (mean elevation of 3059 m) (Figure 4.1). Approximately 22 percent of this area is above treeline (i.e. bare rock and alpine tundra), 58 percent is forested, and 20 percent is nonforested below treeline (i.e grasslands, wetlands, shrublands, open water, and developed) (land cover information accessed: <http://www.mrlc.gov/nlcd2011.php>). The lowest elevations are characterized by gentle sloping topographic features while the highest elevations exhibit steep and complex topography. The Continental Divide intersects the study domain from north to south, therefore dominant eastern (western) aspects are located on the eastern (western) side of the study area (Figure 4.1). The study domain is located within the headwaters of both the Upper Colorado River Basin and Missouri River Basin and the majority of the domain is comprised of Federal Lands, including Rocky Mountain National Park and the Arapaho and Roosevelt National Forests and associated Wilderness. The Front Range Mountains accumulate continental seasonal snowpacks [*Trujillo and Molotch,* 2014] that can be characterized by persistent, transitional, and intermittent snow cover zones [*Richer et al.*, 2013] and generally exhibit peak snow accumulation during the springtime months of April and May each year.

4.3.2 Model description

SnowModel is a spatially distributed snowpack evolution modeling system specifically designed to be applicable over a wide range of topography, land cover, and climate conditions where precipitation falls as snow [*Liston and Elder,* 2006b]. SnowModel includes four sub-models: MicroMet [*Liston and Elder*, 2006a], which is a meteorological distribution model; EnBal [*Liston*, 1995], which calculates surface exchanges between the snow and atmosphere ;

SnowPack [*Liston and Hall*, 1995], which simulates the seasonal evolution of snowpack properties; and SnowTran-3D [*Liston et al.*, 2007], which accounts for snow redistribution by wind. Spatially varying fields of elevation and land cover, along with temporally varying meteorological forcing data, are required to run SnowModel, and it can be operated at varying grid resolutions as fine as 1 m. SnowModel simulates the spatial distribution and seasonal evolution of snow using the first-order physics described in the sub-models above (see citations). The ability of SnowModel to accurately represent snow sublimation is particularly important for the simulation of the spatial distribution of SWE in complex forested and nonforested mountainous terrain. In addition to calculating surface sublimation from the snowpack, SnowModel also simulates blowing snow sublimation processes important in alpine and tundra environments as well as canopy interception and sublimation in forested environments. The equations used for calculating each component of snow sublimation are described below.

4.3.2.1 Surface sublimation

Surface sublimation is computed within SnowModel based on the turbulent flux of latent heat (Q_E) and the latent heat of sublimation (L_s) [*Oke*, 1987]. The turbulent flux of latent heat (Q_E) is calculated using the bulk aerodynamic flux formulation described by *Price and Dunne* [1976]

$$Q_E = \rho L_s C_E \zeta (q_r - q_0) \tag{4.1}$$

where ρ is the air density, ζ is the non-dimensional atmospheric stability parameter, q_r and q_s are the specific humidity at the reference height and snow surface, respectively, and C_E is the transfer coefficient for latent heat,

$$C_E = \frac{k^2 u_r}{\left[\ln\left(z_r / z_0\right)\right]^2} \tag{4.2}$$

where k is von Karman's constant (0.41), u_r is the wind speed at reference height (z_r), and z_0 is the aerodynamic roughness length. The atmospheric stability parameter (ζ) is calculated based on the parameterization presented by [*Louis*, 1979]. In unstable atmospheric conditions, the bulk Richardson number (Ri)

$$Ri = \frac{g}{\theta}\frac{\partial\theta/\partial z}{\left(\partial u/\partial z\right)^2} \tag{4.3}$$

is greater than 0, and the atmospheric stability parameter is calculated by

$$\zeta = 1 - \frac{\eta Ri}{1+\gamma\left|Ri\right|^{0.5}} \tag{4.4}$$

where g is the acceleration due to gravity, θ is the potential temperature, η = 9.4, and

$$\gamma = \varphi\eta\frac{C_E}{u_r}\left(\frac{z_r}{z_0}\right)^{0.5} \tag{4.5}$$

where φ = 5.3. In stable atmospheric conditions ($Ri > 0$)

$$\zeta = \left[1+\left(\frac{\eta}{2}\right)Ri\right]^{-2}. \tag{4.6}$$

This system of equations along with the other energy balance equations described by the EnBal sub-model are solved iteratively for snow surface temperature [*Liston*, 1995].

4.3.2.2 Canopy sublimation

The sublimation rate of snow held within the forest canopy (Q_{cs}) is computed within SnowModel based on a nondimensional canopy exposure coefficient (C_e), the canopy-intercepted load (I) at time (t), and the sublimation-loss rate coefficient (Ψ_s)

$$Q_{cs} = C_e I \Psi_s dt\,. \tag{4.7}$$

Refer to *Liston and Elder* [2006b] for details on the canopy exposure coefficient, canopy-intercepted load, and sublimation-loss rate coefficient.

4.3.2.3 Blowing sublimation

The sublimation rate of wind-transported snow per unit area of snow cover (Q_v) is computed within SnowModel as

$$Q_v(x^*) = \Psi_S \phi_S h_* + \int_{h_*}^{z_t} \Psi_t(x^*, z)\phi_t(x^*, z)dz \tag{4.8}$$

where x^* is the horizontal coordinate in a reference frame defined by the windflow direction, the subscripts *S* and *t* represent the saltation and turbulent suspension layers, respectively, h_* is the height of the saltation layer and z_t is the height of the turbulent suspension layer, Ψ is the sublimation loss-rate coefficient, and ϕ is the vertical mass-concentration distribution. Refer to *Liston and Sturm* [1998] for detail on the sublimation loss-rate coefficient and for a description of model computation of wind-transport of snow in saltation and suspension.

4.3.3 Model simulations

SnowModel was run across the 3600 km^2 model domain (Figure 4.1) at a grid resolution of 100 m (360000 model domain cells) for an hourly time step from WY 2011 through WY 2015. The spatially varying fields of elevation and land cover used for these simulations were provided by the USGS national elevation dataset and national land cover database spatial datasets (30 m grid resolution) (http://ned.usgs.gov and http://www.mrlc.gov/nlcd2011.php, respectively) and were resampled to a 100 m grid resolution. The land cover dataset was reclassified based on the predefined vegetation types defined by SnowModel [*Liston and Elder*, 2006b]. Spatially and temporally distributed meteorological forcing data used to drive model simulations, included air temperature, precipitation, relative humidity, wind speed, and wind direction. MicroMet [*Liston and Elder*, 2006a] uses meteorological data from point locations and performs spatial and temporal interpolations to create the spatially distributed forcing data. The sub-model also provides the option to assimilate observed incoming shortwave and longwave

radiation and surface pressure into modeled meteorological forcings [*Liston and Elder*, 2006a]. In this study, hourly observations from 34 meteorological stations within the model domain were utilized within MicroMet (Table 4.1; Figure 4.1). The forcing data can generally be described as SNOTEL stations and meteorological stations; the SNOTEL stations (n = 18) provided air temperature and precipitation observations, and the meteorological stations (n = 16) provided air temperature, relative humidity, and wind speed and direction observations. Additionally, observations from the US-NR1 AmeriFlux tower [*Turnipseed et al.*, 2002] were used to assimilate observed incoming shortwave and longwave radiation and surface pressure into the modeled forcing data. The default northern hemisphere monthly lapse rates for air temperature and vapor pressure and precipitation adjustment factors for elevation [refer to Table 1 from *Liston and Elder*, 2006a] were used. Additionally, an adjustment factor for wind speed increase and decrease with elevation (similar to that of precipitation) of 2.0 km^{-1} was applied. The wind speed adjustment was derived from observed meteorological station wind speeds with elevation to aid the simulation of wind fields in areas with sparse observations, such as the northeastern portion of the study domain (Figure 4.1). Station data from each of the sites listed in Table 4.1 were quality assured according to the quality checking procedures outlined by *Meek and Hatfield* [1994] and *Serreze et al.* [1999]. All station observations were resampled to an hourly time interval for local standard time. Gap filling of missing meteorological data from individual stations was not completed as missing values were filled by the spatial interpolations completed by MicroMet.

4.3.4 Model verification

4.3.4.1 Snow water equivalent

Daily observations of SWE at SNOTEL stations within the model domain (Table 4.1) were used to assess the performance of modeled snow cover mass balance for each WY. Snow pillows that measure SWE at SNOTEL stations are located in small forested openings, and to ensure that the modeled SWE at SNOTEL stations by SnowModel was not influenced by forest canopy processes (e.g. canopy interception and sublimation), land cover grids (100 m) that overlap SNOTEL station locations were classified as the grassland vegetation type. Modeled SWE for each WY was evaluated versus observed SWE at each SNOTEL station within the model domain. Although the main focus of this paper is the simulation of snow sublimation, it was also important to assess the ability of the model to accurately simulate the snow cover mass balance so the relative importance of snow sublimation losses could be assessed.

4.3.4.2 Snow sublimation

Measurements of water vapor fluxes by the eddy covariance (EC) method were collected during the winter periods of the study and used to quantify snow sublimation at four sites within the model domain. Snow sublimation has been quantified using the EC method by many studies [e.g., *Pomeroy and Essery*, 1999; *Molotch et al.*, 2007; *Marks et al.*, 2008; *Helgason and Pomeroy*, 2012b; *Knowles et al.*, 2012; *Reba et al.*, 2012; *Sexstone et al.*, 2016b], and *Sexstone et al.* [2016b] provides a discussion of the relative merits and limitations of this method for monitoring surface sublimation. Eddy covariance measurements were made at the Arrow (forested opening) [*Sexstone et al.*, 2016b], Andrews Meadow (subalpine meadow), US-NR1 (subalpine forest) [*Turnipseed et al.*, 2002], and T-Van (alpine tundra) [*Knowles et al.*, 2012] sites (Figure 4.1). The Arrow site (2955 m) is located within a moderately sloping (20 percent;

290° aspect), large (~ 600 m) grassland opening of surrounding lodgepole pine (*Pinus contorta*) forest. The Andrews Meadow site (3205 m) is located in a small (~ 150 m) subalpine wetland meadow within the Loch Vale watershed, Rocky Mountain National Park. Measurements collected by EC were made at the Arrow and Andrews Meadow sites during the snow-covered periods of WY 2014 and WY 2015. The US-NR1 site (3050 m) is an AmeriFlux tower that is positioned within subalpine forest composed of subalpine fir (*Abies lasiocarpa*), Engelmann spruce (*Picea engelmannii*), and lodgepole pine with EC instrumentation located approximately 10 m above the top of the forest canopy. The T-Van site (3503 m) is positioned within gently sloping (8 percent) alpine tundra located on Niwot Ridge. Both the US-NR1 and T-Van sites are located within the Niwot Ridge LTER study area and EC measurements at these sites were collected during October 2011 through December 2014 of the study period. Water vapor fluxes were calculated at each site based on the covariance between vertical wind speed and water vapor density fluctuations. Post processing of the EC water vapor fluxes consisted of the standard EC corrections, data screening, and gap-filling [e.g., *Reba et al.*, 2009]. A detailed description of the post processing methods used for the Arrow and Andrews Meadow sites is described in *Sexstone et al.* [2016b], and details for post processing of US-NR1 and T-Van fluxes is described by *Burns et al.* [2014] and *Knowles et al.* [2012], respectively.

Modeled cumulative and daily snow sublimation was compared to water vapor fluxes measured at EC sites within the model domain. The evaluation of modeled snow sublimation at the Arrow, Andrews Meadow, and T-Van sites included a comparison of simulated surface and blowing sublimation to the observed EC sublimation flux. Blowing snow sublimation that occurs below the height of EC instrumentation (~1.5 – 3.0 m above the snow surface) is expected to be measured by these sensors [*Pomeroy and Essery*, 1999]. However, in high wind speeds, blowing

snow within suspension may sublimate above the height of the sensors [*Pomeroy and Male*, 1992; *Pomeroy and Gray*, 1995]. Winter time water vapor fluxes measured at the US-NR1 site include snow sublimation from both surface sublimation from the subcanopy and canopy sublimation from intercepted snow [*Molotch et al.*, 2007]; thus, a comparison of the sum of simulated surface and canopy sublimation was made with the *in-situ* EC observations at this site.

4.4 Results and Discussion

4.4.1 Meteorological conditions

Mean SNOTEL air temperature and total precipitation from November through April for the five years analyzed represents a wide range in winter precipitation and to a lesser extent mean air temperature across the domain (Table 4.2). Winter precipitation in WY 2011 represents a relatively wet year and WY 2012 represents a relatively dry year, with WY 2012 receiving less than half of the precipitation observed in WY 2011. Mean air temperatures in WY 2011 and WY 2013 (WY 2012 and WY 2015) represent relatively colder (warmer) snow season air temperatures across the domain. Air temperatures are often positively correlated with sublimation rates and total seasonal snow sublimation has been suggested to scale with total precipitation [e.g., *Reba et al.*, 2012; *Sexstone et al.*, 2016b]; therefore, evaluating the spatial and temporal variability of snow sublimation in the context of relative meteorological conditions may be important for understanding the intra- and inter-annual variability of these water vapor fluxes.

4.4.2 Snow water equivalent model verification

Initial simulations show that the model is able to represent the seasonal evolution of SWE at some SNOTEL stations, but shows poor results at others (Figure 4.2). Further evaluation showed that the poor results occur at sites located in a favorable position for high above canopy wind speeds and are caused by blowing snow transport and surface/blowing sublimation (e.g.,

Figure 4.2c and 4.2d). These errors are related to trying to represent a SNOTEL snow pillow (~ 4 - 5 m^2) by a 10,000 m^2 model grid [*Kashipazha*, 2012; *Meromy et al.*, 2013]. Given that SNOTEL stations are most often sited within small sheltered forest openings where little wind redistribution is expected [*Meyer et al.*, 2012], modeled blowing snow transport was subsequently turned off at SNOTEL station model grids, which markedly improved simulation results (Figure 4.3). Modeled SWE is biased low at SNOTEL sites, but the magnitude of these simulation errors is variable from site to site (Figure 4.3). The correlation coefficient (*r*), Nash-Sutcliffe efficiency (*NSE*), percent bias (*PBias*) and root mean squared error (*RMSE*) of modeled versus observed SWE at all SNOTEL sites (n = 18) across all years is 0.92, 0.81, -14.7%, and 88.5 mm, respectively. Model errors in SWE simulation may be attributed to differences in precipitation gage undercatch among SNOTEL stations [e.g., *Goodison et al.*, 1998; *Fassnacht*, 2004; *Meyer et al.*, 2012]. Additionally, modeled SWE at some stations, such as the Niwot SNOTEL (Figure 4.3), show an early onset of snowmelt not reflected by the SNOTEL observations, which contributes to the low bias of modeled SWE. Modeled snowmelt errors may be related to a high bias of solar radiation inputs, as the SNOTEL model grids are not shaded by the surrounding forested area but SNOTEL snow pillows often are. These precipitation and snowmelt errors could likely be lessened through assimilating the SNOTEL SWE observations into SnowModel to adjust the precipitation inputs and snowmelt rates [*Liston and Hiemstra*, 2008]. However, it is also possible that the negative bias of modeled SWE could be related to an overestimation of modeled surface sublimation within the forested openings where the SNOTEL sites are located, since some canopy is actually present around most SNOTEL stations and could reduce wind movement across the snow surface.

4.4.3 Snow sublimation model verification

The modeled versus observed snow sublimation at the Arrow and US-NR1 sites show similar magnitudes and temporal evolution, but discrepancies are observed at the Andrews Meadow and T-Van sites (Figure 4.4). Modeled snow sublimation at the Andrews Meadow shows a consistent low bias when compared to the EC observations. These biases may be related to site specific conditions that were not well represented by model simulations. For instance changes of surface layer conditions between the subalpine meadow where Andrews Meadow is sited compared to the steep talus field upwind from the site could be responsible for differences in observed and modeled snow sublimation. The large discrepancies in modeled versus observed snow sublimation at the T-Van may be related to the representativeness of the *in-situ* EC observations made at 3 m above the surface. In very high wind speeds, characteristic of the T-Van site, eddy covariance sensors close to the snow surface may only be measuring water vapor fluxes from the surface sublimation component [*Knowles et al.*, 2012] because the majority of blowing snow transport and sublimation is expected to occur from blowing snow within suspension [*Pomeroy and Male*, 1992], above the height of the EC instrumentation and up to a height of approximately 10 m [*Pomeroy and Gray*, 1995]. However, at moderate wind speeds when the friction velocity in approaching the threshold for drifting snow [e.g., *Schmidt*, 1980; *Clifton et al.*, 2006], more characteristic of the Arrow and Andrews Meadow sites, much of the blowing sublimation may occur during saltation [e.g., *Pomeroy and Gray*, 1990; *Dai and Huang*, 2014] or lower suspension movement and sensed by the EC instrumentation. Therefore, in subsequent sections a comparison will be made between *in-situ* EC observations with both modeled snow sublimation (sum of surface, canopy, and blowing sublimation) and modeled snow sublimation excluding blowing sublimation (sum of surface and canopy sublimation).

The seasonal mean daily observed and modeled snow sublimation rates are shown to be fairly consistent from year-to-year at each site (Figure 4.5). The mean observed (modeled) sublimation rate over all years with valid data is 0.35 mm day^{-1} (0.36 mm day^{-1}) at the Arrow site, 0.48 mm day^{-1} (0.25 mm day^{-1}) at the Andrews Meadow site, 1.35 mm day^{-1} (1.52 mm day^{-1}) at the US-NR1 site, and 0.62 mm day^{-1} (2.76 mm day^{-1}) at the T-Van site. The mean modeled snow sublimation excluding blowing sublimation at the T-Van site is 1.07 mm day^{-1}, which compares more favorably with the observed mean at this site, but is still biased high (Figure 4.5b). A comparison between daily observed and modeled snow sublimation is displayed in Figure 4.6 and summary statistics are provided in Table 4.3. There is considerable scatter around the one-to-one line at the Arrow and US-NR1 sites, but the mean correlation coefficient of 0.66 and 0.62 and *PBias* of 5.8% and 14.9%, respectively, were satisfactory at these sites. The Andrews Meadow site shows a low bias of modeled snow sublimation with mean correlation coefficient of 0.52 and *PBias* of -48.8%. A high bias was observed at the T-Van site, with modeled daily snow sublimation excluding blowing sublimation exceeding observed daily snow sublimation (mean r = 0.42 and *PBias* = 75.5%).

The verification of modeled snow sublimation with EC observations presented here provides confidence that SnowModel is able to realistically represent the seasonal evolution and magnitude of surface and canopy sublimation within the range of EC measurement uncertainty [*Knowles et al.*, 2012; *Knowles et al.*, 2015b; *Sexstone et al.*, 2016b] at the Arrow and US-NR1 sites, but also highlights potential limitations in modeling specific site conditions at the Andrews Meadow and T-Van sites. The low bias of modeled snow sublimation at the Andrews Meadow site may be related the challenges with EC observations and/or modeling the atmospheric boundary layer in complex terrain. The Andrews Meadow site is located in a flat subalpine

meadow with limited fetch that is surrounded by steep and rugged bedrock cliffs (see photograph in Figure 4.1) which can create challenges for both EC measurements [*Turnipseed et al.*, 2003; *Turnipseed et al.*, 2004] and windflow modeling [e.g., *Musselman et al.*, 2015]. Additionally, the discrepancies between modeled blowing sublimation and EC observations at the T-Van site highlights the challenges of measuring both surface and blowing sublimation fluxes in alpine environments. *Knowles et al.* [2012] assumed that measured EC sublimation from the T-Van site (2007 through 2009) was representative of surface sublimation and estimated winter blowing sublimation to be on the order of 188 – 281 mm, which is similar to the modeled blowing sublimation at T-Van during WY 2012. *Knowles et al.* [2012] also found snow sublimation fluxes from the T-Van site to be snow limited because snow was often blown free from the site, which may help explain the high bias of modeled surface sublimation compared to EC observations. Given that model verification of blowing sublimation was not possible with the experimental setup of this study, blowing sublimation is considered to be an important uncertainty in the modeled snow sublimation. These findings suggest that future investigations should focus on an experimental setup for measuring both surface and blowing sublimation fluxes in alpine regions.

It is likely that modeled snow sublimation is somewhat sensitive to parameter representations of the aerodynamic roughness length (z_0) [e.g., *Reba et al.*, 2014] and/or the atmospheric stability parameter (ζ) [e.g., *Andreas et al.*, 2010], and may also be sensitive to the representation of snow albedo given the importance of solar radiation within the snow cover energy balance [*Marks and Dozier*, 1992]. However, these parameters are expected to exhibit spatial variability across the domain, and the parameterizations in SnowModel have been developed to generally represent processes across many snow-covered regions. Additionally,

modeled snow sublimation across the domain is expected to be most sensitive to the uncertainties in the spatially distributed meteorological forcing data; therefore, this study did not focus on calibrating site specific parameters to the EC observations.

4.4.4 Model simulation results

In the following, results are presented from SnowModel simulations over five water years (WY 2011 through WY 2015) for the 40 km x 90 km study domain within the Front Range Mountains of north-central Colorado, U.S.A (Figure 4.1).

4.4.4.1 Spatial variability of snow sublimation

Domain-wide mean total surface sublimation ranged from 42 mm in WY 2012 to 61 mm in WY 2011 (Table 4.4). Surface sublimation was generally smallest at the lowest elevations that receive short snow cover durations as well as within forested areas (i.e. subcanopy) while the greatest surface sublimation occurred at the highest elevations in alpine areas (Figure 4.7). The mean accumulated surface sublimation over each snow season highlights that the greatest surface sublimation occurs in alpine areas on the eastern side of the Continental Divide (Figure 4.8). This is likely because Mean total canopy sublimation across the domain ranged from 99 mm in WY 2012 to 170 mm in WY 2011 (Table 4.4). Canopy sublimation increased with increasing snowfall events, which is strongly correlated with total winter precipitation. Coniferous forests dominate the land cover across the domain (Figure 4.1), and within these areas, canopy sublimation was shown to increase with increasing elevation (Figure 4.7). Total canopy sublimation was variable from year-to-year with the greatest variability occurring in the northern half of the domain (Figure 4.8). Blowing sublimation was limited to nonforested areas above and below treeline and was shown to increase with elevation (Figure 4.8). The mean total blowing sublimation across the domain ranged from 27 mm in WY 2015 to 73 mm in WY 2011 (Table

4.4), however, localized totals in high elevation alpine areas often exceeded 1000 mm (Figure 4.7).

Few studies have evaluated the spatial and temporal variability of snow sublimation across the basin scale within mountainous areas that contain both forested and alpine areas; however, the results presented in this study are comparable to model simulations of snow sublimation within a 201 km^2 domain in Berchtesgaden National Park, Germany [*Strasser et al.*, 2008]. *Strasser et al.* [2008] found snow sublimation to exhibit considerable variability across the domain with snow sublimation in the valley bottoms and forested areas on the order of 100 mm and snow sublimation from localized alpine ridges up to 1200 mm. A comparison of seasonal snow sublimation from this study (Table 4.4) with results from *Strasser et al.* [2008, refer to Table 2] shows that the domain averaged surface, canopy, and blowing sublimation rates observed in this study are similar but greater. Additionally, both studies highlight that domain averaged canopy sublimation is most important, followed by surface sublimation then blowing sublimation; however these averages are highly influenced by the percentage of forested and alpine areas across the domain.

4.4.4.2 Percentage of snowfall lost to snow sublimation

Annual snowfall totals (Figure 4.9) were variable from year-to-year and scale according to the summarized relative precipitation conditions at SNOTEL sites (Table 4.2). Snowfall totals increased with elevation and also showed a pattern of greater snowfall amounts in the northern half of the domain. Annual snowmelt totals (Figure 4.9) highlight the role that wind redistribution of snow, snow sublimation, as well as inputs from precipitation as rain play in the mass balance of precipitation falling as snow versus snowmelt input into the soil.

Across the model domain, the mean total snow sublimation (sum of surface, canopy, and blowing sublimation) ranged from 170 mm in WY 2012 to 304 mm in WY 2011 and the mean percentage of snowfall lost to snow sublimation ranged from 37% in WY 2015 to 50% in WY 2012 (Table 4.4). The mean five-year seasonal sublimation rates are greatest at highest elevations, particularly on the windward side of ridges within alpine areas because of the combination of surface and blowing sublimation (Figure 4.10). However, total sublimation in forested areas is also substantial, and the greatest percentage of snowfall lost to sublimation occurs within forested areas because of the efficiency of canopy sublimation of intercepted snow as well as the lower amount of snowfall received in the lower elevation forested areas (Figure 4.10).

A key finding of this research is that on average 43 percent of annual snowfall is lost to snow sublimation in north-central Colorado Rocky Mountains. Investigations in the Arctic and Canadian Prairies have estimated that 15 – 50 percent of the snow cover is returned to the atmosphere by snow sublimation [*Liston and Sturm*, 2004]. Additionally, estimations of snow sublimation in mountainous areas vary greatly and generally range between 10 – 60 percent of annual snowfall, but many of these investigations are based on site-specific measurements that do not take into account the spatial variability of this process. Recent modeling studies of the importance of snow sublimation in mountainous areas have presented varying results. *Strasser et al.* [2008] show that snow sublimation can vary by as much as 10 – 90 percent of annual snowfall across Berchtesgaden National Park, Germany, but on average 22 percent of snowfall is lost to snow sublimation. Additionally, *MacDonald et al.* [2010] estimated snow sublimation losses to account for 20 – 32 percent of cumulative snowfall in the alpine of the Canadian Rocky

Mountains, and *Gascoin et al.* [2013] suggested snow sublimation accounts for 71 percent of total ablation in the Dry Andes of Chile.

The assessment of the importance of modeled snow sublimation in the snow-cover mass balance is particularly valuable given the range of relative meteorological conditions over the five years of this study (Table 4.2). Total snow sublimation generally increases with increasing snowfall and snow-cover duration (Table 4.4). However, the importance of snow sublimation in snow ablation is greatest in the low snow years with warm temperatures (Tables 4.2 and 4.4). This is particularly evident when comparing WY 2011 and WY 2012, which were very high and low snow years in this region, and account for 42 percent and 50 percent of total ablation, respectively. In the context of changing climate, these results have important implications for future regional snow water resources.

4.4.4.3 Variability of snow sublimation between land covers

To assess the variability of snow sublimation between different land cover types, the study domain was classified into three land cover categories: alpine (i.e. above treeline), forested, and nonforested below treeline (refer to the *Study Domain* section above). The mean total snow sublimation over each year was greatest within the alpine and included substantial blowing and surface sublimation (Figure 4.11). Mean total snow sublimation within the forests consisted of both canopy and surface sublimation and was slightly less than that of the alpine area, but mean total canopy sublimation was greater than each of the individual sublimation components within all land covers (Figure 4.11, Table 4.4). The mean total snow sublimation within open areas below treeline (i.e. nonforested below treeline) included a moderate contribution from surface sublimation as well as small contributions from canopy and blowing sublimation and was considerably less than the mean total snow sublimation in alpine and

forested areas (Figure 4.11). When the model domain land cover distribution is considered (approximately 22% alpine, 58% forest, and 20% open below treeline), the weighted percentage of total mean snow sublimation across the domain that occurs in the alpine, forest, and open below treeline is 29%, 65%, 6%, respectively. This suggests that snow sublimation fluxes in forested area play a particularly important role in the snow cover mass balance across the model domain. The spatial variability of snow sublimation across the model domain is shown to be largely driven by differences in land cover type. Therefore, future water balance studies considering losses from snow sublimation should account for differences related to land cover distribution [e.g., *Knowles et al.*, 2015b], and measurement campaigns in mountainous regions should consider an experimental setup that represents snow sublimation from alpine, forested, and openings below treeline.

4.4.5 Model uncertainty

The greatest uncertainty in modeling snow sublimation across the domain is likely related to uncertainties in the spatially interpolated meteorological forcing data, particularly the precipitation and wind speed datasets. Winter precipitation is notoriously difficult to measure at gages because of wind effects [*Goodison et al.*, 1998], and reliable measurements of precipitation in alpine areas are rarely available. Additionally, although there is good spatial coverage of SNOTEL precipitation gages across the model domain, these gages are generally located below treeline at similar elevations, making a thorough evaluation of the precipitation lapse rate used by the model challenging. Uncertainties in the precipitation forcing data do not likely have an influence on modeled snow sublimation rates; however, they could have a strong influence on the calculated importance of snow sublimation in the snow-cover mass balance. Modeled snow sublimation is also expected to be very sensitive to the uncertainties and errors in

the spatially distributed wind speeds [*Dadic et al.*, 2013]. *Gascoin et al.* [2013] found that the windflow model used by SnowModel [*Liston et al.*, 2007] performed well representing the synoptic wind conditions in high elevation areas, but that the model was not able to represent windflow conditions important in the valley locations that are influenced by local topography and the diurnal cycle. These uncertainties may explain the need for this study to include a wind speed correction factor for elevation. *Musselman et al.* [2015] evaluated three windflow models, including that of *Liston et al.* [2007], and found that the snow-cover mass balance was highly sensitive to the model configuration; differences in simulated windflow lead to a range of blowing sublimation from 10.5 to 19 percent of seasonal snowfall [*Musselman et al.*, 2015]. Therefore, the potential errors related to modeled windflow are expected to be particularly important for the uncertainty in modeled snow sublimation across the domain.

4.5 Conclusions

This study has investigated the spatial and temporal variability and importance of snow sublimation across the north-central Colorado Rocky Mountains using a process-based snow model. Model verification shows that modeled SWE at SNOTEL stations compares well to observations but is biased slightly low because of gage undercatch of precipitation measurements and the influence of canopy shading by surrounding forested areas. Also, snow sublimation observations by EC generally compare well to modeled values at sites where surface and canopy sublimation are the dominant snow sublimation fluxes. However, EC observations are shown to have limited utility for verification of modeled blowing sublimation because these fluxes often occur from the turbulent suspension of snow and cannot always be resolved by EC observations. Modeled snow sublimation was shown to exhibit substantial spatial and temporal variability across the model domain, with the greatest cumulative snow sublimation occurring at the highest

elevations and in years with the greatest snowfall. The spatial variability of snow sublimation was well correlated with land cover type, with substantial snow sublimation rates occurring in alpine and forested areas, and relatively low sublimation rates occurring in open areas below treeline. Across the model domain, snow sublimation from forested areas (canopy plus surface sublimation) dominated water vapor losses from the snowpack, indicating the importance of canopy sublimation in this region. On average, snow sublimation losses were equivalent to 43 percent of seasonal snowfall and the importance of snow sublimation (as a percentage of total snowfall) was shown to increase in low snow years. These results suggest that snow sublimation is a significant component of the winter water balance in this region and have important implications for future water management and decision making.

Table 4.1. List of SNOTEL and meteorological stations used as forcing data within SnowModel. *T* is air temperature; *P* is precipitation; *RH* is relative humidity; *WS* and *WD* are wind speed and direction, respectively, and the subscript denotes measurement height; *Pa* is surface pressure; *SI* is incoming shortwave radiation; *LI* is incoming longwave radiation; *SWE* is snow water equivalent; and SUB_{EC} is snow sublimation measured by eddy covariance.

Station Name	Station Type	Station ID	Station Elevation (m)	Water Years	Forcing Variables	Model Verification
Hourglass Lake	SNOTEL	1122	2869	11,12,13,14,15	*T, P*	*SWE*
Long Draw Resv	SNOTEL	1123	3052	11,12,13,14,15	*T, P*	*SWE*
Joe Wright	SNOTEL	551	3094	11,12,13,14,15	*T, P*	*SWE*
Willow Park	SNOTEL	870	3263	11,12,13,14,15	*T, P*	*SWE*
Lake Irene	SNOTEL	565	3254	11,12,13,14,15	*T, P*	*SWE*
Phantom Valley	SNOTEL	688	2748	11,12,13,14,15	*T, P*	*SWE*
Stillwater Creek	SNOTEL	793	2675	11,12,13,14,15	*T, P*	*SWE*
Bear Lake	SNOTEL	322	2909	11,12,13,14,15	*T, P*	*SWE*
Wild Basin	SNOTEL	1042	2878	11,12,13,14,15	*T, P*	*SWE*
Copeland Lake	SNOTEL	412	2608	11,12,13,14,15	*T, P*	*SWE*
Sawtooth	SNOTEL	1251	2968	15	*T, P*	*SWE*
University Camp	SNOTEL	838	3152	11,12,13,14,15	*T, P*	*SWE*
Niwot	SNOTEL	663	3033	11,12,13,14,15	*T, P*	*SWE*
Lake Eldora	SNOTEL	564	2964	11,12,13,14,15	*T, P*	*SWE*
High Lonesome	SNOTEL	1187	3263	14,15	*T, P*	*SWE*
Arrow	SNOTEL	305	2941	11,12,13	*T, P*	*SWE*
Fool Creek	SNOTEL	1186	3399	12,13,14,15	*T, P*	*SWE*
Berthoud Summit	SNOTEL	335	3448	11,12,13,14,15	*T, P*	*SWE*
Arrow	USGS	2201	2955	11,12,13,14,15	*T, RH,* WS_3, WD_3	SUB_{EC}
Cabin	USGS	2202	2810	11,12,13,14,15	*T, RH*	---
Snow Mtn Ranch	USGS	2203	2673	11,12,13,14,15	*T, RH,* WS_3, WD_3	---
Ranch Creek	USGS	2204	3603	11,12,13,14,15	*T, RH,* WS_2, WD_2	---
High Lonesome	USGS	2205	3309	11,12,13,14,15	*T, RH*	---
Main	USGS	2206	3162	11,12,13,14,15	*T, RH,* $WS_{2,6}$, $WD_{2,6}$	---
Andrews Meadow	USGS	2207	3205	11,12,13,14,15	*T, RH,* WS_4, WD_4	SUB_{EC}
Sharkstooth	USGS	2208	3514	11,12,13,14,15	*T, RH,* WS_3, WD_3	---
Estes Park	RAWS	3301	2397	11,12,13,14,15	*T, RH,* $WS_{6,}$ WD_6	---
Harbison Meadow	RAWS	3302	2648	11,12,13,14,15	*T, RH,* $WS_{6,}$ WD_6	---
Pickle Gulch	RAWS	3303	2840	11,12,13,14,15	*T, RH,* $WS_{6,}$ WD_6	---
Cameron Pass	CAIC	4401	3223	12,13,14,15	*T, RH,* $WS_{6,}$ WD_6	---
Berthoud Pass	CAIC	4402	3615	11,12,13,14,15	*T, RH,* WS_6, WD_6	---
D1	LTER	5501	3738	11,12,13,14,15	*T, RH,* WS_9, WD_9	---
US-NR1	Ameriflux	5502	3050	11,12,13,14,15	*T, RH,* WS_{10}, WD_{10}, *Pa, SI, LI*	SUB_{EC}
T-Van	LTER	5503	3503	11,12,13,14,15	*T, RH,* WS_3, WD_3	SUB_{EC}

Table 4.2. Mean SNOTEL air temperature and precipitation (November through April) for stations with five years of valid data from WY 2011 through WY 2015. T_{rank} is the rank of mean air temperature from 1 (coldest) to 5 (warmest) and P_{rank} are the rank of mean total precipitation from 1 (driest) to 5 (wettest).

	T (°C)	T_{rank}	P (mm)	P_{rank}	relative met conditions (T, P)
WY2011	-4.4	2	1554	5	cold, wet
WY2012	-3.1	4	782	1	warm, dry
WY2013	-4.4	1	1000	2	cold, dry
WY2014	-4.0	3	1312	4	average, wet
WY2015	-2.6	5	1117	3	warm, average
Mean	-3.7	---	1153	---	---

Table 4.3. Performance statistics for *in-situ* snow sublimation at EC stations compared to (a) modeled total snow sublimation and (b) modeled total snow sublimation minus the blowing snow sublimation component. Performance statistics are Nash-Sutcliffe efficiency (*NSE*), Pearson's r coefficient (*r*), Percent bias (*PBias*), and Root mean squared error (*RMSE*).

(a) Total snow sublimation

		WY2011	WY2012	WY2013	WY2014	WY2015
Arrow	*NSE*	---	---	---	-0.99	0.26
	r	---	---	---	0.69	0.62
	PBias	---	---	---	48.5	-37.0
	RMSE	---	---	---	0.43	0.32
Andrews Meadow	*NSE*	---	---	---	-1.41	-0.28
	r	---	---	---	0.37	0.67
	PBias	---	---	---	-49.9	-47.6
	RMSE	---	---	---	0.37	0.34
US-NR1	*NSE*	-1.92	-0.27	-0.30	-0.21	0.01
	r	0.49	0.65	0.72	0.53	0.72
	PBias	27.7	7.0	23.2	-2.9	19.6
	RMSE	1.31	1.02	1.13	1.40	1.07
T-Van	*NSE*	-67	-26	-127	-69	-278
	r	-0.02	0.14	0.05	0.08	-0.05
	PBias	379	196	347	345	530
	RMSE	5.7	3.4	6.3	5.5	6.2

(b) Total snow sublimation minus blowing snow

		WY2011	WY2012	WY2013	WY2014	WY2015
Arrow	*NSE*	---	---	---	0.38	0.26
	r	---	---	---	0.72	0.63
	PBias	---	---	---	8.8	-38.8
	RMSE	---	---	---	0.24	0.32
Andrews Meadow	*NSE*	---	---	---	-1.33	-0.25
	r	---	---	---	0.38	0.69
	PBias	---	---	---	-51.8	-52.7
	RMSE	---	---	---	0.37	0.34
US-NR1	*NSE*	-1.92	-0.27	-0.30	-0.21	0.01
	r	0.49	0.65	0.72	0.53	0.72
	PBias	27.7	7.0	23.2	-2.9	19.6
	RMSE	1.3	1.0	1.1	1.4	1.1
T-Van	*NSE*	-0.33	-2.5	-3.3	-2.2	-8.7
	r	0.46	0.37	0.28	0.46	0.53
	PBias	31.0	57.7	77.3	72.8	139
	RMSE	0.79	1.2	1.2	1.2	1.2

Table 4.4. Total snow sublimation, total precipitation falling as snow, and percentage of snowfall lost to snow sublimation across the model domain for each water year of the modeling study.

Water year	2011	2012	2013	2014	2015	Mean
Surface Sublimation (mm)	61	42	46	53	45	49
Canopy Sublimation (mm)	170	99	116	157	109	130
Blowing Sublimation (mm)	73	30	28	41	27	40
Total Snow Sublimation (mm)	304	170	189	250	181	219
Total Snowfall (mm)	723	340	428	576	496	513
Sublimation Loss (%)	42	50	44	43	37	43

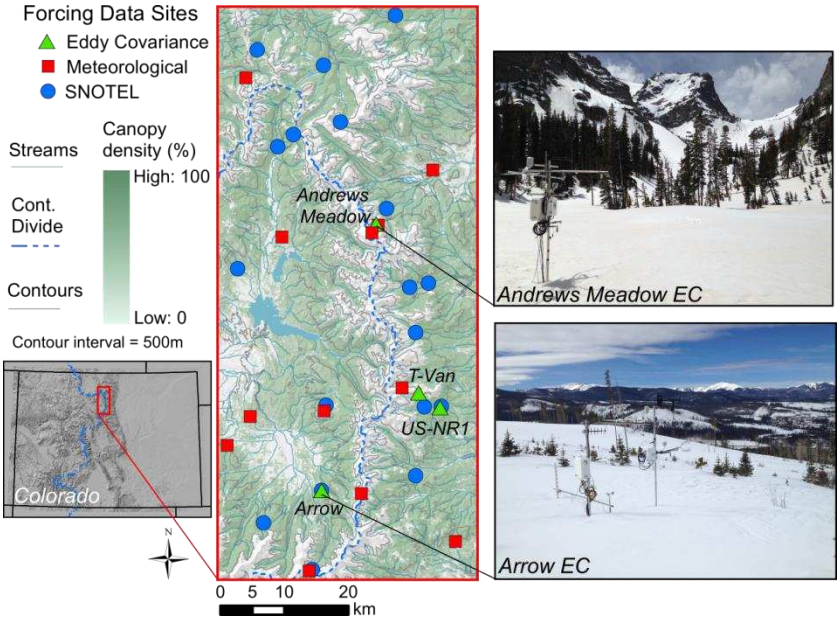

Figure 4.1. Map of study domain located within the north-central Colorado Rocky Mountains, U.S.A. The locations of SNOTEL stations are shown by blue circles, meteorological stations are shown by red squares, and eddy covariance stations are shown by green triangles.

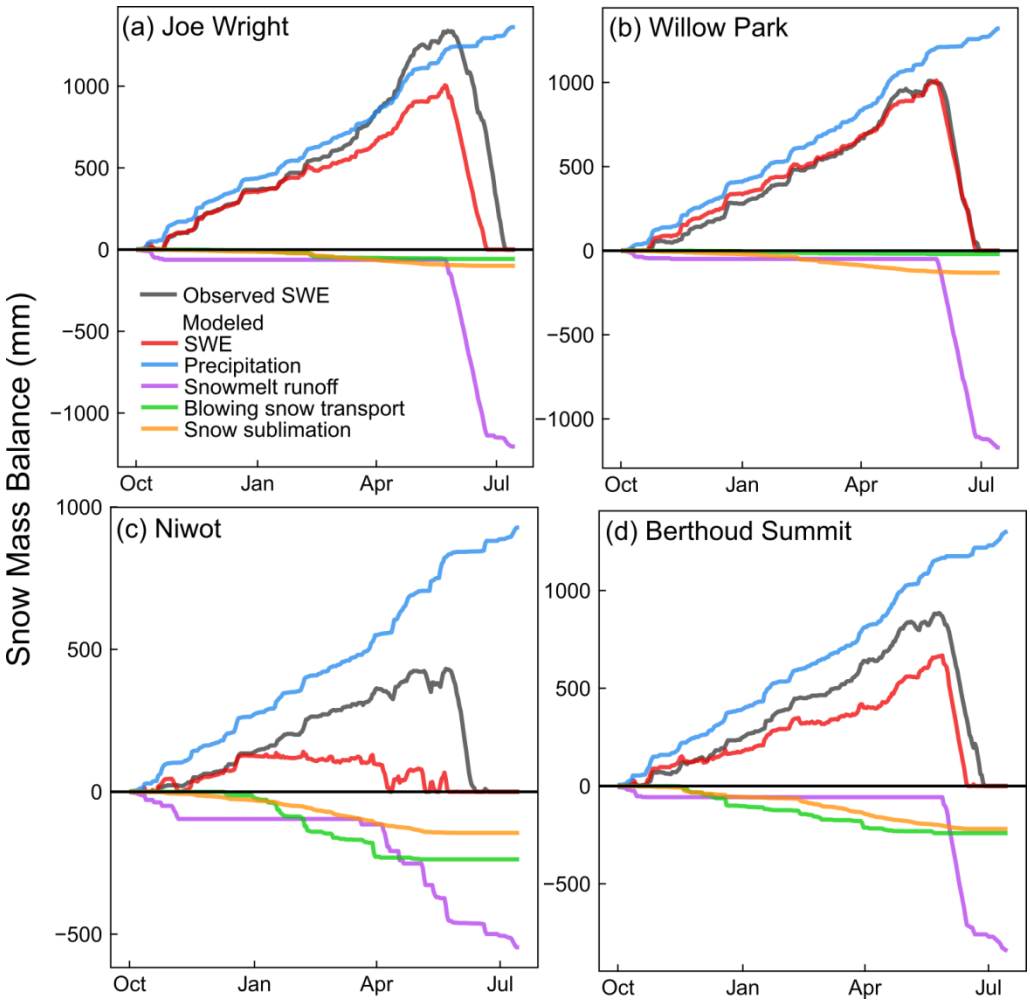

Figure 4.2. Cumulative modeled snow mass balance components compared to observed snow water equivalent at the (a) Joe Wright, (b) Willow Park, (c) Niwot, and (d) Berthoud Summit SNOTEL stations for the WY2011 model simulation.

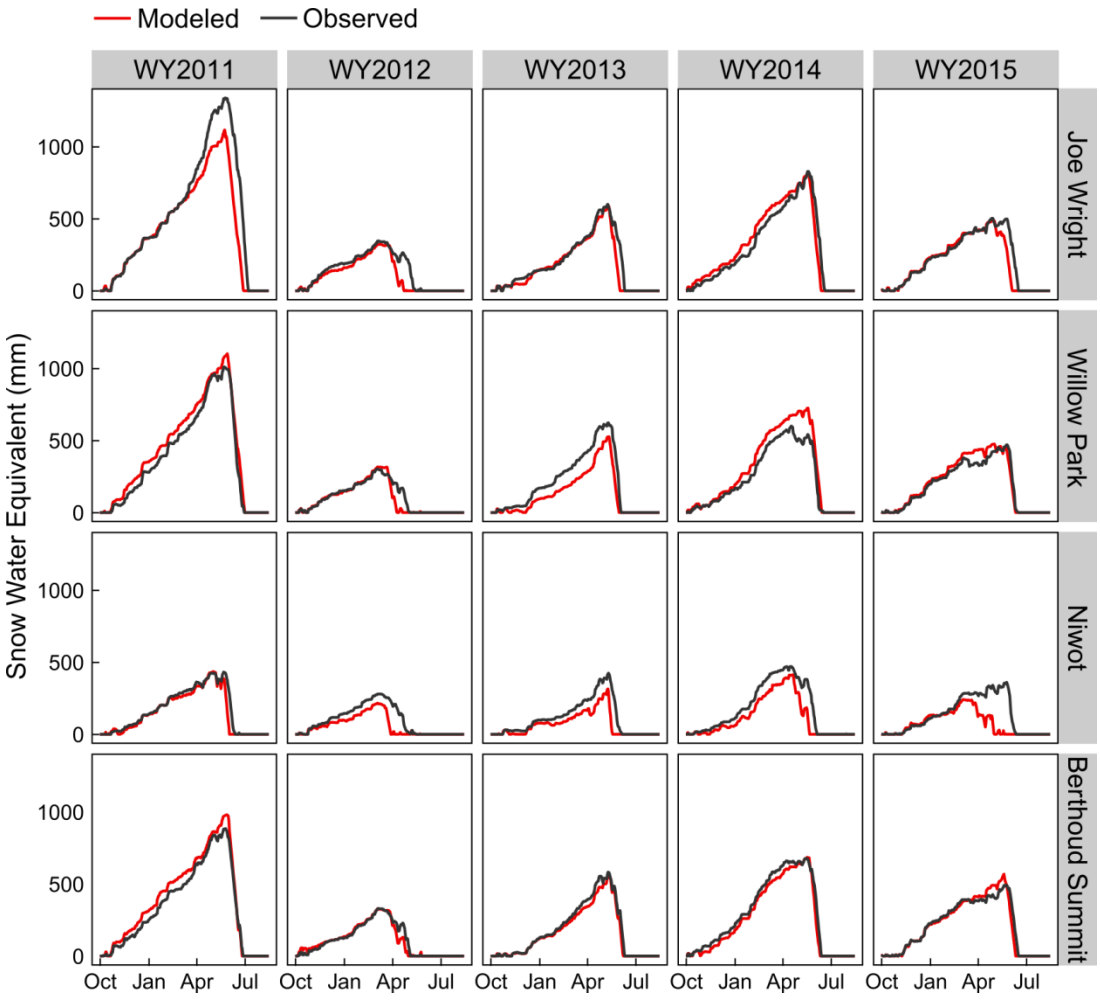

Figure 4.3. Modeled versus observed snow water equivalent at selected SNOTEL stations for each water year simulation.

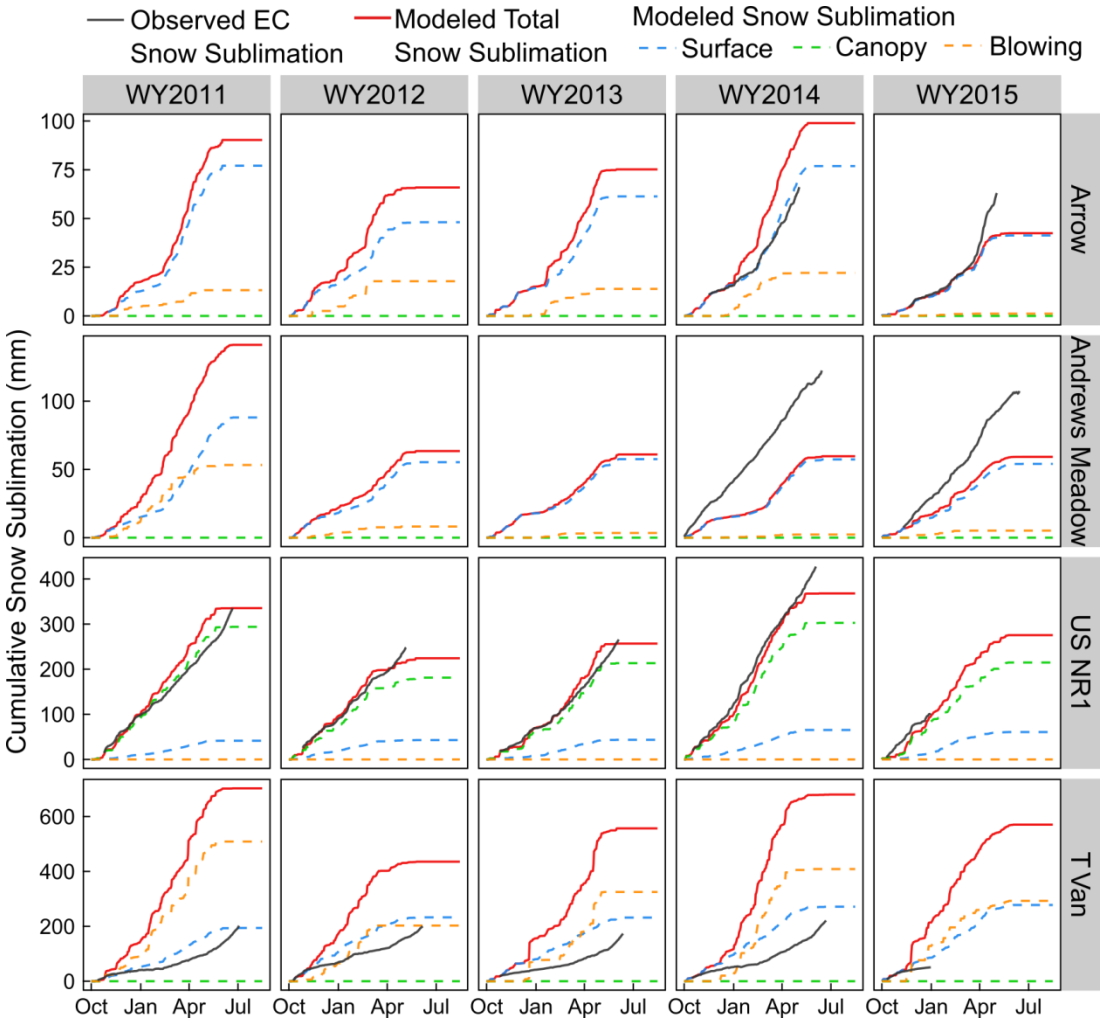

Figure 4.4. Cumulative observed snow sublimation at eddy covariance stations (black line) compared to cumulative modeled snow sublimation (red line), surface sublimation (blue dashed line), canopy sublimation (green dashed line), and blowing sublimation (orange dashed line) for each water year of study.

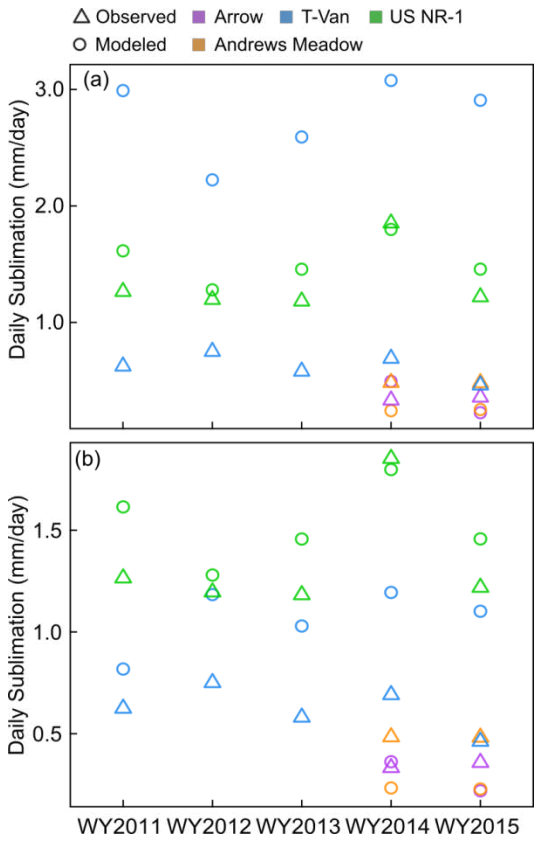

Figure 4.5. Observed (triangles) daily snow sublimation at eddy covariance stations compared to modeled (circles) daily (a) snow sublimation and (b) snow sublimation minus blowing sublimation for each water year of study.

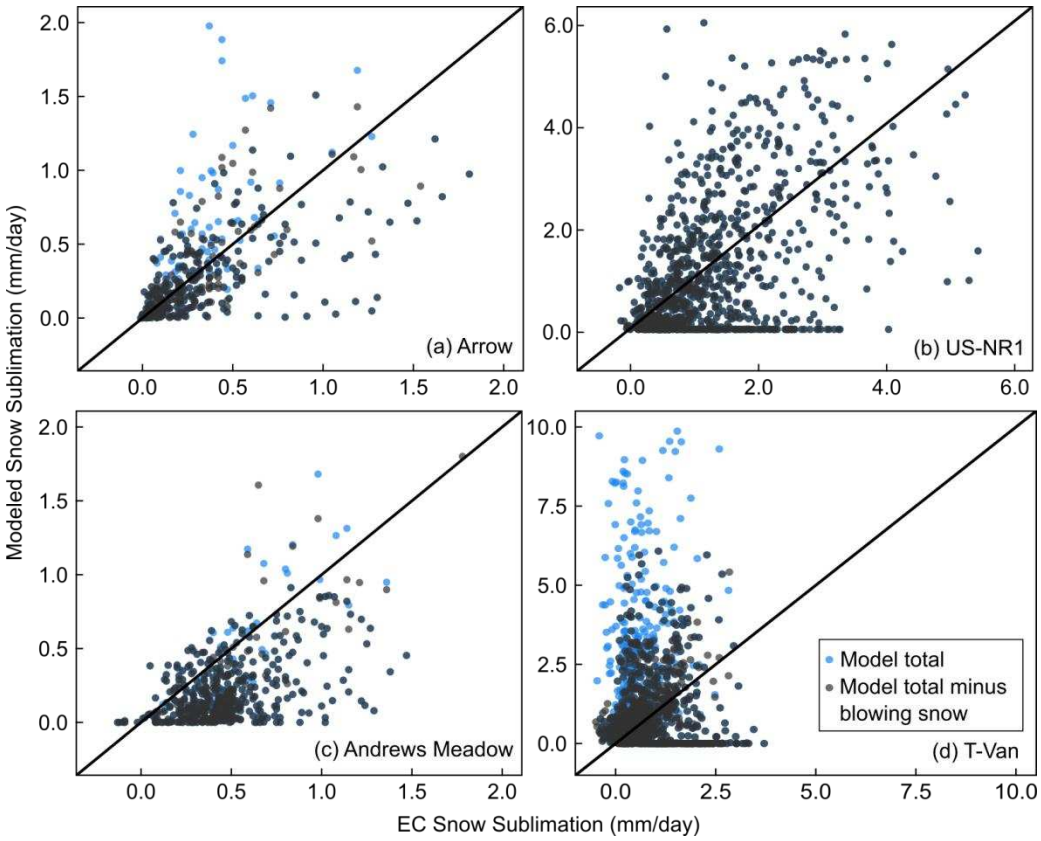

Figure 4.6. Daily modeled versus observed sublimation (mm day^{-1}) at the (a) Arrow site, (b) US-NR1 site, (c) Andrews Meadow site, and (d) T-Van site. Blue dots represent modeled daily snow sublimation and black dots represent modeled daily snow sublimation minus blowing sublimation. The 1:1 line is shown in on each plot.

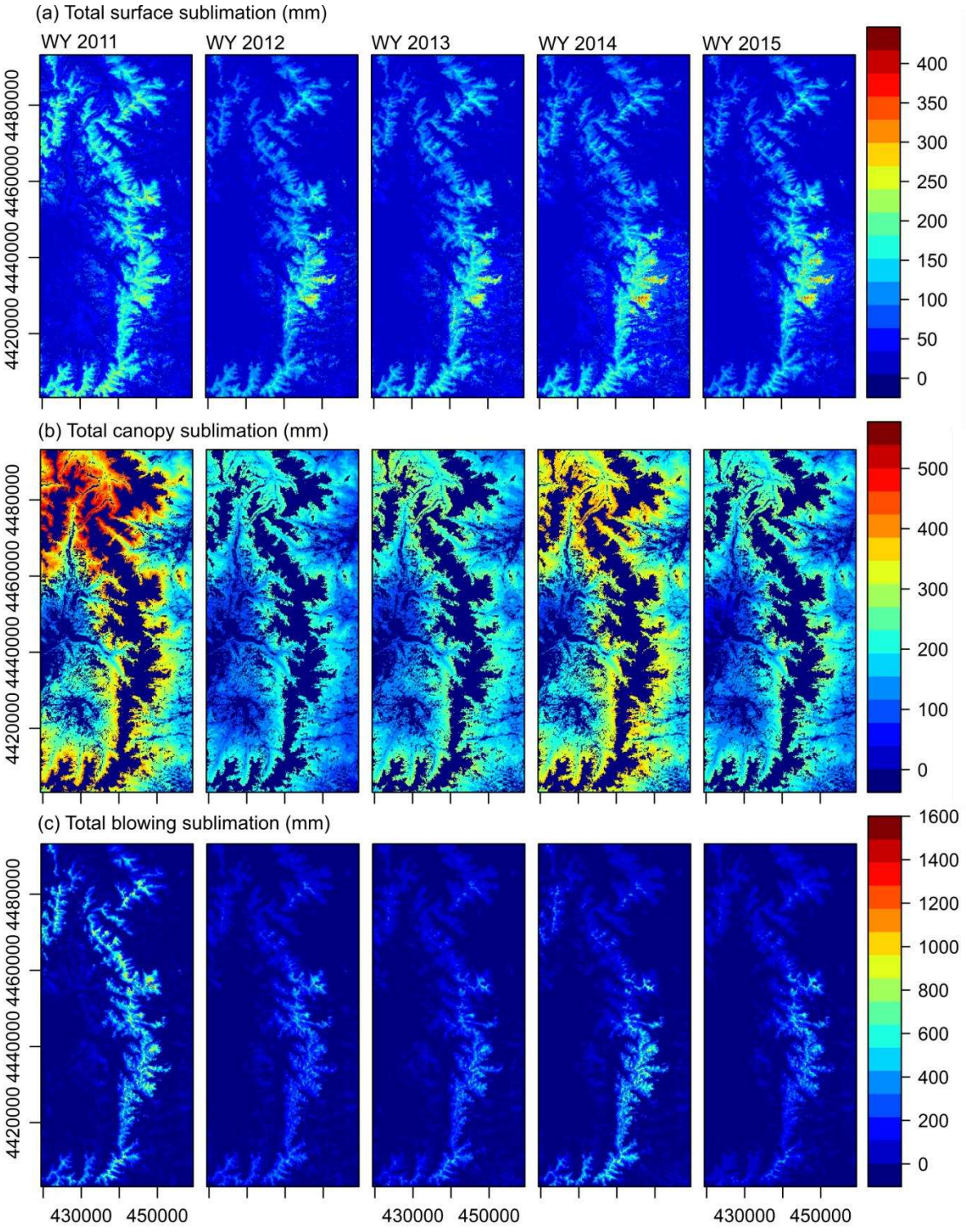

Figure 4.7. Modeled total (a) surface, (b) canopy, and (c) blowing sublimation across the domain for each water year of the study.

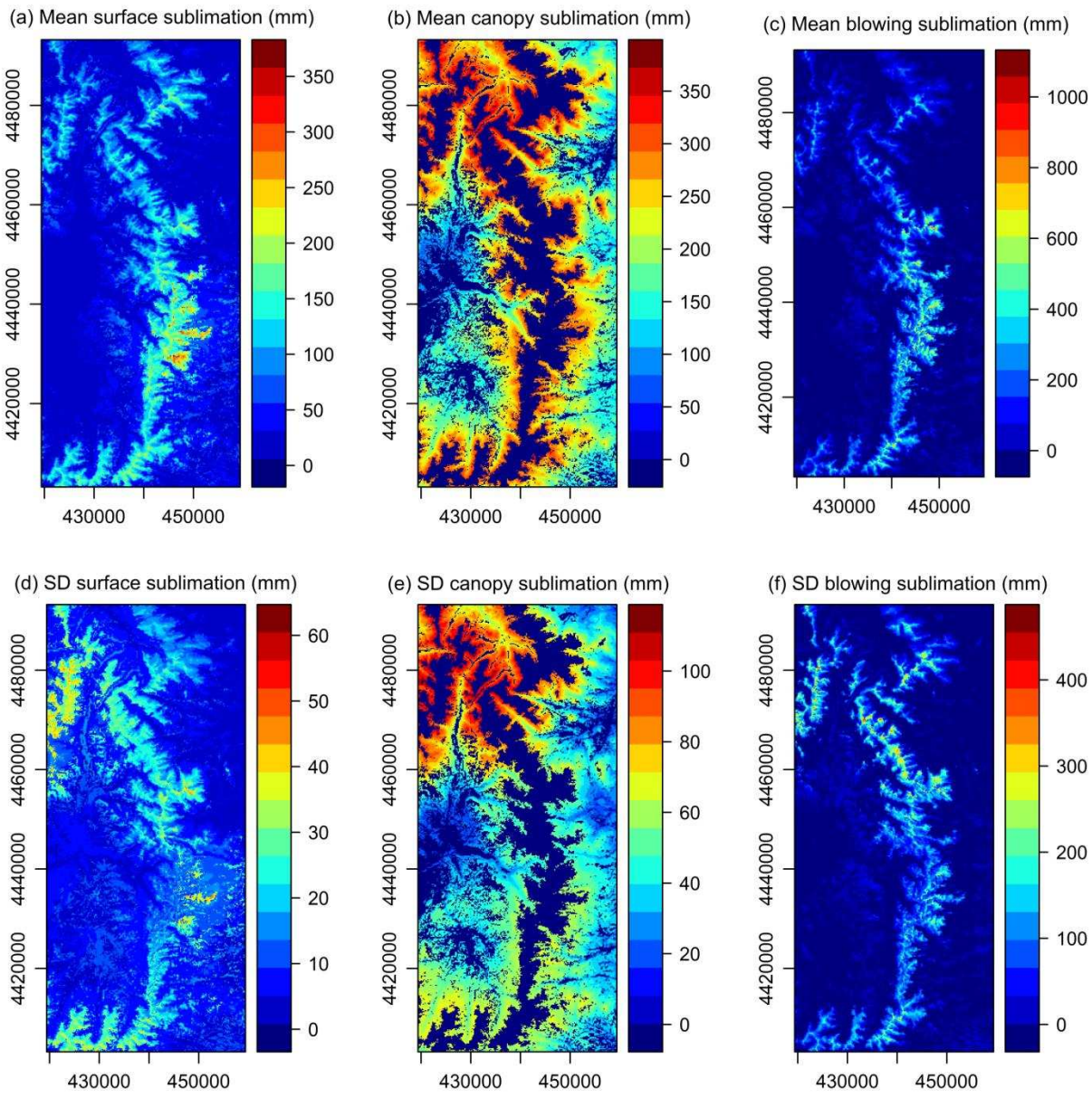

Figure 4.8. Spatial variability of the 5-year modeled mean total (a) surface sublimation, (b) canopy sublimation, (c) blowing snow sublimation and standard deviation of (d) surface sublimation, (e) canopy sublimation, and (f) blowing snow sublimation across the domain.

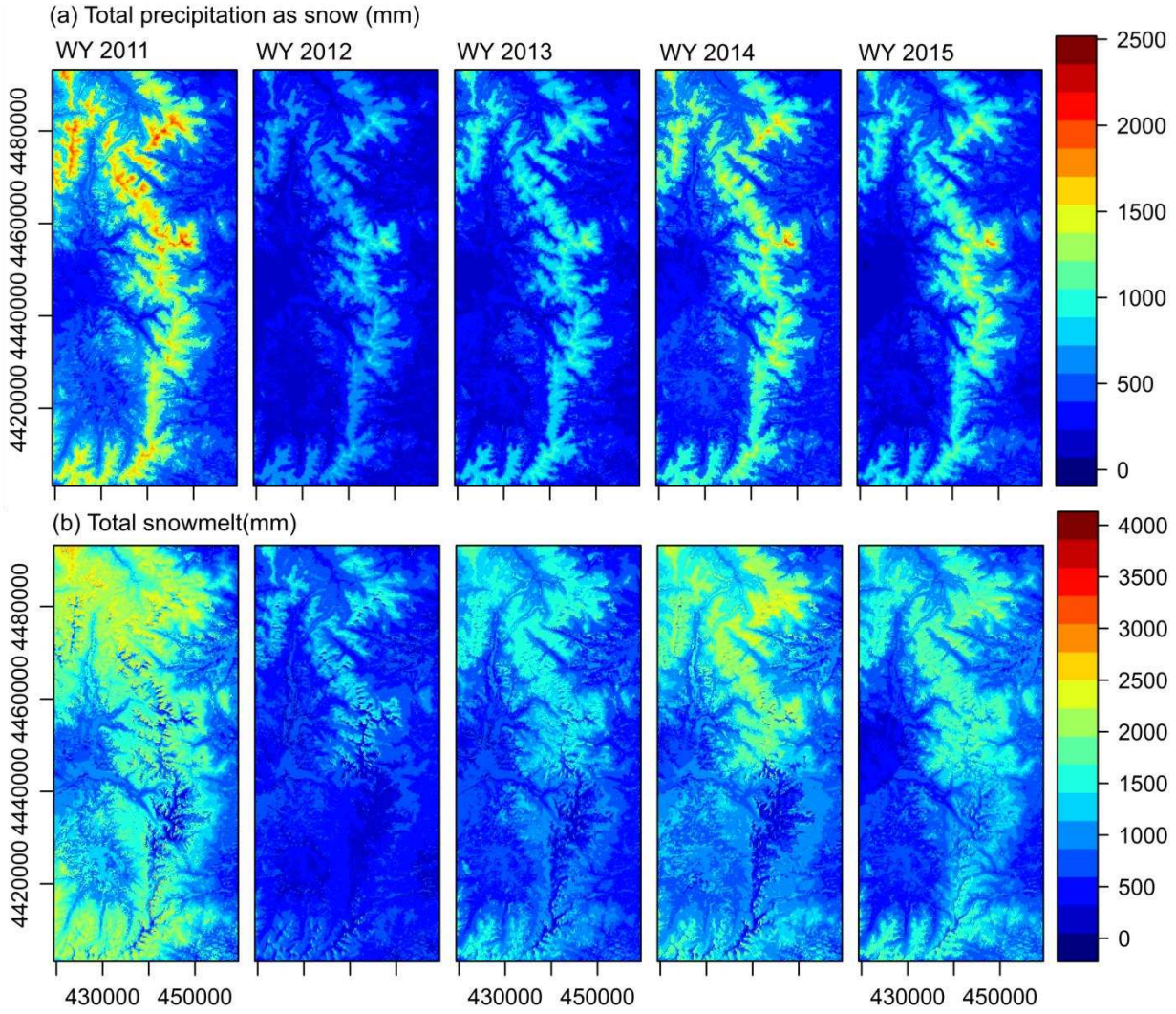

Figure 4.9. Modeled total (a) precipitation as snow and (b) snowmelt across the domain for each water year of the study.

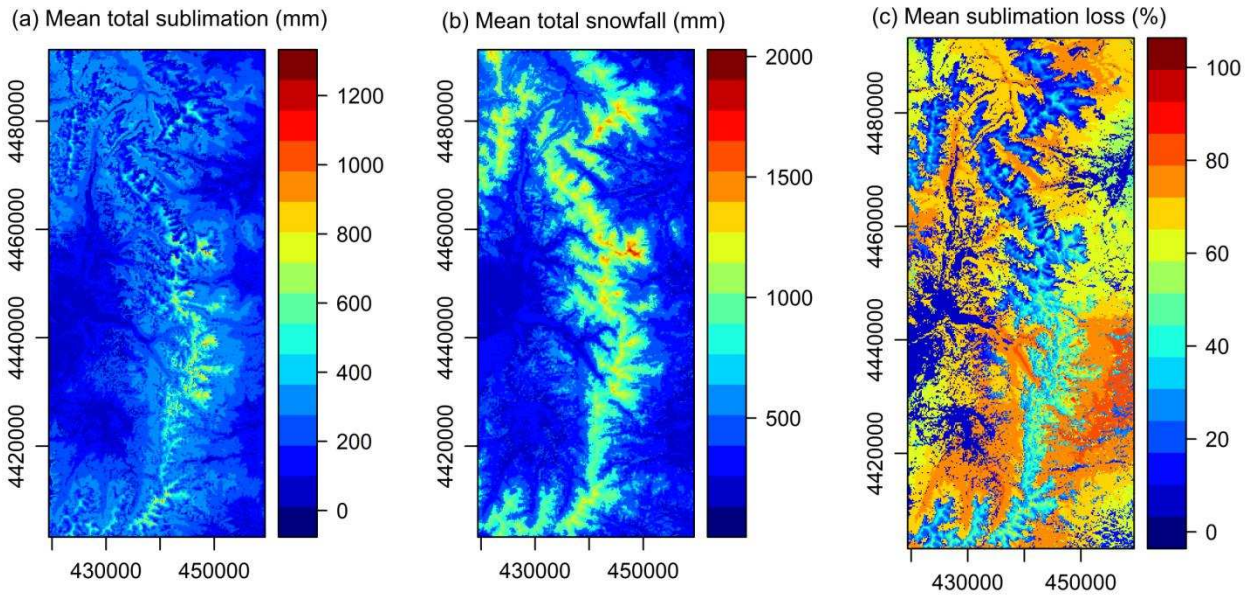

Figure 4.10. 5-year modeled mean (a) total snow sublimation, (b) total snowfall, and (c) percent of snowfall lost to snow sublimation across the domain.

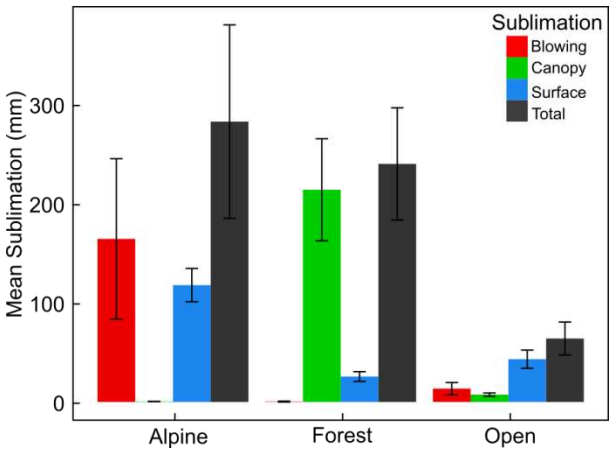

Figure 4.11. 5-year modeled mean (bar) and standard deviation (error bar) of each component of total snow sublimation summarized by land cover type.

CHAPTER 5 – SYNTHESIS OF RESEARCH CONTRIBUTIONS AND FUTURE INVESTIGATIONS

5.1 Synthesis of research

Through a combination of ground-based measurements, remote sensing observations, and snow evolution modeling, the research presented in this dissertation evaluates two of the key uncertainties in characterizing the seasonal evolution of the snowpack: (1) the nature and scale of the spatial variability and distribution of snow in complex mountainous terrain, and (2) the magnitude and variability of seasonal snow sublimation fluxes between the snowpack and atmosphere. The science question motivating this research is: *How does snow sublimation vary spatially and temporally in seasonally snow-covered environments and what is the role of this process in shaping the spatial distribution of the snowpack across varying land covers within mountainous terrain?* Chapters 2 through 4 of this dissertation have attempted to evaluate key gaps in knowledge that are central to this overarching science question.

In Chapter 2, fine resolution airborne lidar-derived snow depth datasets [*Harpold et al.*, 2014b] were used to evaluate the spatial variability of snow within areas comparable to coarse scale model grids (500 m resolution grids). This evaluation of subgrid snow distributions within complex mountainous terrain is particularly applicable for physically-based modeling applications run at a scale too large to resolve processes driving snow distributions [e.g., *Liston*, 2004]. The subgrid coefficient of variation of snow depth was shown to exhibit substantial variability in mountainous terrain and was well correlated with mean snow depth, land cover type, as well as canopy and topography characteristics. A simple statistical model for predicting the subgrid coefficient of variation of snow depth was developed for both alpine and subalpine areas. These results provide a useful parameterization of subgrid snow distribution for future

modeling applications in this region, and also an important methodology that could be used to create a more robust parameterization developed by measurements across many mountainous regions as airborne lidar datasets become more readily available.

The research in Chapter 3 presents measurements of seasonal snow sublimation from two forested openings within the Colorado Rocky Mountains. Specifically, this study evaluates the relative merits and propagated uncertainty of four methods for quantifying surface sublimation in complex mountainous terrain: the eddy covariance (EC), Bowen ratio-energy balance (BR), bulk aerodynamic flux (BF), and aerodynamic profile (AP) methods. Biases between methods are evaluated over a range of environmental conditions, which highlight limitations and uncertainties of each method. Mean propagated uncertainty was calculated to be 24 percent, 46 percent, 46 percent, and 94 percent of the seasonal total surface sublimation for the EC, BR, BF, and AP methods, respectively. The results of this research highlight the challenges related to measuring surface sublimation in snow-covered regions, and provide an important analysis of measurement uncertainty. These results can be used by researchers seeking to quantify snow sublimation in future investigations to determine which method may be most applicable for their application. Additionally, the surface sublimation rates quantified in Chapter 3 help to refine surface sublimation estimates for forested openings in the Colorado Rocky Mountains.

In Chapter 4, a distributed snow evolution model [SnowModel; *Liston and Elder*, 2006b] is applied across a 3600 km^2 model domain in the northern Colorado Rocky Mountains. The model is run at a grid resolution of 100 m for an hourly time step over five water years (WY 2011 through WY 2015). Results from model simulations were evaluated against *in-situ* measurements of snow water equivalent (SWE) at SNOTEL stations and snow sublimation fluxes at eddy covariance stations to assess model accuracy and representation of snow

sublimation. Model verification at both SNOTEL and EC model grids show satisfactory performance, but simulations exhibit a low bias and high bias of modeled SWE and snow sublimation, respectively. Both canopy sublimation in forested areas and blowing sublimation in alpine areas had significant contributions to total snow sublimation across the model domain, which ranged from 170 mm to 304 mm over the five water years. Results from the modeling study have considerable uncertainty, but provide important insight into the variability and importance of snow sublimation in the Rocky Mountains of Colorado.

The research presented in this dissertation supports the common theme that snow sublimation plays an important role in both the overall snow-cover mass balance as well as the spatial variability of snow distributions in complex mountainous terrain [e.g., *Strasser et al.*, 2008]. A substantial finding of this work is that on average, modeled snow sublimation (Chapter 4) is equivalent to 43 percent of the total snowfall across the northern Colorado model domain. Although there is significant uncertainty in process-based modeling [e.g., *Raleigh et al.*, 2015], careful evaluation of modeled SWE evolution at SNOTEL sites and modeled snow sublimation at EC sites show satisfactory performance. Additionally, surface sublimation from two forested openings within the model domain presented in Chapter 3 was equivalent to 10 percent to total winter precipitation on average and is expected to represent the lower bound of snow sublimation rates within the domain. Therefore, these results suggest snow sublimation is a very important process for determining the water balance of the mountainous regions in Colorado.

In addition to influencing the magnitudes of snow water equivalent available for melt, results suggest that snow sublimation exhibits spatial and temporal variability that influences snow distribution and melt patterns. The fine resolution airborne lidar snow depth datasets presented in Chapter 2 highlight distinct patterns of snow variability and amounts between

subalpine and alpine land covers, and when considering the modeled snow sublimation from the same region presented in Chapter 4, it is expected that snow sublimation was an important process contributing to the snow distribution observed by airborne lidar. As highlighted by the results of modeled snow sublimation in Chapter 4, it is expected that the spatial variations in snow sublimation occur at the hillslope scale (100s of meters) and are likely well correlated with changes in the land cover type (e.g., forested openings below treeline, forests, and alpine). Additionally, ground observations of snow sublimation presented in Chapters 3 and 4 show that the greatest seasonal snow sublimation rates often occur close to peak snow accumulation and during snowmelt. These temporal variations highlight the importance of snow sublimation processes for water resources forecasts even when snow distributions can be accurately characterized around peak snow accumulation [e.g., *Elder et al.*, 1991; *Balk and Elder*, 2000; *Fassnacht et al.*, 2003; *Molotch et al.*, 2005; *Painter et al.*, 2016].

The findings of this study have important implications for snow hydrology research and offer ideas for future investigations. Future applications of water resources forecasting, whether it be through process-based modeling [e.g., *Lehning et al.*, 2006; *Liston and Elder*, 2006b; *Pomeroy et al.*, 2007] or airborne lidar observations [e.g., *Deems et al.*, 2013; *Painter et al.*, 2016], should account for snow sublimation losses throughout the snow accumulation and snowmelt periods. Although process-based models show promise for modeling the spatial and temporal variability snow sublimation, additional collection of ground observations of snow sublimation across varying ecosystem types [e.g., *Knowles et al.*, 2015b] will also provide valuable model constraints and improve model representations. Lastly, this research highlights the considerable uncertainty in both measurements and modeling of snow sublimation, which should be carefully considered and reported in future investigations as to provide bounds of

confidence on reported results. Ideas for future investigations related to the results presented by this study are outlined below.

5.2 Future research investigations

Airborne lidar measurements of snow depth offer a unique ability to improve snow model process representations that drive snow distributions within complex mountainous terrain. Future investigations could utilize the methods for parameterization of subgrid snow depth variability developed in Chapter 2 across varying snow-covered topographies and climates to (1) develop additional localized models for subgrid snow depth coefficient of variation and (2) evaluate consistencies amongst regional observations to develop a more robust parametrization for complex mountainous terrain. The methodology presented in Chapter 2 could also be used in future investigations to evaluate parameterizations of other critical input parameters for snow evolution (e.g. snow covered area) and/or hydrological (e.g. soil moisture) modeling applications. For snow modeling applications that are run at a fine grid resolution that can resolve processes driving snow distribution (e.g. snow redistribution by wind in alpine areas), airborne lidar measurements could be particularly useful for direct model evaluation [e.g., *Groot Zwaaftink et al.*, 2013]. Future research could evaluate the ability of snow model simulations to accurately characterize the spatial distribution of snow depth using detailed airborne lidar observations, and subsequently infer snow model deficiencies based on errors in modeled snow depth. Snow redistribution by wind in alpine areas was shown to be an important process related to subgrid snow distribution representations (e.g., Chapter 2) and regional snow sublimation estimations (e.g., Chapter 4), and a detailed study on the temporal evolution of snow redistribution in alpine areas using airborne lidar would be particularly useful for evaluating model representations [e.g., *Musselman et al.*, 2015].

Measurements and modeling of snow sublimation presented in this research provide advances related to understanding the importance of these fluxes in snow evolution within the Colorado Rocky Mountains, but also provide much opportunity for future investigations to build upon. The limitations of methods used for quantifying snow sublimation suggest future research could focus on (1) evaluating methodological improvements for sampling in certain challenging environmental conditions, such as in low turbulence when deposition (i.e. downward snow sublimation) may be occurring, or during snow redistribution events when blowing snow sublimation may occur above the height instrumentation, and (2) evaluating representivity of measurement locations given the complexities of forested and nonforested mountainous terrain. Also, the substantial propagated uncertainty for each method highlighted in Chapter 3 suggests that special care should be taken to consider and report uncertainty in measured and modeled snow sublimation in future investigations. Given that canopy and blowing sublimation components were estimated as a significant contribution of overall snow sublimation losses from the snowpack (e.g., Chapter 4), future research aimed at measuring these processes across varying forest and topography characteristics to evaluate their variability could help to refine and improve the accuracy of model representations.

Lastly, future investigations should continue to pursue testing and improving process representations within snow models; however, should also focus on the testing of the utility of current model systems for water resources forecasting applications to evaluate potential deficiencies. For example, the snow evolution model used in this research [SnowModel; *Liston and Elder*, 2006b] could be coupled with a hydrological model such as the USGS Precipitation Runoff Modeling System (PRMS) and used in a forecasting mode through short-term forecasting of meteorological forcing data. Future water resources management likely will benefit from use

of physically-based snow models that can account for the snow processes such as wind redistribution, canopy interception, and snow sublimation that shape the spatial and temporal evolution and distribution of snow in complex mountainous terrain.

REFERENCES

Akaike, H. (1974), A new look at the statistical model identification, *IEEE Transactions on Automatic Control*, *19*, 716-723.

Andreas, E. L. (2002), Parameterizing scalar transfer over snow and ice: A review, *Journal of Hydrometeorology*, *3*, 417-432.

Andreas, E. L., R. E. Jordan, and A. P. Makshtas (2005), Parameterizing turbulent exchange over sea ice: The Ice Station Weddell results, *Boundary-Layer Meteorology*, *114*, 439-460.

Andreas, E. L., P. O. G. Persson, R. E. Jordan, T. W. Horst, P. S. Guest, A. A. Grachev, and C. W. Fairall (2010), Parameterizing Turbulent Exchange over Sea Ice in Winter, *Journal of Hydrometeorology*, *11*, 87-104.

Arck, M., and D. Scherer (2002), Problems in the determination of sensible heat flux over snow, *Geografiska Annaler*, *84A*, 157-169.

Arya, S. P. (1988), *Introduction to micrometeorology*, 307 pp., Academic Press, San Diego, California.

Bales, R. C., N. P. Molotch, T. H. Painter, M. D. Dettinger, R. Rice, and J. Dozier (2006), Mountain hydrology of the western United States, *Water Resources Research*, *42*, W08432.

Balk, B., and K. Elder (2000), Combining binary decision tree and geostatistical methods to estimate snow distribution in a mountain watershed, *Water Resources Research*, *36*, 13-26.

Barlow, R. (1989), *Statistics. A Guide to the Use of Statistical Methods in the Physical Sciences*, Wiley, Chichester, England.

Barnett, T. P., J. C. Adam, and D. P. Lettenmaier (2005), Potential impacts of a warming climate on water availability in snow-dominated regions, *Nature*, *438*, 303-309.

Barry, R. G. (2008), *Mountain weather and climate*, 3rd ed., 506 pp., Cambridge University Press, New York, New York.

Biederman, J. A., P. D. Brooks, A. A. Harpold, D. J. Gochis, E. Gutmann, D. E. Reed, E. Pendall, and B. E. Ewers (2014), Multiscale observations of snow accumulation and peak snowpack following widespread, insect-induced lodgepole pine mortality, *Ecohydrology*, *7*, 150-162.

Bierkens, M. F. P., V. A. Bell, P. Burek, N. Chaney, L. E. Condon, C. H. David, A. de Roo, P. Doll, N. Drost, J. S. Famiglietti, M. Florke, D. J. Gochis, P. Houser, R. Hut, J. Keune, S. Kollet, R. M. Maxwell, J. T. Reager, L. Samaniego, E. Sudicky, E. H. Sutanudjaja, N. van de Giesen, H. Winsemius, and E. F. Wood (2015), Hyper-resolution global hydrological modelling: what is next? "Everywhere and locally relevant", *Hydrological Processes*, *29*, 310-320.

Blad, B., and N. Rosenberg (1974), Lysimetric calibration of the Bowen ratio-energy balance method for evapotranspiration estimation in the Central Great Plains, *Journal of Applied Meteorology*, *13*, 227-236.

Blanken, P. D., M. W. Williams, S. P. Burns, R. K. Monson, J. Knowles, K. Chowanski, and T. Ackerman (2009), A comparison of water and carbon dioxide exchange at a windy alpine tundra and subalpine forest site near Niwot Ridge, Colorado, *Biogeochemistry*, *95*, 61-76.

Blöschl, G. (1999), Scaling issues in snow hydrology, *Hydrological Processes*, *13*, 2149-2175.

Boon, S. (2012), Snow accumulation following forest disturbance, *Ecohydrology*, *5*, 279-285.

Bowen, I. S. (1926), The Ratio of Heat Losses by Conduction and by Evaporation from any Water Surface, *Physical Review*, *27*, 779-787.

Box, J. E., and K. Steffen (2001), Sublimation on the Greenland ice sheet from automated weather station observations, *Journal of Geophysical Research-Atmospheres*, *106*, 33965-33981.

Brotzge, J. A., and K. C. Crawford (2003), Examination of the surface energy budget: A comparison of eddy correlation and Bowen ratio measurement systems, *Journal of Hydrometeorology*, *4*, 160-178.

Broxton, P. D., A. A. Harpold, J. A. Biederman, P. A. Troch, N. P. Molotch, and P. D. Brooks (2015), Quantifying the effects of vegetation structure on snow accumulation and ablation in mixed-conifer forests, *Ecohydrology*, *8*, 1073-1094.

Bühler, Y., M. Marty, L. Egli, J. Veitinger, T. Jonas, P. Thee, and C. Ginzler (2015), Snow depth mapping in high-alpine catchments using digital photogrammetry, *The Cryosphere*, *9*, 229-243.

Burns, S. P., N. P. Molotch, M. W. Williams, J. F. Knowles, B. Seok, R. K. Monson, A. A. Turnipseed, and P. D. Blanken (2014), Snow Temperature Changes within a Seasonal Snowpack and Their Relationship to Turbulent Fluxes of Sensible and Latent Heat, *Journal of Hydrometeorology*, *15*, 117-142.

Carroll, T., D. Cline, C. Olheiser, A. Rost, A. Nilsson, G. Fall, C. Bovitz, and L. Li (2006), NOAA's National Snow Analyses, *Proceedings of the 74th Annual Western Snow Conference*, *74*, 31-43.

Clark, M. P., J. Hendrikx, A. G. Slater, D. Kavetski, B. Anderson, N. J. Cullen, T. Kerr, E. O. Hreinsson, and R. A. Woods (2011), Representing spatial variability of snow water equivalent in hydrologic and land-surface models: A review, *Water Resources Research*, *47*, W07539.

Clifton, A., J. D. Ruedi, and M. Lehning (2006), Snow saltation threshold measurements in a drifting-snow wind tunnel, *Journal of Glaciology*, *52*, 585-596.

Cline, D., S. Yueh, B. Chapman, B. Stankov, A. Gasiewski, D. Masters, K. Elder, R. Kelly, T. H. Painter, S. Miller, S. Katzberg, and L. Mahrt (2009), NASA Cold Land Processes Experiment (CLPX 2002/03): Airborne Remote Sensing, *Journal of Hydrometeorology*, *10*, 338-346.

Cline, D. W. (1997a), Effect of seasonality of snow accumulation and melt on snow surface energy exchanges at a continental Alpine site, *Journal of Applied Meteorology, 36*, 32-51.

Cline, D. W. (1997b), Snow surface energy exchanges and snowmelt at a continental, midlatitude Alpine site, *Water Resources Research, 33*, 689-701.

Clow, D. W. (2010), Changes in the Timing of Snowmelt and Streamflow in Colorado: A Response to Recent Warming, *Journal of Climate*, *23*, 2293-2306.

Dadic, R., R. Mott, M. Lehning, M. Carenzo, B. Anderson, and A. Mackintosh (2013), Sensitivity of turbulent fluxes to wind speed over snow surfaces in different climatic settings, *Advances in Water Resources*, *55*, 178-189.

Dai, X., and N. Huang (2014), Numerical simulation of drifting snow sublimation in the saltation layer, *Scientific Reports, 4*, 6611.

DeCosmo, J., K. B. Katsaros, S. D. Smith, R. J. Anderson, W. A. Oost, K. Bumke, and H. Chadwick (1996), Air-sea exchange of water vapor and sensible heat: The humidity exchange over the sea (HEXOS) results, *Journal of Geophysical Research-Oceans*, *101*, 12001-12016.

Deems, J. S. (2007), Quantifying scale relationships in snow distributions, Unpublished Ph.D. thesis, 125 pp, Colorado State Univeristy, Fort Collins, Colorado, USA.

Deems, J. S., S. R. Fassnacht, and K. J. Elder (2006), Fractal Distribution of Snow Depth from Lidar Data, *Journal of Hydrometeorology*, *7*, 285-297.

Deems, J. S., S. R. Fassnacht, and K. J. Elder (2008), Interannual Consistency in Fractal Snow Depth Patterns at Two Colorado Mountain Sites, *Journal of Hydrometeorology, 9*, 977-988.

Deems, J. S., T. H. Painter, and D. C. Finnegan (2013), Lidar measurement of snow depth: a review, *Journal of Glaciology*, *59*, 467-479.

Déry, S. J., P. A. Taylor, and J. B. Xiao (1998), The thermodynamic effects of sublimating, blowing snow in the atmospheric boundary layer, *Boundary-Layer Meteorology*, *89*, 251-283.

Dewalle, D. R., and J. R. Meiman (1971), Energy Exchange and Late Season Snowmelt in a Small Opening in Colorado Subalpine Forest, *Water Resources Research, 7*, 184-188.

Doesken, N. J., and A. Judson (1996), *The snow booklet : a guide to the science, climatology, and measurement of snow in the United States*, 2nd ed., 86 pp., Colorado Climate Center, Dept. of Atmospheric Science, Colorado State University, Fort Collins, CO.

Dozier, J. (1980), A Clear-Sky Spectral Solar Radiation Model for Snow-Covered Mountainous Terrain, *Water Resources Research, 16*, 709-718.

Dozier, J. (2011), Mountain hydrology, snow color, and the fourth paradigm, *Eos, Transactions American Geophysical Union*, *92*, 373-374.

Drexler, J. Z., R. L. Snyder, D. Spano, and K. T. U. Paw (2004), A review of models and micrometeorological methods used to estimate wetland evapotranspiration, *Hydrological Processes*, *18*, 2071-2101.

Egli, L., and T. Jonas (2009), Hysteretic dynamics of seasonal snow depth distribution in the Swiss Alps, *Geophysical Research Letters*, *36*, L02501.

Elder, K., J. Dozier, and J. Michaelsen (1991), Snow Accumulation and Distribution in an Alpine Watershed, *Water Resources Research*, *27*, 1541-1552.

Elder, K., W. Rosenthal, and R. E. Davis (1998), Estimating the spatial distribution of snow water equivalence in a montane watershed, *Hydrological Processes*, *12*, 1793-1808.

Ellis, C. R., and J. W. Pomeroy (2007), Estimating sub-canopy shortwave irradiance to melting snow on forested slopes, *Hydrological Processes*, *21*, 2581-2593.

Erickson, T. A., M. W. Williams, and A. Winstral (2005), Persistence of topographic controls on the spatial distribution of snow in rugged mountain terrain, Colorado, United States, *Water Resources Research*, *41*, W04014.

Erxleben, J., K. Elder, and R. Davis (2002), Comparison of spatial interpolation methods for estimating snow distribution in the Colorado Rocky Mountains, *Hydrological Processes*, *16*, 3627-3649.

Falge, E., D. Baldocchi, R. Olson, P. Anthoni, M. Aubinet, C. Bernhofer, G. Burba, R. Ceulemans, R. Clement, H. Dolman, A. Granier, P. Gross, T. Grunwald, D. Hollinger, N. O. Jensen, G. Katul, P. Keronen, A. Kowalski, C. T. Lai, B. E. Law, T. Meyers, H. Moncrieff, E. Moors, J. W. Munger, K. Pilegaard, U. Rannik, C. Rebmann, A. Suyker, J. Tenhunen, K. Tu, S. Verma, T. Vesala, K. Wilson, and S. Wofsy (2001), Gap filling strategies for defensible annual sums of net ecosystem exchange, *Agricultural and Forest Meteorology*, *107*, 43-69.

Fassnacht, S. R. (2004), Estimating Alter-shielded gauge snowfall undercatch, snowpack sublimation, and blowing snow transport at six sites in the coterminous USA, *Hydrological Processes*, *18*, 3481-3492.

Fassnacht, S. R., and E. D. Soulis (2002), Implications during transitional periods of improvements to the snow processes in the land surface scheme - hydrological model WATCLASS, *Atmosphere-Ocean*, *40*, 389-403.

Fassnacht, S. R., and J. S. Deems (2006), Measurement sampling and scaling for deep montane snow depth data, *Hydrological Processes*, *20*, 829-838.

Fassnacht, S. R., and M. Hultstrand (2015), Snowpack variability and trends at long-term stations in northern Colorado, USA, *Proceedings of the International Association of Hydrological Sciences*, *371*, 131-136.

Fassnacht, S. R., K. A. Dressler, and R. C. Bales (2003), Snow water equivalent interpolation for the Colorado River Basin from snow telemetry (SNOTEL) data, *Water Resources Research*, *39*, 1208, doi:1210.1029/2002wr001512.

Fassnacht, S. R., K. A. Dressler, D. M. Hultstrand, R. C. Bales, and G. Patterson (2012), Temporal inconsistencies in coarse-scale snow water equivalent patterns: Colorado River Basin snow telemetry-topography regressions, *Pirineos*, *167*, 165-185.

Fletcher, S. J., G. E. Liston, C. A. Hiemstra, and S. D. Miller (2012), Assimilating MODIS and AMSR-E Snow Observations in a Snow Evolution Model, *Journal of Hydrometeorology*, *13*, 1475-1492.

Foken, T. (2008), The energy balance closure problem: an overview, *Ecological Applications*, *18*, 1351-1367.

Gascoin, S., S. Lhermitte, C. Kinnard, K. Bortels, and G. E. Liston (2013), Wind effects on snow cover in Pascua-Lama, Dry Andes of Chile, *Advances in Water Resources*, *55*, 25-39.

Goodison, B., P. Louie, and D. Yang (1998), *WMO Solid Precipitation Measurement Intercomparison Final Report*. WMO Instruments and Observing Methods Report No. 67, WMO/TD No. 872.

Grachev, A. A., E. L. Andreas, C. W. Fairall, P. S. Guest, and P. O. G. Persson (2007), SHEBA flux-profile relationships in the stable atmospheric boundary layer, *Boundary-Layer Meteorology*, *124*, 315-333.

Graham, C. B., W. van Verseveld, H. R. Barnard, and J. J. McDonnell (2010), Estimating the deep seepage component of the hillslope and catchment water balance within a measurement uncertainty framework, *Hydrological Processes*, *24*, 3631-3647.

Groot Zwaaftink, C. D., R. Mott, and M. Lehning (2013), Seasonal simulation of drifting snow sublimation in Alpine terrain, *Water Resources Research*, *49*, 1581-1590.

Grünewald, T., M. Schirmer, R. Mott, and M. Lehning (2010), Spatial and temporal variability of snow depth and ablation rates in a small mountain catchment, *The Cryosphere*, *4*, 215-225.

Grünewald, T., J. Stötter, J. W. Pomeroy, R. Dadic, I. Moreno Baños, J. Marturià, M. Spross, C. Hopkinson, P. Burlando, and M. Lehning (2013), Statistical modelling of the snow depth distribution in open alpine terrain, *Hydrology and Earth System Sciences*, *17*, 3005-3021.

Gustafson, J. R., P. D. Brooks, N. P. Molotch, and W. C. Veatch (2010), Estimating snow sublimation using natural chemical and isotopic tracers across a gradient of solar radiation, *Water Resources Research*, *46*, W12511.

Harpold, A., P. Brooks, S. Rajagopal, I. Heidbuchel, A. Jardine, and C. Stielstra (2012), Changes in snowpack accumulation and ablation in the intermountain west, *Water Resources Research*, *48*, W11501.

Harpold, A. A., J. A. Biederman, K. Condon, M. Merino, Y. Korgaonkar, T. C. Nan, L. L. Sloat, M. Ross, and P. D. Brooks (2014a), Changes in snow accumulation and ablation following the Las Conchas Forest Fire, New Mexico, USA, *Ecohydrology*, *7*, 440-452.

Harpold, A. A., Q. Guo, N. Molotch, P. D. Brooks, R. Bales, J. C. Fernandez-Diaz, K. N. Musselman, T. L. Swetnam, P. Kirchner, M. W. Meadows, J. Flanagan, and R. Lucas (2014b), LiDAR-derived snowpack data sets from mixed conifer forests across the Western United States, *Water Resources Research*, *50*, 2749-2755.

Hedstrom, N. R., and J. W. Pomeroy (1998), Measurements and modelling of snow interception in the boreal forest, *Hydrological Processes*, *12*, 1611-1625.

Helgason, W., and J. W. Pomeroy (2012a), Characteristics of the Near-Surface Boundary Layer within a Mountain Valley during Winter, *Journal of Applied Meteorology and Climatology*, *51*, 583-597.

Helgason, W., and J. Pomeroy (2012b), Problems Closing the Energy Balance over a Homogeneous Snow Cover during Midwinter, *Journal of Hydrometeorology*, *13*, 557-572.

Hiemstra, C. A., G. E. Liston, and W. A. Reiners (2006), Observing, modelling, and validating snow redistribution by wind in a Wyoming upper treeline landscape, *Ecological Modelling*, *197*, 35-51.

Hiller, R., M. J. Zeeman, and W. Eugster (2008), Eddy-covariance flux measurements in the complex terrain of an Alpine valley in Switzerland, *Boundary-Layer Meteorology*, *127*, 449-467.

Hood, E., M. Williams, and D. Cline (1999), Sublimation from a seasonal snowpack at a continental, mid-latitude alpine site, *Hydrological Processes*, *13*, 1781-1797.

Hopkinson, C., M. Sitar, L. Chasmer, and P. Treitz (2004), Mapping snowpack depth beneath forest canopies using airborne lidar, *Photogrammetric Engineering and Remote Sensing*, *70*, 323-330.

Irmak, S., A. Kilic, and S. Chatterjee (2014), On the Equality Assumption of Latent and Sensible Heat Energy Transfer Coefficients of the Bowen Ratio Theory for Evapotranspiration Estimations: Another Look at the Potential Causes of Inequalities, *Climate*, *2*, 181.

Jackson, S. I., and T. D. Prowse (2009), Spatial variation of snowmelt and sublimation in a high-elevation semi-desert basin of western Canada, *Hydrological Processes*, *23*, 2611-2627.

Jonas, T., C. Marty, and J. Magnusson (2009), Estimating the snow water equivalent from snow depth measurements in the Swiss Alps, *Journal of Hydrology*, *378*, 161-167.

Jost, G., M. Weiler, D. R. Gluns, and Y. Alila (2007), The influence of forest and topography on snow accumulation and melt at the watershed-scale, *Journal of Hydrology*, *347*, 101-115.

Kaimal, J. C., and J. J. Finnigan (1994), *Atmospheric boundary layer flows : their structure and measurement*, 289 pp., Oxford University Press, New York, New York.

Kashipazha, A. H. (2012), Practical snow depth sampling around six snow telemetry (SNOTEL) stations in Colorado and Wyoming, United States, Unpublished M.S. thesis, 189 pp, Colorado State University, Fort Collins, Colorado, USA.

Kattelmann, R., and K. Elder (1991), Hydrologic characteristics and water balance of an Alpine Basin in the Sierra Nevada, *Water Resources Research*, *27*, 1553-1562.

Kerr, T., M. Clark, J. Hendrikx, and B. Anderson (2013), Snow distribution in a steep mid-latitude alpine catchment, *Advances in Water Resources*, *55*, 17-24.

Kirchner, P. B., R. C. Bales, N. P. Molotch, J. Flanagan, and Q. Guo (2014), LiDAR measurement of seasonal snow accumulation along an elevation gradient in the southern Sierra Nevada, California, *Hydrology and Earth System Sciences*, *18*, 4261-4275.

Knowles, J. F., P. D. Blanken, M. W. Williams, and K. M. Chowanski (2012), Energy and surface moisture seasonally limit evaporation and sublimation from snow-free alpine tundra, *Agricultural and Forest Meteorology*, *157*, 106-115.

Knowles, J. F., S. P. Burns, P. D. Blanken, and R. K. Monson (2015a), Fluxes of energy, water, and carbon dioxide from mountain ecosystems at Niwot Ridge, Colorado, *Plant Ecology & Diversity*, *8*, 663-676.

Knowles, J. F., A. A. Harpold, R. Cowie, M. Zeliff, H. R. Barnard, S. P. Burns, P. D. Blanken, J. F. Morse, and M. W. Williams (2015b), The relative contributions of alpine and subalpine ecosystems to the water balance of a mountainous, headwater catchment, *Hydrological Processes*, *29*, 4794-4808.

Knowles, N., M. D. Dettinger, and D. R. Cayan (2006), Trends in Snowfall versus Rainfall in the Western United States, *Journal of Climate*, *19*, 4545-4559.

Kumar, S. V., C. D. Peters-Lidard, Y. Tian, P. R. Houser, J. Geiger, S. Olden, L. Lighty, J. L. Eastman, B. Doty, P. Dirmeyer, J. Adams, K. Mitchell, E. F. Wood, and J. Sheffield (2006), Land information system: An interoperable framework for high resolution land surface modeling, *Environmental Modelling & Software*, *21*, 1402-1415.

Lang, H. (1981), Is Evaporation an Important Component in High Alpine Hydrology?, *Nordic Hydrology*, *12*, 217-224.

Lapen, D. R., and L. W. Martz (1996), An investigation of the spatial association between snow depth and topography in a Prairie agricultural landscape using digital terrain analysis, *Journal of Hydrology*, *184*, 277-298.

Lee, Y. H., and L. Mahrt (2004), An evaluation of snowmelt and sublimation over short vegetation in land surface modelling, *Hydrological Processes*, *18*, 3543-3557.

Lehning, M., I. Völksch, D. Gustafsson, T. A. Nguyen, M. Stähli, and M. Zappa (2006), ALPINE3D: a detailed model of mountain surface processes and its application to snow hydrology, *Hydrological Processes*, *20*, 2111-2128.

Liston, G. E. (1995), Local Advection of Momentum, Heat, and Moisture during the Melt of Patchy Snow Covers, *Journal of Applied Meteorology*, *34*, 1705-1715.

Liston, G. E. (1999), Interrelationships among snow distribution, snowmelt, and snow cover depletion: Implications for atmospheric, hydrologic, and ecologic modeling, *Journal of Applied Meteorology*, *38*, 1474-1487.

Liston, G. E. (2004), Representing subgrid snow cover heterogeneities in regional and global models, *Journal of Climate*, *17*, 1381-1397.

Liston, G. E., and D. K. Hall (1995), An Energy-Balance Model of Lake-Ice Evolution, *Journal of Glaciology*, *41*, 373-382.

Liston, G. E., and M. Sturm (1998), A snow-transport model for complex terrain, *Journal of Glaciology*, *44*, 498-516.

Liston, G. E., and M. Sturm (2004), The role of winter sublimation in the Arctic moisture budget, *Nordic Hydrology*, *35*, 325-334.

Liston, G. E., and K. Elder (2006a), A meteorological distribution system for high-resolution terrestrial modeling (MicroMet), *Journal of Hydrometeorology*, *7*, 217-234.

Liston, G. E., and K. Elder (2006b), A distributed snow-evolution modeling system (SnowModel), *Journal of Hydrometeorology*, *7*, 1259-1276.

Liston, G. E., and C. A. Hiemstra (2008), A Simple Data Assimilation System for Complex Snow Distributions (SnowAssim), *Journal of Hydrometeorology*, *9*, 989-1004.

Liston, G. E., and C. A. Hiemstra (2011), Representing Grass- and Shrub-Snow-Atmosphere Interactions in Climate System Models, *Journal of Climate*, *24*, 2061-2079.

Liston, G. E., R. B. Haehnel, M. Sturm, C. A. Hiemstra, S. Berezovskaya, and R. D. Tabler (2007), Simulating complex snow distributions in windy environments using SnowTran-3D, *Journal of Glaciology*, *53*, 241-256.

Lopez-Moreno, J. I., S. R. Fassnacht, J. T. Heath, K. N. Musselman, J. Revuelto, J. Latron, E. Moran-Tejeda, and T. Jonas (2013), Small scale spatial variability of snow density and depth over complex alpine terrain: Implications for estimating snow water equivalent, *Advances in Water Resources*, *55*, 40-52.

López-Moreno, J. I., and D. Nogués-Bravo (2006), Interpolating local snow depth data: an evaluation of methods, *Hydrological Processes*, *20*, 2217-2232.

López-Moreno, J. I., S. R. Fassnacht, S. Beguería, and J. B. P. Latron (2011), Variability of snow depth at the plot scale: implications for mean depth estimation and sampling strategies, *The Cryosphere*, *5*, 617-629.

López-Moreno, J. I., J. Revuelto, S. R. Fassnacht, C. Azorín-Molina, S. M. Vicente-Serrano, E. Morán-Tejeda, and G. A. Sexstone (2015), Snowpack variability across various spatio-temporal resolutions, *Hydrological Processes*, *29*, 1213-1224.

Louis, J.-F. (1979), A parametric model of vertical eddy fluxes in the atmosphere, *Boundary-Layer Meteorology*, *17*, 187-202.

MacDonald, M. K., J. W. Pomeroy, and A. Pietroniro (2010), On the importance of sublimation to an alpine snow mass balance in the Canadian Rocky Mountains, *Hydrology and Earth System Sciences*, *14*, 1401-1415.

Mallows, C. L. (1973), Some Comments on Cp, *Technometrics*, *15*, 661.

Marks, D., and J. Dozier (1992), Climate and Energy Exchange at the Snow Surface in the Alpine Region of the Sierra-Nevada .2. Snow Cover Energy-Balance, *Water Resources Research*, *28*, 3043-3054.

Marks, D., M. Reba, J. Pomeroy, T. Link, A. Winstral, G. Flerchinger, and K. Elder (2008), Comparing Simulated and Measured Sensible and Latent Heat Fluxes over Snow under a Pine Canopy to Improve an Energy Balance Snowmelt Model, *Journal of Hydrometeorology*, *9*, 1506-1522.

Martinec, J., and A. Rango (1981), Areal distribution of snow water equivalent evaluated by snow cover monitoring, *Water Resources Research*, *17*, 1480-1488.

Mauder, M., and T. Foken (2004), *Documentation and instruction manual of the eddy covariance software package TK2*, Univ. of Bayreuth, Bayreuth, Germany.

McCabe, G. J., and D. M. Wolock (2007), Warming may create substantial water supply shortages in the Colorado River basin, *Geophysical Research Letters*, *34*, L22708.

McGrath, D., L. Sass, S. O'Neel, A. Arendt, G. Wolken, A. Gusmeroli, C. Kienholz, and C. McNeil (2015), End-of-winter snow depth variability on glaciers in Alaska, *Journal of Geophysical Research: Earth Surface*, *120*, 1530-1550.

McKay, D. C., and G. W. Thurtell (1978), Measurements of the Energy Fluxes Involved in the Energy Budget of a Snow Cover, *Journal of Applied Meteorology*, *17*, 339-349.

Meek, D., and J. Hatfield (1994), Data quality checking for single station meteorological databases, *Agricultural and Forest Meteorology*, *69*, 85-109.

Meiman, J. R. (1968), Snow accumulation related to elevation, aspect, and forest canopy, *Proceedings of a Workshop Seminar on Snow Hydrology*, 35-47, Canadian National Committee for the International Hydrological Decade, Ottawa, Ont.

Meiman, J. R., and L. O. Grant (1974), *Snow-air interactions and mangement of mountain watershed snowpack*. Environmetal Resources Center, Colorado State Unversity, Fort Collins, CO, 36 pp.

Meromy, L., N. P. Molotch, T. E. Link, S. R. Fassnacht, and R. Rice (2013), Subgrid variability of snow water equivalent at operational snow stations in the western USA, *Hydrological Processes*, *27*, 2383-2400.

Meyer, J. D. D., J. M. Jin, and S. Y. Wang (2012), Systematic Patterns of the Inconsistency between Snow Water Equivalent and Accumulated Precipitation as Reported by the Snowpack Telemetry Network, *Journal of Hydrometeorology*, *13*, 1970-1976.

Milly, P. C., J. Betancourt, M. Falkenmark, R. M. Hirsch, Z. W. Kundzewicz, D. P. Lettenmaier, and R. J. Stouffer (2008), Climate change. Stationarity is dead: whither water management?, *Science*, *319*, 573-574.

Mizukami, N., and S. Perica (2008), Spatiotemporal Characteristics of Snowpack Density in the Mountainous Regions of the Western United States, *Journal of Hydrometeorology*, *9*, 1416-1426.

Molotch, N. P., and R. C. Bales (2005), Scaling snow observations from the point to the grid element: Implications for observation network design, *Water Resources Research*, *41*, W11421.

Molotch, N. P., M. T. Colee, R. C. Bales, and J. Dozier (2005), Estimating the spatial distribution of snow water equivalent in an alpine basin using binary regression tree models: the impact of digital elevation data and independent variable selection, *Hydrological Processes*, *19*, 1459-1479.

Molotch, N. P., P. D. Blanken, M. W. Williams, A. A. Turnipseed, R. K. Monson, and S. A. Margulis (2007), Estimating sublimation of intercepted and sub-canopy snow using eddy covariance systems, *Hydrological Processes*, *21*, 1567-1575.

Moncrieff, J. B., Y. Malhi, and R. Leuning (1996), The propagation of errors in long-term measurements of land-atmosphere fluxes of carbon and water, *Global Change Biology*, *2*, 231-240.

Montesi, J., K. Elder, R. A. Schmidt, and R. E. Davis (2004), Sublimation of intercepted snow within a subalpine forest canopy at two elevations, *Journal of Hydrometeorology*, *5*, 763-773.

Moreo, M. T., R. J. Laczniak, and D. I. Stannard (2007), Evapotranspiration rate measurements of vegetation typical of ground-water discharge areas in the Basin and Range carbonate-rock aquifer system, Nevada and Utah, September 2005-August 2006, U.S. Geological Survey Scientific-Investigations Report, 2007-5078, 36 pp.

Mote, P. W. (2006), Climate-driven variability and trends in mountain snowpack in western North America, *Journal of Climate*, *19*, 6209-6220.

Mott, R., L. Egli, T. Grünewald, N. Dawes, C. Manes, M. Bavay, and M. Lehning (2011), Micrometeorological processes driving snow ablation in an Alpine catchment, *The Cryosphere*, *5*, 1083-1098.

Musselman, K. N., N. P. Molotch, and P. D. Brooks (2008), Effects of vegetation on snow accumulation and ablation in a mid-latitude sub-alpine forest, *Hydrological Processes*, *22*, 2767-2776.

Musselman, K. N., J. W. Pomeroy, R. L. H. Essery, and N. Leroux (2015), Impact of windflow calculations on simulations of alpine snow accumulation, redistribution and ablation, *Hydrological Processes*, *29*, 3983-3999.

Musselman, K. N., N. P. Molotch, S. A. Margulis, P. B. Kirchner, and R. C. Bales (2012), Influence of canopy structure and direct beam solar irradiance on snowmelt rates in a mixed conifer forest, *Agricultural and Forest Meteorology*, *161*, 46-56.

Nolan, M., C. Larsen, and M. Sturm (2015), Mapping snow depth from manned aircraft on landscape scales at centimeter resolution using structure-from-motion photogrammetry, *The Cryosphere*, *9*, 1445-1463.

Nolin, A. W. (2010), Recent advances in remote sensing of seasonal snow, *Journal of Glaciology*, *56*, 1141-1150.

Ohmura, A. (1982), Objective Criteria for Rejecting Data for Bowen Ratio Flux Calculations, *Journal of Applied Meteorology*, *21*, 595-598.

Oke, T. R. (1987), *Boundary layer climates*, 2nd ed., 435 pp., Routledge Publishing, New York, New York.

Pagano, T., A. Wood, K. Werner, and R. Tama-Sweet (2014), Western U.S. Water Supply Forecasting: A Tradition Evolves, *Eos, Transactions American Geophysical Union*, *95*, 28-29.

Painter, T. H., J. S. Deems, J. Belnap, A. F. Hamlet, C. C. Landry, and B. Udall (2010), Response of Colorado River runoff to dust radiative forcing in snow, *Proc Natl Acad Sci U S A*, *107*, 17125-17130.

Painter, T. H., D. F. Berisford, J. W. Boardman, K. J. Bormann, J. S. Deems, F. Gehrke, A. Hedrick, M. Joyce, R. Laidlaw, D. Marks, C. Mattmann, B. McGurk, P. Ramirez, M. Richardson, S. M. Skiles, F. C. Seidel, and A. Winstral (2016), The Airborne Snow Observatory: Fusion of scanning lidar, imaging spectrometer, and physically-based modeling for mapping snow water equivalent and snow albedo, *Remote Sensing of Environment*, *184*, 139-152.

Payero, J. O., C. M. U. Neale, J. L. Wright, and R. G. Allen (2003), Guidelines for validating Bowen ratio data, *Transactions of the Asae*, *46*, 1051-1060.

Pomeroy, J. W., and D. M. Gray (1990), Saltation of snow, *Water Resources Research*, *26*, 1583-1594.

Pomeroy, J. W., and D. H. Male (1992), Steady-state suspension of snow, *Journal of Hydrology*, *136*, 275-301.

Pomeroy, J. W., and D. M. Gray (1995), *Snow Accumulation, Relocation and Management*, National Hydrology Research Institute Science Report No. 7, NHRI, Environment Canada, Saskatoon, 144 pp.

Pomeroy, J. W., and R. L. H. Essery (1999), Turbulent fluxes during blowing snow: field tests of model sublimation predictions, *Hydrological Processes, 13*, 2963-2975.

Pomeroy, J. W., B. Toth, R. J. Granger, N. R. Hedstrom, and R. L. H. Essery (2003), Variation in surface energetics during snowmelt in a subarctic mountain catchment, *Journal of Hydrometeorology*, *4*, 702-719.

Pomeroy, J. W., D. M. Gray, K. R. Shook, B. Toth, R. L. H. Essery, A. Pietroniro, and N. Hedstrom (1998), An evaluation of snow accumulation and ablation processes for land surface modelling, *Hydrological Processes, 12*, 2339-2367.

Pomeroy, J. W., D. M. Gray, T. Brown, N. R. Hedstrom, W. L. Quinton, R. J. Granger, and S. K. Carey (2007), The cold regions hydrological model: a platform for basing process representation and model structure on physical evidence, *Hydrological Processes, 21*, 2650-2667.

Pomeroy, J. W., D. Marks, T. Link, C. Ellis, J. Hardy, A. Rowlands, and R. Granger (2009), The impact of coniferous forest temperature on incoming longwave radiation to melting snow, *Hydrological Processes, 23*, 2513-2525.

Price, A. G., and T. Dunne (1976), Energy balance computations of snowmelt in a subarctic area, *Water Resources Research, 12*, 686-694.

Pugh, E., and E. Small (2012), The impact of pine beetle infestation on snow accumulation and melt in the headwaters of the Colorado River, *Ecohydrology*, *5*, 467-477.

Raleigh, M. S., J. D. Lundquist, and M. P. Clark (2015), Exploring the impact of forcing error characteristics on physically based snow simulations within a global sensitivity analysis framework, *Hydrology and Earth System Sciences*, *19*, 3153-3179.

Rauscher, S. A., J. S. Pal, N. S. Diffenbaugh, and M. M. Benedetti (2008), Future changes in snowmelt-driven runoff timing over the western US, *Geophysical Research Letters*, *35*, L16703.

Reba, M. L., T. E. Link, D. Marks, and J. Pomeroy (2009), An assessment of corrections for eddy covariance measured turbulent fluxes over snow in mountain environments, *Water Resources Research, 45*, W00D38.

Reba, M. L., J. Pomeroy, D. Marks, and T. E. Link (2012), Estimating surface sublimation losses from snowpacks in a mountain catchment using eddy covariance and turbulent transfer calculations, *Hydrological Processes*, *26*, 3699-3711.

Reba, M. L., D. Marks, T. E. Link, J. Pomeroy, and A. Winstral (2014), Sensitivity of model parameterizations for simulated latent heat flux at the snow surface for complex mountain sites, *Hydrological Processes, 28*, 868-881.

Revuelto, J., J. I. López-Moreno, C. Azorin-Molina, and S. M. Vicente-Serrano (2014), Topographic control of snowpack distribution in a small catchment in the central Spanish Pyrenees: intra- and inter-annual persistence, *The Cryosphere, 8*, 1989-2006.

Revuelto, J., J. I. Lopez-Moreno, C. Azorin-Molina, and S. M. Vicente-Serrano (2015), Canopy influence on snow depth distribution in a pine stand determined from terrestrial laser data, *Water Resources Research, 51*, 3476-3489.

Richer, E. E., S. K. Kampf, S. R. Fassnacht, and C. C. Moore (2013), Spatiotemporal index for analyzing controls on snow climatology: application in the Colorado Front Range, *Physical Geography, 34*, 85-107.

Schmidt, R. A. (1980), Threshold wind-speeds and elastic impact in snow transport, *Journal of Glaciology, 26*, 453-467.

Schmidt, R. A., C. A. Troendle, and J. R. Meiman (1998), Sublimation of snowpacks in subalpine conifer forests, *Canadian Journal of Forest Research, 28*, 501-513.

Schotanus, P., F. T. M. Nieuwstadt, and H. A. R. De Bruin (1983), Temperature measurement with a sonic anemometer and its application to heat and moisture fluxes, *Boundary-Layer Meteorology, 26*, 81-93.

Schuepp, P. H., M. Y. Leclerc, J. I. Macpherson, and R. L. Desjardins (1990), Footprint Prediction of Scalar Fluxes from Analytical Solutions of the Diffusion Equation, *Boundary-Layer Meteorology, 50*, 353-373.

Serreze, M. C., M. P. Clark, R. L. Armstrong, D. A. McGinnis, and R. S. Pulwarty (1999), Characteristics of the western United States snowpack from snowpack telemetry (SNOTEL) data, *Water Resources Research, 35*, 2145-2160.

Sexstone, G. A., and S. R. Fassnacht (2014), What drives basin scale spatial variability of snowpack properties in northern Colorado?, *The Cryosphere, 8*, 329-344.

Sexstone, G. A., S. R. Fassnacht, J. I. López-Moreno, and C. A. Hiemstra (2016a), Subgrid snow depth coefficient of variation within complex mountainous terrain, *The Cryosphere, in review*.

Sexstone, G. A., D. W. Clow, D. I. Stannard, and S. R. Fassnacht (2016b), Comparison of methods for quantifying surface sublimation over seasonally snow-covered terrain, *Hydrological Processes*, doi: 10.1002/hyp.10864.

Sexstone, G. A., D. W. Clow, S. R. Fassnacht, G. E. Liston, C. A. Hiemstra, and J. F. Knowles (2016c), Modeling the variability and importance of snow sublimation in the north-central Colorado Rocky Mountains, *Water Resources Research, in preparation*.

Seyfried, M. S., and B. P. Wilcox (1995), Scale and the Nature of Spatial Variability - Field Examples Having Implications for Hydrologic Modeling, *Water Resources Research, 31*, 173-184.

Slater, A. G., C. A. Schlosser, C. E. Desborough, A. J. Pitman, A. Henderson-Sellers, A. Robock, K. Y. Vinnikov, K. Mitchell, A. Boone, H. Braden, F. Chen, P. M. Cox, P. de Rosnay, R. E. Dickinson, Y. J. Dai, Q. Duan, J. Entin, P. Etchevers, N. Gedney, Y. M. Gusev, F. Habets, J. Kim, V. Koren, E. A. Kowalczyk, O. N. Nasonova, J. Noilhan, S. Schaake, A. B. Shmakin, T. G. Smirnova, D. Verseghy, P. Wetzel, X. Yue, Z. L. Yang, and Q. Zeng (2001), The representation of snow in land surface schemes: Results from PILPS 2(d), *Journal of Hydrometeorology*, *2*, 7-25.

Stannard, D. I. (1997), A theoretically based determination of Bowen-ratio fetch requirements, *Boundary-Layer Meteorology*, *83*, 375-406.

Stannard, D. I., J. H. Blanford, W. P. Kustas, W. D. Nichols, S. A. Amer, T. J. Schmugge, and M. A. Weltz (1994), Interpretation of Surface Flux Measurements in Heterogeneous Terrain during the Monsoon 90 Experiment, *Water Resources Research*, *30*, 1227-1239.

Stewart, I. T. (2009), Changes in snowpack and snowmelt runoff for key mountain regions, *Hydrological Processes*, *23*, 78-94.

Storr, D., and H. L. Ferguson (1974), On the Ambiguity of Bowen Ratios over Freezing and Melting Surfaces, *Journal of Applied Meteorology*, *13*, 509-511.

Strasser, U., M. Bernhardt, M. Weber, G. E. Liston, and W. Mauser (2008), Is snow sublimation important in the alpine water balance?, *The Cryosphere*, *2*, 53-66.

Sturm, M., and A. M. Wagner (2010), Using repeated patterns in snow distribution modeling: An Arctic example, *Water Resources Research*, *46*, W12549.

Sturm, M., J. Holmgren, and G. E. Liston (1995), A Seasonal Snow Cover Classification-System for Local to Global Applications, *Journal of Climate*, *8*, 1261-1283.

Sturm, M., B. Taras, G. E. Liston, C. Derksen, T. Jonas, and J. Lea (2010), Estimating Snow Water Equivalent Using Snow Depth Data and Climate Classes, *Journal of Hydrometeorology*, *11*, 1380-1394.

Suding, K. N., E. C. Farrer, A. J. King, L. Kueppers, and M. J. Spasojevic (2015), Vegetation change at high elevation: scale dependence and interactive effects on Niwot Ridge, *Plant Ecology & Diversity*, *8*, 713-725.

Svoma, B. M. (2016), Difficulties in Determining Snowpack Sublimation in Complex Terrain at the Macroscale, *Advances in Meteorology*, *2016*, 10.

Tanner, B., J. Greene, and G. Bingham (1987), A Bowen ratio design for long-term measurements, *Proceedings ASCE 1987 International Winter Meeting*, ASCE, St. Joseph, Mich.

Tanner, C. B. (1960), Energy Balance Approach to Evapotranspiration from Crops, *Soil Science Society of America Journal*, *24*, 1-9.

Taylor, J. R. (1997), *An Introduction to Error Analysis*, 2nd ed., 327 pp., University Science Books, Sausalito, California.

Trujillo, E., and N. P. Molotch (2014), Snowpack regimes of the Western United States, *Water Resources Research, 50*, 5611-5623.

Trujillo, E., and M. Lehning (2015), Theoretical analysis of errors when estimating snow distribution through point measurements, *The Cryosphere, 9*, 1249-1264.

Trujillo, E., J. A. Ramirez, and K. J. Elder (2007), Topographic, meteorologic, and canopy controls on the scaling characteristics of the spatial distribution of snow depth fields, *Water Resources Research, 43*, W07409.

Turnipseed, A. A., P. D. Blanken, D. E. Anderson, and R. K. Monson (2002), Energy budget above a high-elevation subalpine forest in complex topography, *Agricultural and Forest Meteorology, 110*, 177-201.

Turnipseed, A. A., D. E. Anderson, P. D. Blanken, W. M. Baugh, and R. K. Monson (2003), Airflows and turbulent flux measurements in mountainous terrain Part 1. Canopy and local effects, *Agricultural and Forest Meteorology, 119*, 1-21.

Turnipseed, A. A., D. E. Anderson, S. Burns, P. D. Blanken, and R. K. Monson (2004), Airflows and turbulent flux measurements in mountainous terrain: Part 2: Mesoscale effects, *Agricultural and Forest Meteorology, 125*, 187-205.

USDA Forest Service (2011), Mountain Pine Beetle on the Front Range, available at http://www.fs.usda.gov/Internet/FSE_DOCUMENTS/stelprdb5340091.pdf.

Veatch, W., P. D. Brooks, J. R. Gustafson, and N. P. Molotch (2009), Quantifying the effects of forest canopy cover on net snow accumulation at a continental, mid-latitude site, *Ecohydrology, 2*, 115-128.

Vickers, D., and L. Mahrt (1997), Quality control and flux sampling problems for tower and aircraft data, *Journal of Atmospheric and Oceanic Technology, 14*, 512-526.

Viviroli, D., R. Weingartner, and B. Messerli (2003), Assessing the Hydrological Significance of the World's Mountains, *Mountain Research and Development, 23*, 32-40.

Webb, E. K., G. I. Pearman, and R. Leuning (1980), Correction of flux measurements for density effects due to heat and water vapour transfer, *Quarterly Journal of the Royal Meteorological Society, 106*, 85-100.

Weiss, A. D. (2001), Topographic Position and Landforms Analysis, *ESRI User Conference*, San Diego, California.

Westerling, A. L., H. G. Hidalgo, D. R. Cayan, and T. W. Swetnam (2006), Warming and earlier spring increase western U.S. forest wildfire activity, *Science, 313*, 940-943.

Wilson, K., A. Goldstein, E. Falge, M. Aubinet, D. Baldocchi, P. Berbigier, C. Bernhofer, R. Ceulemans, H. Dolman, C. Field, A. Grelle, A. Ibrom, B. E. Law, A. Kowalski, T. Meyers, J. Moncrieff, R. Monson, W. Oechel, J. Tenhunen, R. Valentini, and S. Verma (2002), Energy balance closure at FLUXNET sites, *Agricultural and Forest Meteorology*, *113*, 223-243.

Winstral, A., and D. Marks (2014), Long-term snow distribution observations in a mountain catchment: Assessing variability, time stability, and the representativeness of an index site, *Water Resources Research*, *50*, 293-305.

Winstral, A., K. Elder, and R. E. Davis (2002), Spatial snow modeling of wind-redistributed snow using terrain-based parameters, *Journal of Hydrometeorology*, *3*, 524-538.

Wood, E. F., J. K. Roundy, T. J. Troy, L. P. H. van Beek, M. F. P. Bierkens, E. Blyth, A. de Roo, P. Doll, M. Ek, J. Famiglietti, D. Gochis, N. van de Giesen, P. Houser, P. R. Jaffe, S. Kollet, B. Lehner, D. P. Lettenmaier, C. Peters-Lidard, M. Sivapalan, J. Sheffield, A. Wade, and P. Whitehead (2011), Hyperresolution global land surface modeling: Meeting a grand challenge for monitoring Earth's terrestrial water, *Water Resources Research*, *47*.

Yang, Z. L., R. E. Dickinson, A. Robock, and K. Y. Vinnikov (1997), Validation of the snow submodel of the biosphere-atmosphere transfer scheme with Russian snow cover and meteorological observational data, *Journal of Climate*, *10*, 353-373.

Zhang, Y. S., M. Ishikawa, T. Ohata, and D. Oyunbaatar (2008), Sublimation from thin snow cover at the edge of the Eurasian cryosphere in Mongolia, *Hydrological Processes*, *22*, 3564-3575.

Zheng, Z., P. B. Kirchner, and R. C. Bales (2016), Topographic and vegetation effects on snow accumulation in the southern Sierra Nevada: a statistical summary from lidar data, *The Cryosphere*, *10*, 257-269.

Zhou, H. F., X. J. Zheng, B. J. Zhou, Q. Dai, and Y. Li (2012), Sublimation over seasonal snowpack at the southeastern edge of a desert in central Eurasia, *Hydrological Processes*, *26*, 3911-3920.

APPENDIX A

A.1. Calculation of snowpack internal energy change

The snowpack thermocouple wires were housed within a white polyvinyl chloride (PVC) pipe (19 mm diameter) and routed from each measurement height to a multiplexer housed at the base of the snowpack. At each measurement height, the thermocouple was exposed to the snow through a north-facing opening in the pipe (13 mm diameter), which was protected from solar radiation using a small radiation shield. Insulation within the pipe between each thermocouple prevented air movement within the pipe.

The snowpack internal energy change ($dU\ dt^{-1}$) was calculated at each site during the snow-accumulation period by measurements of snow depth as well as measurements of snow density and snow temperature for each 10 cm layer within the snowpack. The temperature of each layer was defined based on the average of the upper and lower height of thermocouples buried within the snowpack. The temperature of the uppermost layer (< 10 cm) was defined by a weighted average of snow surface temperature (2 cm layer) and uppermost buried thermocouple measurement (remaining layer below 2 cm snow surface layer). Manual snow pit snow density measurements were collected every 2 – 4 weeks during the snow-accumulation period to estimate the snow density profile at both sites. Snow density estimates were adjusted between site visits using the snow density time series from the nearby Arrow SNOTEL site during WY 2013 (discontinued following WY 2013) and the High Lonesome SNOTEL site during WY 2014 and WY 2015 (Figure 1) (SNOTEL data accessed at <http://www.wcc.nrcs.usda.gov/snow/>).

The accuracy of the snow temperature measurements (T_S) taken along the thermocouple array are particularly sensitive to any errors in the reference temperature measurement (T_{REF}) made by the datalogger multiplexer (Campbell Scientific AM25T). Given that the multiplexer

was insulated by the entire depth of the snowpack, it was not anticipated that T_{REF} would vary at short time scales. To remove any spurious errors in T_S caused by the unexpected fluctuations in T_{REF}, T_{REF} was subtracted from T_S at each time step for each thermocouple (T_S-T_{REF}); a 12 hour running average of T_{REF} (T_{REF_RA}) was then added back to each T_S-T_{REF} to provide corrected measurements of T_S. This technique was justified given that the calculation of $dU\ dt^{-1}$ requires accurate measurements of the relative change in temperature rather than the actual magnitude of T_S.

A.2. Procedure for calculating turbulent fluxes using the aerodynamic profile (AP) method

These supplemental equations outline the iterative procedure adapted from Arya (1988) for calculating the turbulent flux of latent ($Q_{E\text{-}AP}$) and sensible ($Q_{H\text{-}AP}$) heat using the aerodynamic profile method with measurements of temperature and vapor pressure at two heights and wind speed measurements at only one height.

The transfer coefficient for latent (C_E) and sensible (C_H) heat discussed in this study are as follows:

$$C_E = \frac{k^2}{\Phi_m \Phi_v \ln\left(\frac{z_2 - d}{z_1 - d}\right)^2}, C_H = \frac{k^2}{\Phi_m \Phi_h \ln\left(\frac{z_2 - d}{z_1 - d}\right)^2} \qquad \text{(A1a:b)}$$

First, compute the following fixed values and initial assumptions:

$$z_m = d + [(z_2 - d)(z_1 - d)]^{0.5} \qquad \text{(A2)}$$

$$T_k = \frac{T_2 + T_1}{2} + 273.15 \qquad \text{(A3)}$$

$$\Phi_v = \Phi_h = \Phi_m = 1 \text{ (neutral conditions assumed)} \qquad \text{(A4)}$$

$$\Psi_a = \Psi_2 = \Psi_1 = \Psi_1 = 0 \text{ (neutral conditions assumed)} \qquad \text{(A5)}$$

Then, iterate the following equations until convergence of u^*, $Q_{H\text{-}AP}$, and $Q_{E\text{-}AP}$ is obtained:

$$u^* = \frac{k u_a}{\ln\left(\frac{z_a - d}{z_0}\right) - \Psi_a} \tag{A6}$$

$$u_2 = \frac{u^*}{k}\left[\ln\left(\frac{z_2 - d}{z_0}\right) - \Psi_2\right] \tag{A7}$$

$$u_1 = \frac{u^*}{k}\left[\ln\left(\frac{z_1 - d}{z_0}\right) - \Psi_1\right] \tag{A8}$$

$$u_m = \frac{u^*}{k}\left[\ln\left(\frac{z_m - d}{z_0}\right) - \Psi_m\right] \tag{A9}$$

$$Q_{H-AP} = \frac{-\rho c_p k^2 \Delta u \Delta T}{\Phi_m \Phi_h \ln\left(\frac{z_2 - d}{z_1 - d}\right)^2} \tag{A10}$$

$$Q_{E-AP} = \frac{-L_s 0.622 \rho k^2 \Delta u \Delta e}{P \Phi_m \Phi_v \ln\left(\frac{z_2 - d}{z_1 - d}\right)^2} \tag{A11}$$

Calculate the cumulative footprint prediction based on Schuepp et al. (1990), using the mean geometric height (Stannard, 1997), while varying x_L:

$$CNF(x_L) = 100 * \exp^{-u_m(z_m - d)/ku^* x_L} \tag{A12}$$

Compute the atmospheric stability parameter at the upper height:

$$\zeta_2 = \frac{-k(z_2 - d) g (Q_{H-AP} + 0.07 Q_{E-AP})}{\rho c_p T_k (u^*)^3} \tag{A13}$$

Limit the stability parameter in extreme conditions:

If $\zeta_2 > 5$ then $\zeta_2 = 5$, If $\zeta_2 < -10$ then $\zeta_2 = -10$ (A14a:b)

Compute the stability parameter at the anemometer, mean, and lower heights:

$$\zeta_a = \zeta_2\left(\frac{z_a - d}{z_2 - d}\right),\ \ \zeta_m = \zeta_2\left(\frac{z_m - d}{z_2 - d}\right),\ \ \zeta_1 = \zeta_2\left(\frac{z_1 - d}{z_2 - d}\right) \qquad \text{(A15a:c)}$$

Branching calculations depending on stable, neutral, or unstable conditions:

If $\zeta_2 \geq 0$ (stable or neutral conditions):

$$\Psi_a = -5\zeta_a,\ \ \Psi_2 = -5\zeta_2,\ \ \Psi_1 = -5\zeta_1,\ \Psi_m = -5\zeta_m,\ \ \Phi_h = \Phi_v = \Phi_m = 1 + 5\zeta_m \qquad \text{(A16a:e)}$$

Else if $\zeta_2 < 0$ (unstable conditions):

$$x_a = (1 - 15\zeta_a)^{0.25},\ \ x_2 = (1 - 15\zeta_2)^{0.25},\ \ x_1 = (1 - 15\zeta_1)^{0.25},\ x_m = (1 - 15\zeta_m)^{0.25} \qquad \text{(A17a:d)}$$

$$\Psi_a = \ln\left[\left(\frac{1 + x_a^{\,2}}{2}\right)\left(\frac{1 + x_a}{2}\right)^2\right] - 2\tan^{-1} x_a + \frac{\Pi}{2} \qquad \text{(A18a)}$$

$$\Psi_2 = \ln\left[\left(\frac{1 + x_2^{\,2}}{2}\right)\left(\frac{1 + x_2}{2}\right)^2\right] - 2\tan^{-1} x_2 + \frac{\Pi}{2} \qquad \text{(A18b)}$$

$$\Psi_1 = \ln\left[\left(\frac{1 + x_1^{\,2}}{2}\right)\left(\frac{1 + x_1}{2}\right)^2\right] - 2\tan^{-1} x_1 + \frac{\Pi}{2} \qquad \text{(A18c)}$$

$$\Psi_m = \ln\left[\left(\frac{1 + x_m^{\,2}}{2}\right)\left(\frac{1 + x_m}{2}\right)^2\right] - 2\tan^{-1} x_m + \frac{\Pi}{2} \qquad \text{(A18d)}$$

$$\Phi_h = (1 - 15\zeta_m)^{-0.25}, \Phi_v = (1 - 15\zeta_m)^{-0.5}, \Phi_m = (1 - 15\zeta_m)^{-0.25} \qquad \text{(A18e:g)}$$

Return to the Eq A6 for u^*

List of Symbols

c_p – Specific heat capacity of air (1.01 $Jg^{-1}K^{-1}$)
d - Displacement height (assumed to equal 0 m)
g - Acceleration due to gravity (9.81 m s^{-2})
k - von Karman's constant (0.41)
Π - pi (≈ 3.14159)
Δ - Measurement gradient (upper height minus lower height)
T - Air temperature (subscripts: k – mean of heights 1 and 2 in degrees Kelvin; 1, 2 – measurement heights 1 and 2)
u - Wind speed (subscripts: a – at height of anemometer; 1, 2 – at measurement heights 1 and 2)
u^* - Friction velocity

e - Vapor pressure
z - Measurement height above snow surface (subscripts: a – anemometer; m – geometric mean of measurement heights; 1, 2 – measurement heights)
z_0 - Roughness length (0.001 m)
ζ - Atmospheric stability parameter (subscripts: a – at height of anemometer; m – at height of z_m; 1, 2 – at measurement heights 1 and 2)
Φ - Stability flux corrector (subscripts: h – for sensible heat; v – for latent heat; m – for momentum)
Ψ - Stability profile corrector (subscripts: a – at height of anemometer; 1, 2 – at measurement heights 1 and 2)
ρ - Air density
P - Atmospheric pressure
CNF – Cumulative normalized footprint from Schuepp et al. (1990)
x_L – Fetch distance

Table A1: Mean seasonal surface sublimation rates, total seasonal surface sublimation, and surface sublimation losses as a percentage of winter precipitation [$P^{(SCP)}$] for the eddy-covariance (EC) method, bulk-aerodynamic flux (BF) method, Bowen-ratio (BR) method, and aerodynamic-profile (AP) method at the (a) Arrow site and (b) Cabin site during the snow-covered period $^{(SCP)}$, snow-accumulation period $^{(SAP)}$, and snowmelt period $^{(SMP)}$ of WY 2013, WY 2014, and WY 2015.

(a)	Arrow 2013				Arrow 2014				Arrow 2015			
	EC	BF	BR	AP	EC	BF	BR	AP	EC	BF	BR	AP
Sublimation Rate^{SCP} ($mm\ day^{-1}$)	---	0.15	0.20	0.10	0.33	0.15	0.14	0.09	0.36	0.17	---	---
Sublimation Rate^{SAP} ($mm\ day^{-1}$)	---	0.13	0.15	0.10	0.27	0.10	0.10	0.06	0.19	0.09	---	---
Sublimation Rate^{SMP} ($mm\ day^{-1}$)	---	0.22	0.57	0.15	0.60	0.38	0.34	0.22	0.78	0.37	---	---
Total Sublimation^{SCP} (mm)	---	27.2	38.2	19.2	55.3	25.3	23.4	14.8	58.6	27.6	---	---
Total Sublimation^{SAP} (mm)	---	22.3	25.6	15.9	37.2	13.9	13.3	8.1	22.5	10.5	---	---
Total Sublimation^{SMP} (mm)	---	4.9	12.6	3.3	18.1	11.4	10.1	6.8	36.1	17.1	---	---
Total Sublimation as % of P^{SCP}	---	7.9	11.1	5.6	12.8	5.9	5.4	3.4	16.9	7.9	---	---

(b)	Cabin 2013				Cabin 2014			
	EC	BF	BR	AP	EC	BF	BR	AP
Sublimation Rate^{SCP} ($mm\ day^{-1}$)	---	0.10	0.37	0.03	---	0.13	0.34	0.04
Sublimation Rate^{SAP} ($mm\ day^{-1}$)	---	0.03	0.23	0.01	---	0.11	0.28	0.04
Sublimation Rate^{SMP} ($mm\ day^{-1}$)	---	0.20	0.59	0.08	---	0.27	0.70	0.09
Total Sublimation^{SCP} (mm)	---	13.6	53.2	4.9	---	19.4	50.8	6.8
Total Sublimation^{SAP} (mm)	---	2.4	19.4	0.32	---	14.2	37.2	5.1
Total Sublimation^{SMP} (mm)	---	11.2	33.7	4.6	---	5.2	13.5	1.7
Total Sublimation as % of P^{SCP}	---	7.0	27.4	2.5	---	9.2	24.1	3.2